Advanced Engineering Electromagnetics — Constantine Balanis © 1989

CHAPTER 12

INTEGRAL EQUATIONS AND THE MOMENT METHOD

12.1 INTRODUCTION

In Chapter 11 we discussed scattering from conducting objects, such as plates, circular cylinders, and spheres, using geometrical optics, physical optics, and modal solutions. For the plates and cylinders we assumed that their dimensions were of infinite extent. In practice, however, the dimensions of the objects are always finite, although some of them may be very large. Expressions for the radar cross section of finite size scatterers were introduced in the previous chapter. These, however, represent approximate forms, and more accurate expressions are sometimes desired.

The physical optics method of Chapter 7, Section 7.10, was used in the previous chapter to approximate the current induced on the surface of a finite size target, such as the strip and rectangular plate. Radiation integrals were then used to find the field scattered by the target. To derive a more accurate representation of the current induced on the surface of the finite size target, and thus of the scattered fields, two methods will be examined here.

One method, referred to here as the *integral equation* (IE) technique, casts the solution for the induced current in the form of an integral equation (hence its name) where the unknown induced current density is part of the integrand. Numerical techniques such as the *moment method* (MM) [1–6] can then be used to solve for the current density. Once this is accomplished, the fields scattered by the target can be found using the traditional radiation integrals. The total induced current density will be the sum of the physical optics current density and a *fringe wave* current density [7–13] which can be thought of as a perturbation current density introduced by the edge diffractions of the finite size structure. This method will be introduced and applied in this chapter.

The other method, referred to here as the *geometrical theory of diffraction* (GTD) [14–17], is an extension of geometrical optics and accounts for the contributions from the edges of the finite structure using diffraction theory. This method will be introduced and applied in Chapter 13. More extensive discussions of each can be found in the open literature.

12.2 INTEGRAL EQUATION METHOD

The objective of the integral equation (IE) method for scattering is to cast the solution for the unknown current density, which is induced on the surface of the scatterer, in the form of an integral equation where the unknown induced current density is part of the integrand. The integral equation is then solved for the unknown induced current density using numerical techniques such as the *moment method* (MM). To demonstrate the technique, we will initially consider some specific problems. We will start with an electrostatics problem and follow it with time-harmonic problems.

12.2.1 Electrostatic Charge Distribution

In electrostatics, the problem of finding the potential that is due to a given charge distribution is often considered. In physical situations, however, it is seldom possible to specify a charge distribution. Whereas we may connect a conducting body to a voltage source, and thus specify the potential throughout the body, the distribution of charge is obvious only for a few rotationally symmetric geometries. In this section we will consider an integral equation approach to solve for the electric charge distribution once the electric potential is specified. Some of the material here and in other sections is drawn from [18, 19].

From statics we know that a linear electric charge distribution $\rho(\mathbf{r}')$ will create an electric potential, $V(\mathbf{r})$, according to [20]

$$V(\mathbf{r}) = \frac{1}{4\pi\varepsilon_0}\int_{\substack{\text{source}\\(\text{charge})}} \frac{\rho(\mathbf{r}')}{R}\, d\ell' \tag{12-1}$$

where $\mathbf{r}'(x', y', z')$ denotes the source coordinates, $\mathbf{r}(x, y, z)$ denotes the observation coordinates, $d\ell'$ is the path of integration, and R is the distance from any point on the source to the observation point, which is generally represented by

$$R(\mathbf{r}, \mathbf{r}') = |\mathbf{r} - \mathbf{r}'| = \sqrt{(x - x')^2 + (y - y')^2 + (z - z')^2} \tag{12-1a}$$

We see that (12-1) may be used to calculate the potentials that are due to any known line charge density. However, the charge distribution on most configurations of practical interest, i.e., complex geometries, is not usually known, even when the potential on the source is given. It is the nontrivial problem of determining the charge distribution, for a specified potential, that is to be solved here using an integral equation approach.

A. FINITE STRAIGHT WIRE

Consider a straight wire of length ℓ and radius a, placed along the y axis, as shown in Figure 12-1*a*. The wire is given a normalized constant electric potential of 1 V.

Note that (12-1) is valid everywhere, including on the wire itself ($V_{\text{wire}} = 1$ V). Thus, choosing the observation along the wire axis ($x = z = 0$) and representing the charge density on the surface of the wire, (12-1) can be expressed as

$$1 = \frac{1}{4\pi\varepsilon_0}\int_0^{\ell} \frac{\rho(y')}{R(y, y')}\, dy' \qquad 0 \le y \le \ell \tag{12-2}$$

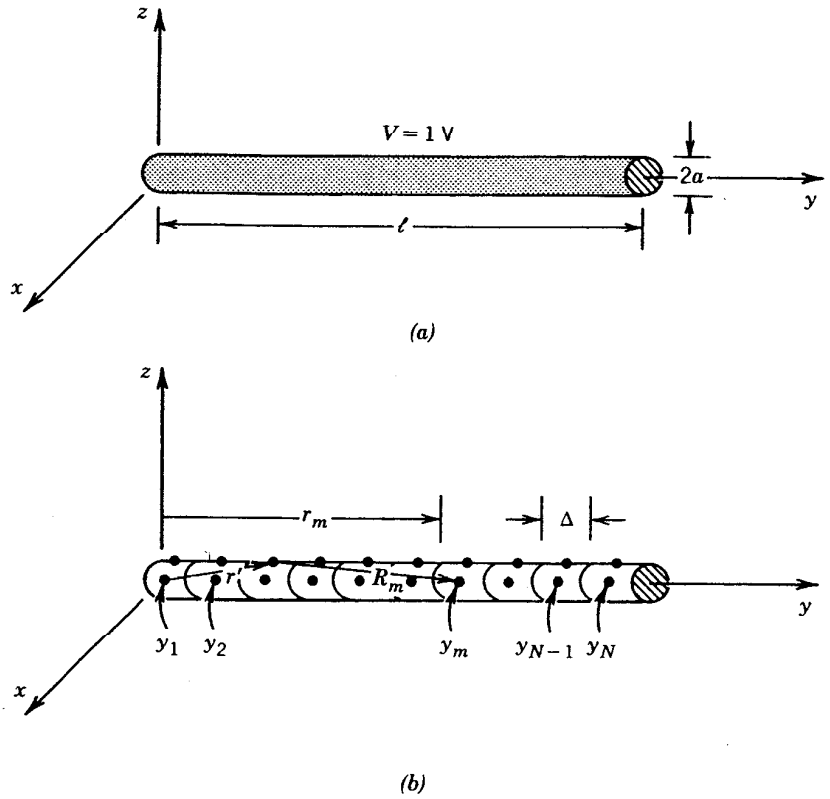

FIGURE 12-1 (*a*) Straight wire of constant potential and (*b*) its segmentation.

where

$$R(y, y') = R(\mathbf{r}, \mathbf{r}')|_{x=z=0} = \sqrt{(y - y')^2 + \left[(x')^2 + (z')^2\right]} = \sqrt{(y - y')^2 + a^2} \tag{12-2a}$$

The observation point is chosen along the wire axis and the charge density is represented along the surface of the wire to avoid $R(y, y') = 0$, which would introduce a singularity in the integrand of (12-2).

It is necessary to solve (12-2) for the unknown $\rho(y')$ (an inversion problem). Equation 12-2 is an integral equation that can be used to find the charge density $\rho(y')$ based on the 1-V potential. The solution may be reached numerically by reducing (12-2) to a series of linear algebraic equations that may be solved by conventional matrix equation techniques. To facilitate this, let us approximate the unknown charge distribution $\rho(y')$ by an expansion of N known terms with constant, but unknown, coefficients, that is

$$\rho(y') = \sum_{n=1}^{N} a_n g_n(y') \tag{12-3}$$

Thus (12-2) may be written, using (12-3), as

$$4\pi\varepsilon_0 = \int_0^{\ell} \frac{1}{R(y, y')} \left[\sum_{n=1}^{N} a_n g_n(y')\right] dy' \tag{12-4}$$

Because (12-4) is a nonsingular integral, its integration and summation can be interchanged and it can be written as

$$4\pi\varepsilon_0 = \sum_{n=1}^{N} a_n \int_0^{\ell} \frac{g_n(y')}{\sqrt{(y-y')^2 + a^2}}\, dy' \tag{12-4a}$$

The wire is now divided into N uniform segments, each of length $\Delta = \ell/N$, as illustrated in Figure 12-1*b*. The $g_n(y')$ functions in the expansion (12-3) are chosen for their ability to accurately model the unknown quantity, while minimizing computation. They are often referred to as *basis* (or expansion) functions, and they will be discussed further in Section 12.2.5. To avoid complexity in this solution, subdomain piecewise constant (or "pulse") functions will be used. These functions, shown in Figure 12-6, are defined to be of a constant value over one segment and zero elsewhere, or

$$g_n(y') = \begin{cases} 0 & y' < (n-1)\Delta \\ 1 & (n-1)\Delta \le y' \le n\Delta \\ 0 & n\Delta < y' \end{cases} \tag{12-5}$$

Many other basis functions are possible, some of which will be introduced later in Section 12.2.5.

Replacing y in (12-4) by a fixed point on the surface of the wire, such as y_m, results in an integrand that is solely a function of y', so the integral may be evaluated. Obviously (12-4) leads to one equation with N unknowns a_n written as

$$4\pi\varepsilon_0 = a_1 \int_0^{\Delta} \frac{g_1(y')}{R(y_m, y')}\, dy' + a_2 \int_{\Delta}^{2\Delta} \frac{g_2(y')}{R(y_m, y')}\, dy' + \cdots$$
$$+ a_n \int_{(n-1)\Delta}^{n\Delta} \frac{g_n(y')}{R(y_m, y')}\, dy' + \cdots + a_N \int_{(N-1)\Delta}^{\ell} \frac{g_N(y')}{R(y_m, y')}\, dy' \tag{12-6}$$

In order to obtain a solution for these N amplitude constants, N linearly independent equations are necessary. These equations may be produced by choosing an observation point y_m on the surface of the wire and at the center of each Δ length element as shown in Figure 12-1*b*. This will result in one equation of the form of (12-6) corresponding to each observation point. For N such points we can reduce (12-6) to

$$4\pi\varepsilon_0 = a_1 \int_0^{\Delta} \frac{g_1(y')}{R(y_1, y')}\, dy' + \cdots + a_N \int_{(N-1)\Delta}^{\ell} \frac{g_N(y')}{R(y_1, y')}\, dy'$$
$$\vdots$$
$$4\pi\varepsilon_0 = a_1 \int_0^{\Delta} \frac{g_1(y')}{R(y_N, y')}\, dy' + \cdots + a_N \int_{(N-1)\Delta}^{\ell} \frac{g_N(y')}{R(y_N, y')}\, dy' \tag{12-6a}$$

We may write (12-6a) more concisely using matrix notation as

$$[V_m] = [Z_{mn}][I_n] \tag{12-7}$$

where each Z_{mn} term is equal to

$$Z_{mn} = \int_0^{\ell} \frac{g_n(y')}{\sqrt{(y_m - y')^2 + a^2}}\, dy' = \int_{(n-1)\Delta}^{n\Delta} \frac{1}{\sqrt{(y_m - y')^2 + a^2}}\, dy' \quad (12\text{-}7a)$$

and

$$[I_n] = [a_n] \quad (12\text{-}7b)$$

$$[V_m] = [4\pi\varepsilon_0] \quad (12\text{-}7c)$$

The V_m column matrix has all terms equal to $4\pi\varepsilon_0$, and the $I_n = a_n$ values are the unknown charge distribution coefficients. Solving (12-7) for $[I_n]$ gives

$$[I_n] = [a_n] = [Z_{mn}]^{-1}[V_m] \quad (12\text{-}8)$$

Either (12-7) or (12-8) may readily be solved on a digital computer by using any of a number of matrix inversion or equation solving routines. Whereas the integrals involved here may be evaluated in closed form by making appropriate approximations, this is not usually possible with more complicated problems. Efficient numerical integration computer subroutines are commonly available in easy-to-use forms.

One closed form evaluation of (12-7a) is to reduce the integral and represent it by

$$Z_{mn} = \begin{cases} 2\ln\left(\dfrac{\dfrac{\Delta}{2} + \sqrt{a^2 + \left(\dfrac{\Delta}{2}\right)^2}}{a}\right) & m = n \quad (12\text{-}9a) \\ \ln\left\{\dfrac{d_{mn}^{+} + \left[(d_{mn}^{+})^2 + a^2\right]^{1/2}}{d_{mn}^{-} + \left[(d_{mn}^{-})^2 + a^2\right]^{1/2}}\right\} & m \neq n \text{ but } |m-n| \leq 2 \quad (12\text{-}9b) \\ \ln\left(\dfrac{d_{mn}^{+}}{d_{mn}^{-}}\right) & |m-n| > 2 \quad (12\text{-}9c) \end{cases}$$

where

$$d_{mn}^{+} = \ell_m + \frac{\Delta}{2} \quad (12\text{-}9d)$$

$$d_{mn}^{-} = \ell_m - \frac{\Delta}{2} \quad (12\text{-}9e)$$

ℓ_m is the distance between the mth matching point and the center of the nth source point.

In summary, the solution of (12-2) for the charge distribution on a wire has been accomplished by approximating the unknown with some basis functions, dividing the wire into segments, and then sequentially enforcing (12-2) at the center of each segment to form a set of linear equations.

Even for the relatively simple straight wire geometry we have discussed, the exact form of the charge distribution is not intuitively apparent. To illustrate the principles of the numerical solution, an example is now presented.

Example 12-1. A 1-m long straight wire of radius $a = 0.001$ m is maintained at a constant potential of 1 V. Determine the linear charge distribution on the wire by dividing the length into 5 and 20 uniform segments. Assume subdomain pulse basis functions.

Solution.

1. $N = 5$. When the 1-m long wire is divided into five uniform segments each of length $\Delta = 0.2$ m, (12-7) reduces to

$$\begin{bmatrix} 10.60 & 1.10 & 0.51 & 0.34 & 0.25 \\ 1.10 & 10.60 & 1.10 & 0.51 & 0.34 \\ 0.51 & 1.10 & 10.60 & 1.10 & 0.51 \\ 0.34 & 0.51 & 1.10 & 10.60 & 1.10 \\ 0.25 & 0.34 & 0.51 & 1.10 & 10.60 \end{bmatrix} \begin{bmatrix} a_1 \\ a_2 \\ a_3 \\ a_4 \\ a_5 \end{bmatrix} = \begin{bmatrix} 1.11 \times 10^{-10} \\ 1.11 \times 10^{-10} \\ \vdots \\ 1.11 \times 10^{-10} \end{bmatrix}$$

Inverting this matrix leads to the amplitude coefficients and subsequent charge distribution of

$$a_1 = 8.81 \text{ pC/m}$$

$$a_2 = 8.09 \text{ pC/m}$$

$$a_3 = 7.97 \text{ pC/m}$$

$$a_4 = 8.09 \text{ pC/m}$$

$$a_5 = 8.81 \text{ pC/m}$$

The charge distribution is shown in Figure 12-2*a*.

2. $N = 20$. Increasing the number of segments to 20 results in a much smoother distribution, as shown plotted in Figure 12-2*b*. As more segments are used, a better approximation of the actual charge distribution is attained, which has smaller discontinuities over the length of the wire.

B. BENT WIRE

In order to illustrate the solution for a more complex structure, let us analyze a body composed of two noncollinear straight wires, that is, a bent wire. If a straight wire is bent, the charge distribution will be altered, although the solution to find it will differ only slightly from the straight wire case. We will assume a bend of angle α, which remains in the yz plane, as shown in Figure 12-3.

For the first segment ℓ_1 of the wire the distance R can be represented by (12-2a). However, for the second segment ℓ_2 we can express the distance as

$$R = \sqrt{(y - y')^2 + (z - z')^2} \tag{12-10}$$

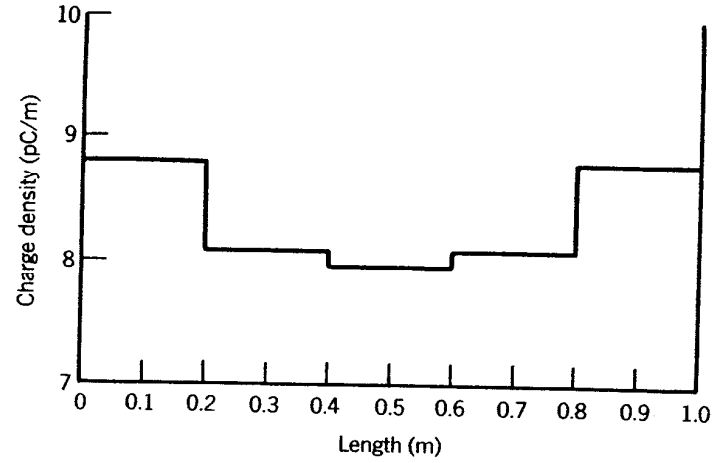

(a)

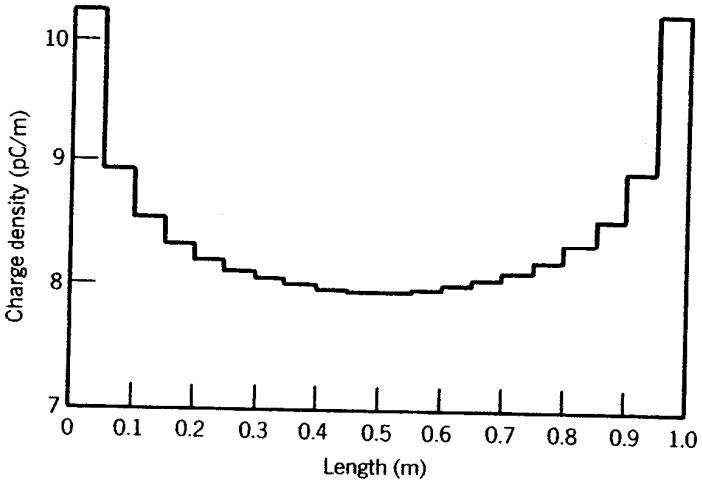

(b)

FIGURE 12-2 Charge distribution on a 1-m straight wire at 1 V. (*a*) $N = 5$. (*b*) $N = 20$.

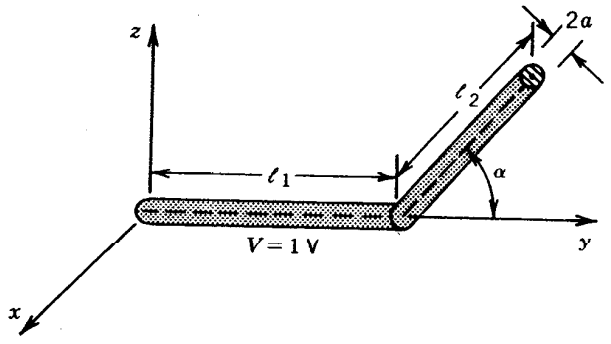

FIGURE 12-3 Geometry for bent wire.

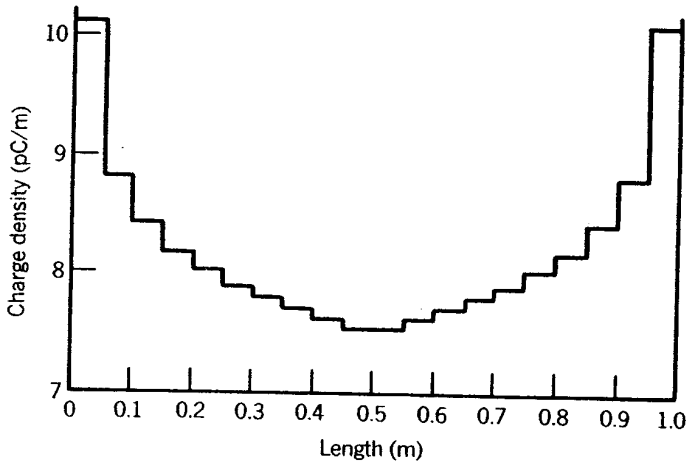

FIGURE 12-4 Charge distribution on a 1-m bent wire ($\alpha = 90°$, $N = 20$).

Also because of the bend, the integral in (12-7a) must be separated into two parts of

$$Z_{mn} = \int_0^{\ell_1} \frac{\rho_n(\ell_1')}{R}\, d\ell_1' + \int_0^{\ell_2} \frac{\rho_n(\ell_2')}{R}\, d\ell_2' \tag{12-11}$$

where ℓ_1 and ℓ_2 are measured along the corresponding straight sections from their left ends.

Example 12-2. Repeat Example 12-1 assuming that the wire has been bent 90° at its midpoint. Subdivide the wire into 20 uniform segments.

Solution. The charge distribution for this case, calculated using (12-10) and (12-11), is plotted in Figure 12-4 for $N = 20$ segments. Note that the charge is relatively more concentrated near the ends of this structure than was the case for a straight wire of Figure 12-2*b*. Further, the overall charge density, and thus capacitance, on the structure has decreased.

Arbitrary wire configurations, including numerous bends and even curved sections, may be analyzed by the methods already outlined here. As with the simple bent wire, the only alterations generally necessary are those required to describe the geometry analytically.

12.2.2 Integral Equation

Now that we have demonstrated the numerical solution of a well known electrostatics integral equation, we will derive and solve a time-harmonic integral equation for an infinite line source above a two-dimensional conducting strip, as shown in Figure 12-5*a*. Once this is accomplished, we will generalize the integral equation formulation for three-dimensional problems in Section 12.3.

Referring to Figure 12-5*a*, the field radiated by a line source of constant current I_z in the absence of the strip (referred to as E_z^d) is given by (11-10a) or

$$E_z^d(\rho) = -\frac{\beta^2 I_z}{4\omega\varepsilon} H_0^{(2)}(\beta\rho) \tag{12-12}$$

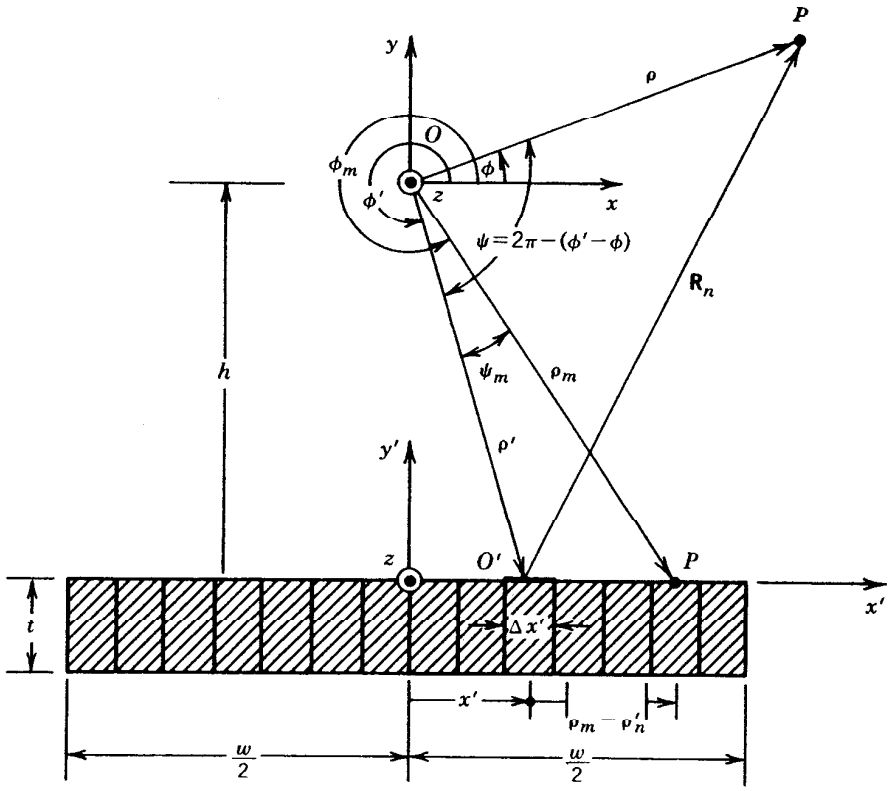

FIGURE 12-5 Geometry of a line source above a two-dimensional finite width strip. (*a*) Boundary conditions and integration on the same surface. (*b*) Boundary conditions and integration not on the same surface.

where $H_0^{(2)}(\beta\rho)$ is the Hankel function of the second kind of order zero. Part of the field given by (12-12) is directed toward the strip, and it induces on it a linear current density J_z (amperes per meter) such that

$$J_z(x')\,\Delta x' = \Delta I_z(x') \tag{12-13}$$

which as $\Delta x' \to 0$ can be written as

$$J_z(x')\,dx' = dI_z(x') \tag{12-13a}$$

The induced current of (12-13a) reradiates and produces an electric field component that will be referred to as *reflected* (or *scattered*) and designated as $E_z^r(\rho)$ [or $E_z^s(\rho)$]. If the strip is subdivided into N segments, each of width $\Delta x_n'$ as shown in Figure 12-5*b*, the scattered field can be written according to (12-12) as

$$E_z^s(\rho) = -\frac{\beta^2}{4\omega\varepsilon}\sum_{n=1}^{N} H_0^{(2)}(\beta R_n)\,\Delta I_z(x_n') = -\frac{\beta^2}{4\omega\varepsilon}\sum_{n=1}^{N} H_0^{(2)}(\beta R_n) J_z(x_n')\,\Delta x_n' \tag{12-14}$$

where x_n' is the position of the nth segment. In the limit, as each segment becomes

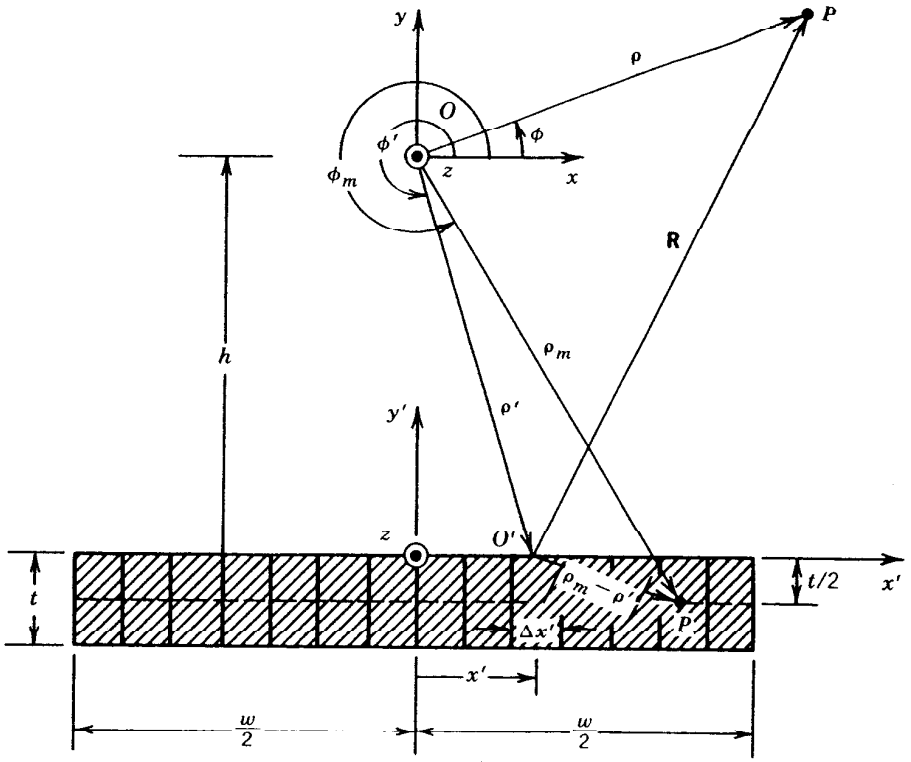

(b)

FIGURE 12-5 (*Continued*).

very small ($\Delta x_n \rightarrow$ small), (12-14) can be written as

$$\boxed{E_z^s(\rho) = -\frac{\beta^2}{4\omega\varepsilon}\int_{\text{strip}} H_0^{(2)}(\beta R)\, dI_z = -\frac{\beta^2}{4\omega\varepsilon}\int_{-w/2}^{w/2} J_z(x') H_0^{(2)}(\beta|\rho - \rho'|)\, dx'} \tag{12-15}$$

since

$$\boxed{R = |\rho - \rho'| = \sqrt{\rho^2 + (\rho')^2 - 2\rho\rho'\cos(\phi - \phi')}} \tag{12-15a}$$

The total field at any observation point, including the strip itself, will be the sum of the direct E_z^d of (12-12) and the scattered E_z^s of (12-15) components. However, to determine the scattered component we need to know the induced current density $J_z(x')$. The objective here then will be to find an equation, which in this case will be in terms of an integral and will be referred as an *integral equation*, that can be used to determine $J_z(x')$. This can be accomplished by choosing the observation point on the strip itself. Doing this, we have that for any observation point $\rho = \rho_m$ on the strip, the total tangential electric field vanishes and it is

given by

$$E_z^t(\rho = \rho_m)\big|_{\text{strip}} = \left[E_z^d(\rho = \rho_m) + E_z^s(\rho = \rho_m)\right]_{\text{strip}} = 0 \tag{12-16}$$

or

$$E_z^s(\rho = \rho_m)\big|_{\text{strip}} = -E_z^d(\rho = \rho_m)\big|_{\text{strip}} \tag{12-16a}$$

Using (12-12) and (12-15), we can write (12-16a) as

$$-\frac{\beta^2 I_z}{4\omega\varepsilon} H_0^{(2)}(\beta\rho_m) = +\frac{\beta^2}{4\omega\varepsilon}\int_{-w/2}^{w/2} J_z(x') H_0^{(2)}(\beta|\rho_m - \rho'|)\, dx' \tag{12-17}$$

which for a unit current I_z (i.e., $I_z = 1$) reduces to

$$\boxed{H_0^{(2)}(\beta\rho_m) = -\int_{-w/2}^{w/2} J_z(x') H_0^{(2)}(\beta|\rho_m - \rho'|)\, dx'} \tag{12-17a}$$

Equation 12-17a is the *electric field integral equation* (EFIE) for the line source above the strip, and it can be used to find the current density $J_z(x')$ based upon a unit current I_z. If I_z is of any other constant value, then all the values of $J_z(x')$ must be multiplied by that same constant value. Electric field integral equations (EFIE) and magnetic field integral equations (MFIE) are discussed in more general forms in Section 12.3.

12.2.3 Radiation Pattern

Once J_z is found, we can then determine the total radiated field of the entire system for any observation point. The total field is composed of two parts: the field radiated from the line source itself (E_z^d) and that which is scattered (reradiated) from the strip (E_z^s). Thus, using (12-12) and (12-15) we can write the total field as

$$\begin{aligned} E_z^t(\rho) &= E_z^d(\rho) + E_z^s(\rho) \\ &= -\frac{\beta^2 I_z}{4\omega\varepsilon} H_0^{(2)}(\beta\rho) - \frac{\beta^2}{4\omega\varepsilon}\int_{-w/2}^{w/2} J_z(x') H_0^{(2)}(\beta|\rho - \rho'|)\, dx' \end{aligned} \tag{12-18}$$

which for a unit amplitude current I_z ($I_z = 1$) reduces to

$$\boxed{E_z^t(\rho) = -\frac{\beta^2}{4\omega\varepsilon}\left[H_0^{(2)}(\beta\rho) + \int_{-w/2}^{w/2} J_z(x') H_0^{(2)}(\beta|\rho - \rho'|)\, dx'\right]} \tag{12-18a}$$

Equation 12-18a can be used to find the total field at any observation point, near or far field. The current density $J_z(x')$ can be found using (12-17a). However, for far-field observations, (12-18a) can be approximated and written in a more simplified form. In general, the distance R is given by (12-15a). However, for

far-field observations ($\rho \gg \rho'$), (12-15a) reduces using the binomial expansion to

$$R \simeq \begin{cases} \rho - \rho' \cos(\phi - \phi') & \text{for phase terms} \quad (12\text{-}19a) \\ \rho & \text{for amplitude terms} \quad (12\text{-}19b) \end{cases}$$

For large arguments, the Hankel functions in (12-18a) can be replaced by their asymptotic form of

$$H_n^{(2)}(\beta z) \overset{\beta z \to \infty}{\simeq} \sqrt{\frac{2j}{\pi \beta z}}\, j^n e^{-j\beta z} \tag{12-20}$$

For $n = 0$, (12-20) reduces to

$$H_0^{(2)}(\beta z) \simeq \sqrt{\frac{2j}{\pi \beta z}}\, e^{-j\beta z} \tag{12-20a}$$

Using (12-19a) through (12-20a), we can write the Hankel functions found in (12-18a) as

$$H_0^{(2)}(\beta \rho) \sim \sqrt{\frac{2j}{\pi \beta \rho}}\, e^{-j\beta \rho} \tag{12-21a}$$

$$H_0^{(2)}(\beta |\rho - \rho'|) \sim \sqrt{\frac{2j}{\pi \beta \rho}}\, e^{-j\beta[\rho - \rho' \cos(\phi - \phi')]}$$

$$\simeq \sqrt{\frac{2j}{\pi \beta \rho}}\, e^{-j\beta \rho + j\beta \rho' \cos(\phi - \phi')} \tag{12-21b}$$

When (12-21a) and (12-21b) are substituted into (12-18a), they reduce it to

$$E_z^t(\rho) \simeq -\frac{\beta^2}{4\omega\varepsilon} \sqrt{\frac{2j}{\pi \beta \rho}}\, e^{-j\beta \rho} \left[1 + \int_{-w/2}^{+w/2} J_z(x')\, e^{j\beta \rho' \cos(\phi - \phi')}\, dx' \right] \tag{12-22}$$

which in normalized form can be written as

$$\boxed{E_z^t \text{ (normalized)} \simeq 1 + \int_{-w/2}^{w/2} J_z(x')\, e^{j\beta \rho' \cos(\phi - \phi')}\, dx'} \tag{12-22a}$$

Equation 12-22a represents the normalized pattern of the line above the strip. It is based on the linear current density $J_z(x')$ that is induced by the source on the strip. The current density can be found using approximate methods or more accurately it can be determined using the integral equation (12-17a).

12.2.4 Point-Matching (Collocation) Method

The next step will be to use a numerical technique to solve the integral equation 12-17a for the unknown current density $J_z(x')$. We first expand $J_z(x')$ into a finite series of the form

$$J_z(x') \simeq \sum_{n=1}^{N} a_n g_n(x') \tag{12-23}$$

where $g_n(x')$ represents *basis* (*expansion*) functions [1, 2]. When (12-23) is substituted into (12-17a), we can write it as

$$H_0^{(2)}(\beta\rho_m) = -\int_{-w/2}^{w/2} \sum_{n=1}^{N} a_n g_n(x') H_0^{(2)}(\beta|\rho_m - \rho_n'|)\, dx'$$

$$H_0^{(2)}(\beta\rho_m) = -\sum_{n=1}^{N} a_n \int_{-w/2}^{w/2} g_n(x') H_0^{(2)}(\beta|\rho_m - \rho_n'|)\, dx' \tag{12-24}$$

which takes the general form

$$\boxed{h = \sum_{n=1}^{N} a_n F(g_n)} \tag{12-25}$$

where

$$h = H_0^{(2)}(\beta\rho_m) \tag{12-25a}$$

$$F(g_n) = -\int_{-w/2}^{w/2} g_n(x') H_0^{(2)}(\beta|\rho_m - \rho_n'|)\, dx' \tag{12-25b}$$

In (12-25) F is referred to as a *linear integral operator*, g_n represents the response function, and h is the known excitation function.

Equation 12-17a is an integral equation derived by enforcing the boundary conditions of vanishing total tangential electric field on the surface of the conducting strip. A numerical solution of (12-17a) is (12-24) or (12-25) through (12-25b) which for a given observation point $\rho = \rho_m$ leads to one equation with N unknowns. This can be repeated N times by choosing N observation points. Such a procedure leads to a system of N linear equations each with N unknowns of the form

$$[H_0^{(2)}(\beta\rho_m)] = \left\{ \sum_{n=1}^{N} a_n \left[-\int_{-w/2}^{w/2} g_n(x') H_0^{(2)}(\beta|\rho_m - \rho_n'|)\, dx' \right] \right\}$$

$$m = 1, 2, \ldots, N \tag{12-26}$$

which can also be written as

$$\boxed{V_m = \sum_{n=1}^{N} I_n Z_{mn}} \tag{12-27}$$

where

$$\boxed{V_m = H_0^{(2)}(\beta\rho_m)} \tag{12-27a}$$

$$\boxed{I_n = a_n} \tag{12-27b}$$

$$\boxed{Z_{mn} = -\int_{-w/2}^{w/2} g_n(x') H_0^{(2)}(\beta|\rho_m - \rho_n'|)\, dx'} \tag{12-27c}$$

In matrix form, (12-27) can be expressed as

$$\boxed{[V_m] = [Z_{mn}][I_n]} \tag{12-28}$$

where the unknown is $[I]_n$ and can be found by solving (12-28), or

$$\boxed{[I_n] = [Z_{mn}]^{-1}[V_n]} \tag{12-28a}$$

Since the system of N linear equations each with N unknowns, as given by (12-26), (12-27), or (12-28), was derived by applying the boundary conditions at N discrete points, the technique is referred to as the *point-matching* (or *collocation*) *method* [1, 2].

Thus by finding the elements of the $[V]$ and $[Z]$, and then the inverse $[Z]^{-1}$, matrices, we can then determine the elements a_n of the $[I]$ matrix. This in turn allows us to approximate $J_z(x')$ using (12-23) which can then be used in (12-18a) to find the total field everywhere. However, for far-field observations, the total field can be found more easily using (12-22) or in normalized form using (12-22a).

12.2.5 Basis Functions

One very important step in any numerical solution is the choice of basis functions. In general, one chooses as basis functions the set that has the ability to accurately represent and resemble the anticipated unknown function, while minimizing the computational effort required to employ it [21–23]. Do not choose basis functions with smoother properties than the unknown being represented.

Theoretically, there are many possible basis sets. However, only a limited number are used in practice. These sets may be divided into two general classes. The first class consists of subdomain functions, which are nonzero only over a part of the domain of the function $g(x')$; its domain is the surface of the structure. The second class contains entire domain functions that exist over the entire domain of the unknown function. The entire domain basis function expansion is analogous to the well known Fourier series expansion method.

A. SUBDOMAIN FUNCTIONS

Of the two types of basis functions, subdomain functions are the most common. Unlike entire domain bases, they may be used without prior knowledge of the nature of the function that they must represent.

The subdomain approach involves subdivision of the structure into N nonoverlapping segments, as illustrated on the axis in Figure 12-6*a*. For clarity, the segments are shown here to be collinear and of equal length, although neither condition is necessary. The basis functions are defined in conjunction with the limits of one or more of the segments.

Perhaps the most common of these basis functions is the conceptually simple piecewise constant, or "pulse" function, shown in Figure 12-6*a*. It is defined by

Piecewise Constant

$$g_n(x') = \begin{cases} 1 & x'_{n-1} \le x' \le x'_n \\ 0 & \text{elsewhere} \end{cases} \tag{12-29}$$

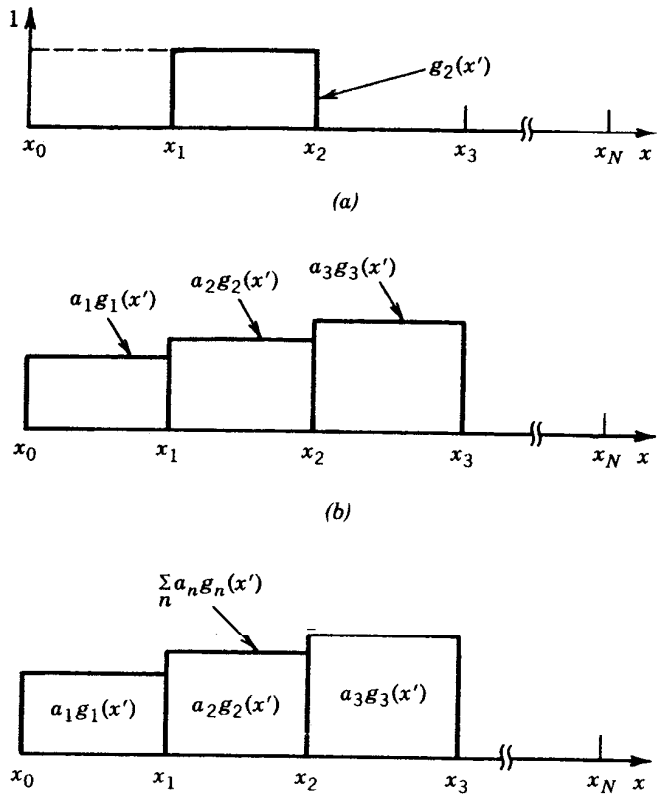

FIGURE 12-6 Piecewise constant subdomain functions. (*a*) Single. (*b*) Multiple. (*c*) Function representation.

Once the associated coefficients are determined, this function will produce a staircase representation of the unknown function, similar to that in Figure 12-6*b* and *c*.

Another common basis set is the piecewise linear, or "triangle," functions seen in Figure 12-7*a*. These are defined by

$$\underline{\text{Piecewise Linear}}$$

$$g_n(x') = \begin{cases} \dfrac{x' - x'_{n-1}}{x'_n - x'_{n-1}} & x'_{n-1} \le x' \le x'_n \\ \dfrac{x'_{n+1} - x'}{x'_{n+1} - x'_n} & x'_n \le x' \le x'_{n+1} \\ 0 & \text{elsewhere} \end{cases} \tag{12-30}$$

and are seen to cover two segments, and overlap adjacent functions (Figure 12-7*b*). The resulting representation (Figure 12-7*c*) is smoother than that for "pulses," but at the cost of increased computational complexity.

Increasing the sophistication of subdomain basis functions beyond the level of the "triangle" may not be warranted by the possible improvement in representation accuracy. However, there are cases where more specialized functions are useful for other reasons. For example, some integral operators may be evaluated without numerical integration when their integrands are multiplied by a $\sin(kx')$ or $\cos(kx')$ function, where x' is the variable of integration. In such examples, considerable

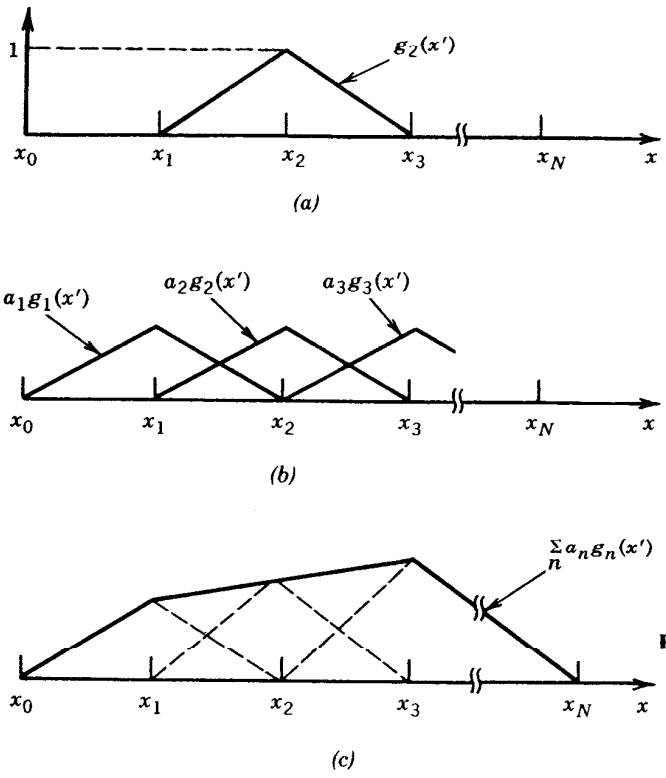

FIGURE 12-7 Piecewise linear subdomain functions. (*a*) Single. (*b*) Multiple. (*c*) Function representation.

advantages in computation time and resistance to errors can be gained by using basis functions like the piecewise sinusoid of Figure 12-8 or truncated cosine of Figure 12-9. These functions are defined by

Piecewise Sinusoid

$$g_n(x') = \begin{cases} \dfrac{\sin\left[\beta(x' - x'_{n-1})\right]}{\sin\left[\beta(x'_n - x'_{n-1})\right]} & x'_{n-1} \le x' \le x'_n \\ \dfrac{\sin\left[\beta(x'_{n+1} - x')\right]}{\sin\left[\beta(x'_{n+1} - x'_n)\right]} & x'_n \le x' \le x'_{n+1} \\ 0 & \text{elsewhere} \end{cases} \tag{12-31}$$

Truncated Cosine

$$g_n(x') = \begin{cases} \cos\left[\beta\left(x' - \dfrac{x'_n - x'_{n-1}}{2}\right)\right] & x'_{n-1} \le x' \le x'_n \\ 0 & \text{elsewhere} \end{cases} \tag{12-32}$$

B. ENTIRE-DOMAIN FUNCTIONS

Entire domain basis functions, as their name implies, are defined and are nonzero over the entire length of the structure being considered. Thus no segmentation is involved in their use.

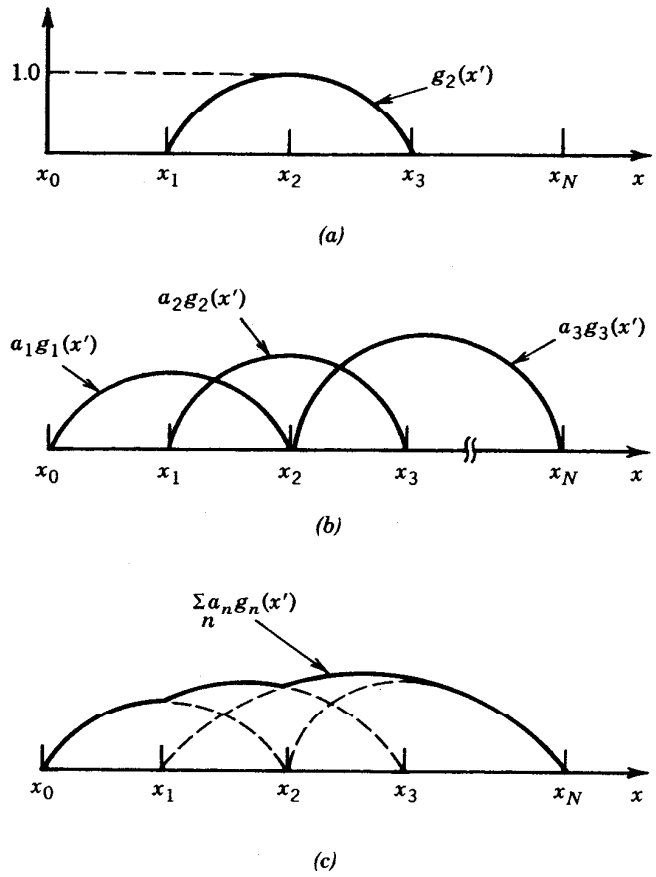

FIGURE 12-8 Piecewise sinusoids subdomain functions. (*a*) Single. (*b*) Multiple. (*c*) Function representation.

A common entire domain basis set is that of sinusoidal functions, where

$$\underline{\text{Entire Domain}}$$

$$g_n(x') = \cos\left[\frac{(2n-1)\pi x'}{\ell}\right] \qquad -\frac{\ell}{2} \le x' \le \frac{\ell}{2} \tag{12-33}$$

Note that this basis set would be particularly useful for modeling the current distribution on a wire dipole, which is known to have primarily sinusoidal distribution. The main advantage of entire domain basis functions lies in problems where the unknown function is assumed a priori to follow a known pattern. Such entire-domain functions may render an acceptable representation of the unknown while using far fewer terms in the expansion of (12-23) than would be necessary for subdomain bases. Representation of a function by entire domain cosine and/or sine functions is similar to the Fourier series expansion of arbitrary functions.

Because we are constrained to use a finite number of functions (or modes, as they are sometimes called), entire domain basis functions usually have difficulty in modeling arbitrary or complicated unknown functions.

Entire domain basis functions, sets like (12-33), can be generated using Tschebyscheff, Maclaurin, Legendre, and Hermite polynomials, or other convenient functions.

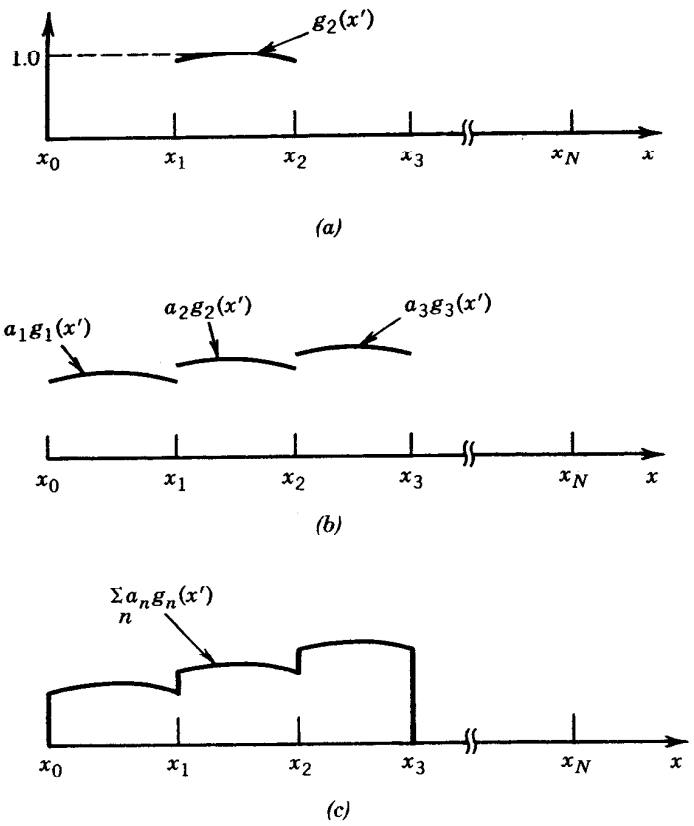

FIGURE 12-9 Truncated cosines subdomain functions. (*a*) Single. (*b*) Multiple. (*c*) Function representation.

12.2.6 Application of Point Matching

If each of the expansion functions $g_n(x')$ in (12-23) is of the subdomain type where each exists only over one segment of the structure, then Z_{mn} of (12-27c) reduces to

$$Z_{mn} = -\int_{x_n}^{x_{n+1}} g_n(x') H_0^{(2)}(\beta|\rho_m - \rho_n'|)\, dx' \tag{12-34}$$

where x_n and x_{n+1} represent, respectively, the lower and upper limits of the segment over which each of the subdomain expansion functions $g_n(x')$ exists. If, in addition, the g_n are subdomain pulse expansion functions of the form

$$g_n(x') = \begin{cases} 1 & x_n \le x' \le x_{n+1} \\ 0 & \text{elsewhere} \end{cases} \tag{12-35}$$

then (12-34) reduces to

$$Z_{mn} = -\int_{x_n}^{x_{n+1}} H_0^{(2)}(\beta|\rho_m - \rho_n'|)\, dx' \tag{12-36}$$

The preceding integral cannot be evaluated exactly in closed form. However, there exist various approximations for its evaluation.

In solving (12-17a) using (12-24) or (12-26), there are few problems that must be addressed. Before we do that, let us first state in words what (12-24) and (12-26) represent. Each equation is a solution to (12-17a), which was derived by enforcing the boundary conditions. These conditions required the total tangential electric field to vanish on the surface of the conductor. For each observation point, the total field consists of the sum of the direct (E_z^d) and scattered (E_z^s) components. Thus, to find the total scattered field at *each observation point* we must add the contributions of the scattered field components *from all* the segments of the strip, which also includes those coming from the segment where the observations are made (referred to as *self-terms*). When the contributions from the segment over which the observation point lies are considered, then the distance $R_{mn} = R_{mm} = |\rho_m - \rho_n'|$ used for evaluating the self-term Z_{mm} in (12-27c) will become zero. This introduces a singularity in the integrand of (12-36) because the Hankel function defined as

$$H_0^{(2)}(\beta\rho) = J_0(\beta\rho) - jY_0(\beta\rho) \tag{12-37}$$

is infinite because $Y_0(0) = \infty$.

For finite thickness strips, the easiest way to get around the problem of evaluating the Hankel function for the self-terms will be to choose observation points away from the surface of the strip over which the integration in (12-36) is performed. For example, the observation points can be selected at the center of each segment along a line that divides the thickness of the strip, while the integration is performed along the upper surface of the strip. These points are designated in Figure 12-5*b* by the distance ρ_m.

Even if the aforementioned procedure is implemented for the evaluation of all the terms of Z_{mn}, including the self-terms, the distance $R_{mn} = |\rho_m - \rho_n'|$ for the self-terms (and some from the neighboring elements) will still sometime be sufficiently small that standard algorithms for computing Bessel functions, and thus Hankel functions, may not be very accurate. For these instances the Hankel functions can be evaluated using asymptotic expressions for small arguments. That is, for cases where the argument of the Hankel functions in (12-36) is small, which may include the self-terms and some of the neighboring elements, the Hankel function can be computed using [24]

$$H_0^{(2)}(\beta\rho) = J_0(\beta\rho) - jY_0(\beta\rho) \overset{\beta\rho \to 0}{\simeq} 1 - j\frac{2}{\pi}\ln\left(\frac{1.781\beta\rho}{2}\right) \tag{12-38}$$

The integral of (12-36) can be evaluated approximately in closed form, even if the observation and source points are chosen to be along the same line. This can be done not only for diagonal (self, $m = n$) but also for the nondiagonal ($m \neq n$) terms. For the diagonal terms ($m = n$) the Hankel function of (12-36) has an integrable singularity, and the integral can be evaluated analytically in closed form using the small argument approximation of (12-38) for the Hankel function. When (12-38) is used, it can be shown that (12-36) reduces to [2]

Diagonal Terms Approximation

$$Z_{nn} \simeq -\Delta x_n\left[1 - j\frac{2}{\pi}\ln\left(\frac{1.781\beta\Delta x_n}{4e}\right)\right] \qquad m = n \tag{12-39}$$

where

$$\Delta x_n = x_{n+1} - x_n \tag{12-39a}$$

$$e = 2.718 \tag{12-39b}$$

For evaluation of the nondiagonal terms of (12-36) the crudest approximation would be to consider the Hankel function over each segment to be essentially constant [2]. To minimize the error using such an approximation, it is recommended that the argument of the Hankel function in (12-36) be represented by its average value over each segment. For straight line segments that average value will be representative of the distance from the center of the segment to the observation point. Thus for the nondiagonal terms, (12-36) can be approximated by

Nondiagonal Terms Approximation

$$Z_{mn} \simeq -\Delta x_n H_0^{(2)}(\beta|R_{mn}|_{av}) = -\Delta x_n H_0^{(2)}(\beta|\rho_m - \rho_n'|_{av}) \qquad m \neq n \quad (12\text{-}40)$$

The average value approximation for the distance R_{mn} in the Hankel function evaluation of (12-36) can also be used for curved surface scattering whereby each segment has been basically approximated by a straight line segment. Crude as it may seem, the average value approximation for the distance yields good results.

12.2.7 Weighting (Testing) Functions

Expansion of (12-24) leads to one equation with N unknowns. It alone is not sufficient to determine the N unknown a_n $(n = 1, 2, \ldots, N)$ constants. To resolve the N constants, it is necessary to have N linearly independent equations. This can be accomplished by evaluating (12-24) (e.g., applying boundary conditions) at N different points, as represented by (12-26). To improve the point-matching solution, however, an inner product $\langle w, g \rangle$ can be defined which is a scalar operation satisfying the laws of

$$\langle w, g \rangle = \langle g, w \rangle \qquad (12\text{-}41a)$$
$$\langle bf + cg, w \rangle = b\langle f, w \rangle + c\langle g, w \rangle \qquad (12\text{-}41b)$$
$$\langle g^*, g \rangle > 0 \quad \text{if } g \neq 0 \qquad (12\text{-}41c)$$
$$\langle g^*, g \rangle = 0 \quad \text{if } g = 0 \qquad (12\text{-}41d)$$

where b and c are scalars and the asterisk (*) indicates complex conjugation. A typical, but not unique, inner product is

$$\langle \mathbf{w}, \mathbf{g} \rangle = \iint_S \mathbf{w}^* \cdot \mathbf{g}\, ds \qquad (12\text{-}42)$$

where the w's are the *weighting* (*testing*) functions and S is the surface of the structure being analyzed. Note that the functions w and g can be vectors. This technique is better known as the *moment method* or *method of moments* (MM) [1, 2].

12.2.8 Moment Method

The collocation (point-matching) method is a numerical technique whose solutions satisfy the electromagnetic boundary conditions (e.g., vanishing tangential electric fields on the surface of an electric conductor) only at discrete points. Between these points the boundary conditions may not be satisfied, and we define the deviation as

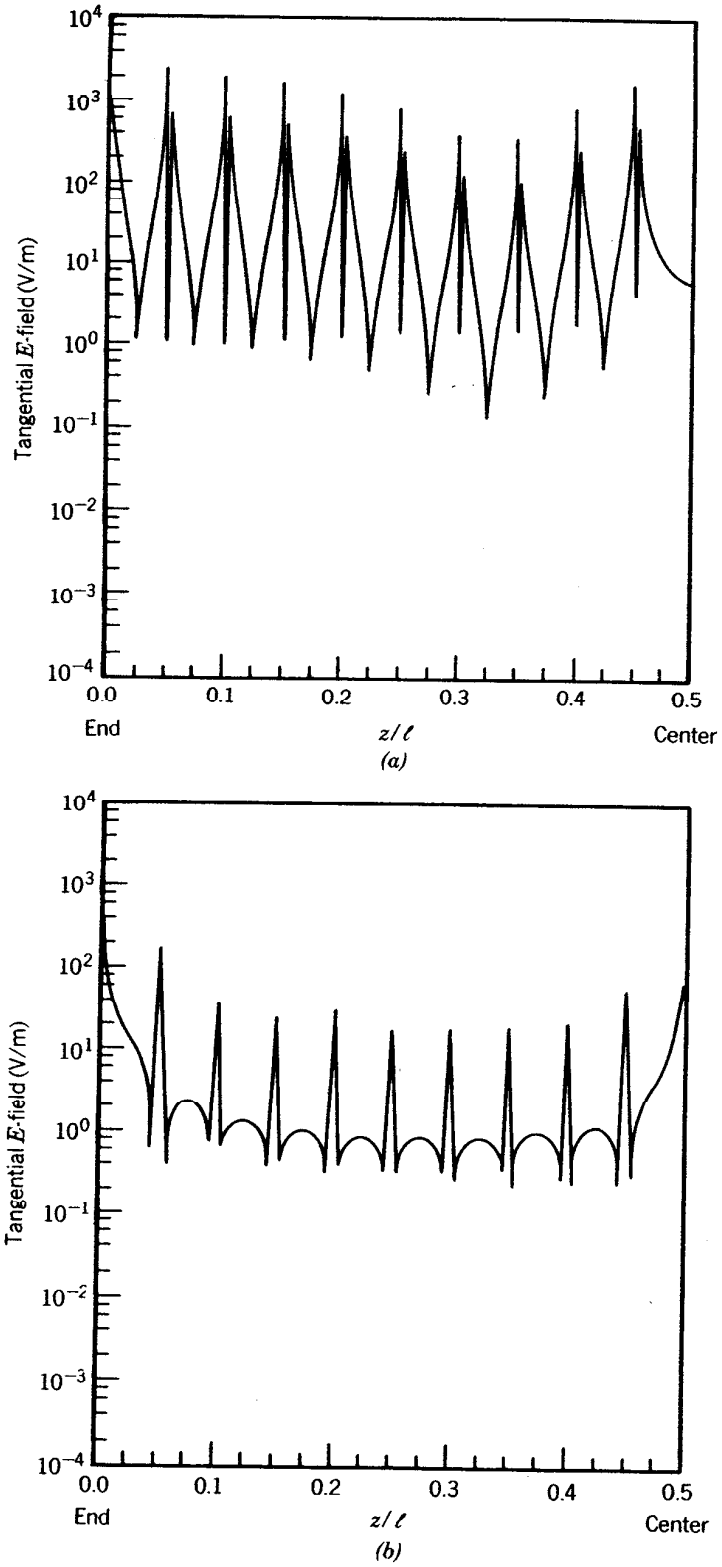

FIGURE 12-10 Tangential electric field on the conducting surface of the $\lambda/2$ dipole. (*Source:* E. K. Miller and F. J. Deadrick, "Some computational aspects of thin-wire modeling" in *Numerical and Asymptotic Techniques in Electromagnetics*, 1975, Springer-Verlag.) (*a*) Pulse basis—point matching. (*b*) Piecewise sinusoids—Galerkin's method.

a *residual* [e.g., residual $= \Delta E|_{\tan} = E(\text{scattered})|_{\tan} + E(\text{incident})|_{\tan} \neq 0$ on the surface of an electric conductor]. For a half-wavelength dipole, a typical residual is shown in Figure 12-10*a* for pulse basis functions and point matching and Figure 12-10*b* exhibits the residual for piecewise sinusoids–Galerkin method [25]. As expected, the pulse basis point matching exhibits the most ill-behaved residual and the piecewise sinusoids–Galerkin method indicates an improved residual. To minimize the residual in such a way that its overall average over the entire structure approaches zero, the method of *weighted residuals* is utilized in conjunction with the inner product of (12-42). This technique, referred as *moment method* (MM), does not lead to a vanishing residual at every point on the surface of a conductor, but it forces the boundary conditions to be satisfied in an average sense over the entire surface.

To accomplish this, we define a set of N *weighting* (or testing) functions $\{w_m\} = w_1, w_2, \ldots, w_N$ in the domain of the operator F. Forming the inner product between each of these functions, (12-25) results in

$$\boxed{\langle w_m, h\rangle = \sum_{n=1}^{N} a_n \langle w_m, F(g_n)\rangle \qquad m = 1, 2, \ldots, N} \tag{12-43}$$

This set of N equations may be written in matrix form as

$$\boxed{[h_m] = [F_{mn}][a_n]} \tag{12-44}$$

where

$$\boxed{[F_{mn}] = \begin{bmatrix} \langle w_1, F(g_1)\rangle & \langle w_1, F(g_2)\rangle & \cdots \\ \langle w_2, F(g_1)\rangle & \langle w_2, F(g_2)\rangle & \\ \vdots & & \vdots \end{bmatrix}} \tag{12-44a}$$

$$\boxed{[a_n] = \begin{bmatrix} a_1 \\ a_2 \\ \vdots \\ a_N \end{bmatrix} \qquad h_m = \begin{bmatrix} \langle w_1, h\rangle \\ \langle w_2, h\rangle \\ \vdots \\ \langle w_N, h\rangle \end{bmatrix}} \tag{12-44b}$$

The matrix of (12-44) may be solved for the a_n by inversion, and it can be written as

$$\boxed{[a_n] = [F_{mn}]^{-1}[h_m]} \tag{12-45}$$

The choice of weighting functions is important in that the elements of $\{w_n\}$ must be linearly independent, so that the N equations in (12-43) will be linearly

independent [1–3, 22, 23]. Further, it will generally be advantageous to choose weighting functions that minimize the computations required to evaluate the inner product.

The condition of linear independence between elements and the advantage of computational simplicity are also important characteristics of basis functions. Because of this, similar types of functions are often used for both weighting and expansion. A particular choice of functions may be to let the weighting and basis function be the same, that is, $w_n = g_n$. This technique is known as *Galerkin's method* [26].

It should be noted that there are N^2 terms to be evaluated in (12-44a). Each term usually requires two or more integrations; at least one to evaluate each $F(g_n)$, and one to perform the inner product of (12-42). When these integrations are to be done numerically, as is often the case, vast amounts of computation time may be necessary.

There is, however, a unique set of weighting functions that reduce the number of required integrations. This is the set of Dirac delta weighting functions

$$\boxed{[w_m] = [\delta(p - p_m)] = [\delta(p - p_1), \delta(p - p_2), \ldots]} \tag{12-46}$$

where p specifies a position with respect to some reference (origin), and p_m represents a point at which the boundary condition is enforced. Using (12-42) and (12-46) reduces (12-43) to

$$\langle \delta(p - p_m), h \rangle = \sum_n a_n \langle \delta(p - p_m), F(g_n) \rangle \qquad m = 1, 2, \ldots, N$$

$$\iint_S \delta(p - p_m) h \, ds = \sum_n a_n \iint_S \delta(p - p_m) F(g_n) \, ds \qquad m = 1, 2, \ldots, N$$

$$\boxed{h|_{p=p_m} = \sum a_n F(g_n)|_{p=p_m} \qquad m = 1, 2, \ldots, N} \tag{12-47}$$

Hence, the only remaining integrations are those specified by $F(g_n)$. This simplification may make possible some solutions that would be impractical if other weighting functions were used. Physically, the use of Dirac delta weighting functions is seen as the relaxation of boundary conditions so that they are enforced only at discrete points on the surface of the structure, hence the name point matching.

An important consideration when using point matching is the positioning of the N points (p_m). While equally spaced points often yield good results, much depends on the basis functions used. When using subsectional basis functions in conjunction with point matching, one match point should be placed on each segment (to maintain linear independence). Placing the points at the center of the segments usually produces the best results. It is important that a match point does not coincide with the "peak" of a triangle or a similar discontinuous function, where the basis function is not differentiably continuous. This may cause errors in some situations.

Because it provides acceptable accuracy along with obvious computational advantages, point matching is easily the most popular testing technique for moment method solutions to electromagnetics problems. The analysis presented here, along with most problems considered in the literature, proceed via point matching.

For the strip problem, a convenient inner product of (12-42) would be

$$\langle w_m, g_n \rangle = \int_{-w/2}^{w/2} w_m^*(x) g_n(x)\, dx \tag{12-48}$$

Applying the inner product of (12-48) on both sides of (12-26), we can write it as

$$V'_m = \sum_{n=1}^{N} I_n Z'_{mn} \qquad m = 1, 2, \ldots, N \tag{12-49}$$

where

$$V'_m = \int_{-w/2}^{w/2} w_m^*(x) H_0^{(2)}(\beta \rho_m)\, dx \tag{12-49a}$$

$$Z'_{mn} = -\int_{-w/2}^{w/2} w_m^*(x) \left[\int_{-w/2}^{w/2} g_n(x') H_0^{(2)}(\beta |\rho_m - \rho'_n|)\, dx' \right] dx \tag{12-49b}$$

or in matrix form as

$$[V']_m = [Z']_{mn} [I]_n \tag{12-50}$$

If the w_m weighting functions are Dirac delta functions [i.e., $w_m(y) = \delta(y - y_m)$], then (12-49) reduces to (12-27) or

$$V'_m = V_m \tag{12-51a}$$

and

$$Z'_{mn} = Z_{mn} \tag{12-51b}$$

The *method of weighted residuals* (moment method) was introduced to minimize the average deviation, from the actual values, of the boundary conditions over the entire structure. However, it is evident that it has complicated the formulation by requiring an integration in the evaluation of the elements of the V' matrix [as given by (12-49a)] and an additional integration in the evaluation of the elements of the Z'_{mn} matrix [as given by (12-49b)]. Therein lies the penalty that is paid to improve the solution.

If both the expansion g_n and the weighting w_m functions are of the subdomain type, each of which exists only over one of the strip segments, then (12-49b) can be written as

$$Z'_{mn} = -\int_{x_m}^{x_{m+1}} w_m^*(x) \left[\int_{x'_n}^{x'_{n+1}} g_n(x') H_0^{(2)}(\beta |\rho_m - \rho'|)\, dx' \right] dx \tag{12-52}$$

where (x_m, x_{m+1}) and (x'_n, x'_{n+1}) represent, respectively, the lower and upper limits

of the strip segments over which the weighting w_m and expansion g_n functions exist. To evaluate the mnth element of Z'_{mn} from (12-49b) or (12-52), we first choose the weighting function w_m, and the region of the segment over which it exists, and weigh the contributions from the g_n expansion function over the region in which it exists. To find the next element $Z'_{m(n+1)}$, we maintain the same weighting function w_m, and the region over which it exists, and weigh the contributions from the g_{n+1} expansion function. We repeat this until the individual contributions from all the N expansion functions (g_n) are weighted by the w_m weighting function. Then we choose the w_{m+1} weighting function, and the region over which it exists, and we weigh individually the contributions from each of the N expansion functions (g_n). We repeat this until all the N weighting functions (w_m), and the regions of the strip over which they exist, are individually weighted by the N expansion functions (g_n). This procedure allows us to form N linear equations, each with N unknowns, that can be solved using matrix inversion methods.

Example 12-3. For the electric line source of Figure 12-5 with $w = 2\lambda$, $t = 0.01\lambda$, and $h = 0.5\lambda$ perform the following.

1. Compute the equivalent current density induced on the open surface of the strip. This equivalent current density is representative of the vector sum of the current densities that flow on the opposite sides of the strip. Use subdomain pulse expansion functions and point matching. Subdivide the strip into 150 segments.
2. Compare the current density of part 1 with the physical optics current density.
3. Compute the normalized far-field amplitude pattern of (12-22a) using the current densities of parts 1 and 2. Compare these patterns with those obtained using a combination of geometrical optics (GO) and geometrical theory of diffraction (GTD) techniques of Chapter 13 and physical optics (PO) and physical theory of diffraction (PTD) techniques of [13].

Solution.

1. Utilizing (12-27) through (12-27b) and (12-36) the current density of (12-23) is computed using (12-28a). It is plotted in Figure 12-11. It is observed that the current density exhibits singularities toward the edges of the strip.
2. The physical optics current density is found using

$$\mathbf{J}_s^{\text{PO}} \simeq 2\hat{n} \times \mathbf{H}^i$$

which reduces using (11-10b) to

$$\mathbf{J}_s^{\text{PO}} \simeq 2\hat{a}_y \times \hat{a}_\phi H_\phi^i|_{\text{strip}} = 2\hat{a}_y \times \left(-\hat{a}_x \sin\phi + \hat{a}_y \cos\phi\right) H_\phi^i\Big|_{\text{strip}}$$

$$= \hat{a}_z 2 \sin\phi H_\phi^i\Big|_{\text{strip}} \simeq -j\hat{a}_z I_z \frac{\beta}{2} \sin\phi_m H_1^{(2)}(\beta\rho_m)$$

$$\mathbf{J}_s^{\text{PO}} = -j\hat{a}_z I_z \frac{\beta}{2}\left(\frac{y_m}{\rho_m}\right) H_1^{(2)}(\beta\rho_m)$$

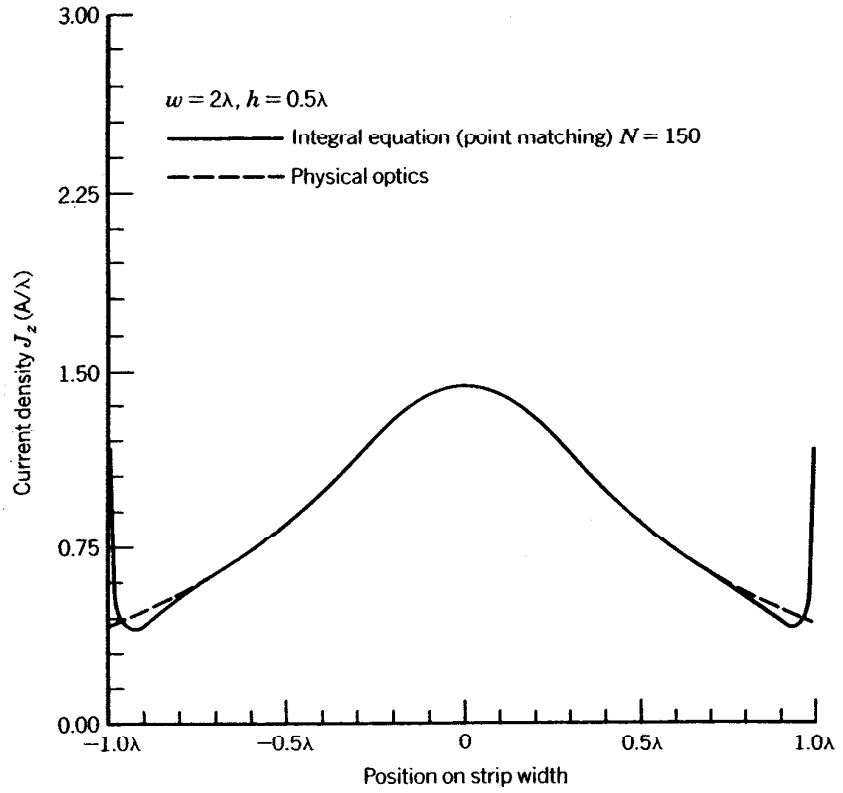

FIGURE 12-11 Current density on a finite width strip that is due to the electric line source above the strip.

The normalized value of this has also been plotted in Figure 12-11 so that it can be compared with the more accurate one obtained in part 1 using the integral equation.

3. The far-field amplitude patterns, based on the current densities of parts 1 and 2, are plotted in Figure 12-12. In addition to the normalized radiation patterns obtained using the current densities of parts 1 and 2, the pattern obtained using geometrical optics (GO) plus first-order diffractions by the geometrical theory of diffraction (GTD), to be discussed in Chapter 13, is also displayed in Figure 12-12. An excellent agreement is indicated between the IE and the GO plus GTD patterns. The pattern obtained using physical optics supplemented by first-order diffractions of the physical theory of diffraction (PTD) [13] is also displayed in Figure 12-12 for comparison purposes. It also compares extremely well with the others. As expected, the only one that does not compare well with the others is that of PO. Its largest differences are in the back lobes.

12.3 ELECTRIC AND MAGNETIC FIELD INTEGRAL EQUATIONS

The key to the solution of any antenna or scattering problem is a knowledge of the physical or equivalent current density distributions on the volume or surface of the antenna or scatterer. Once these are known then the radiated or scattered fields

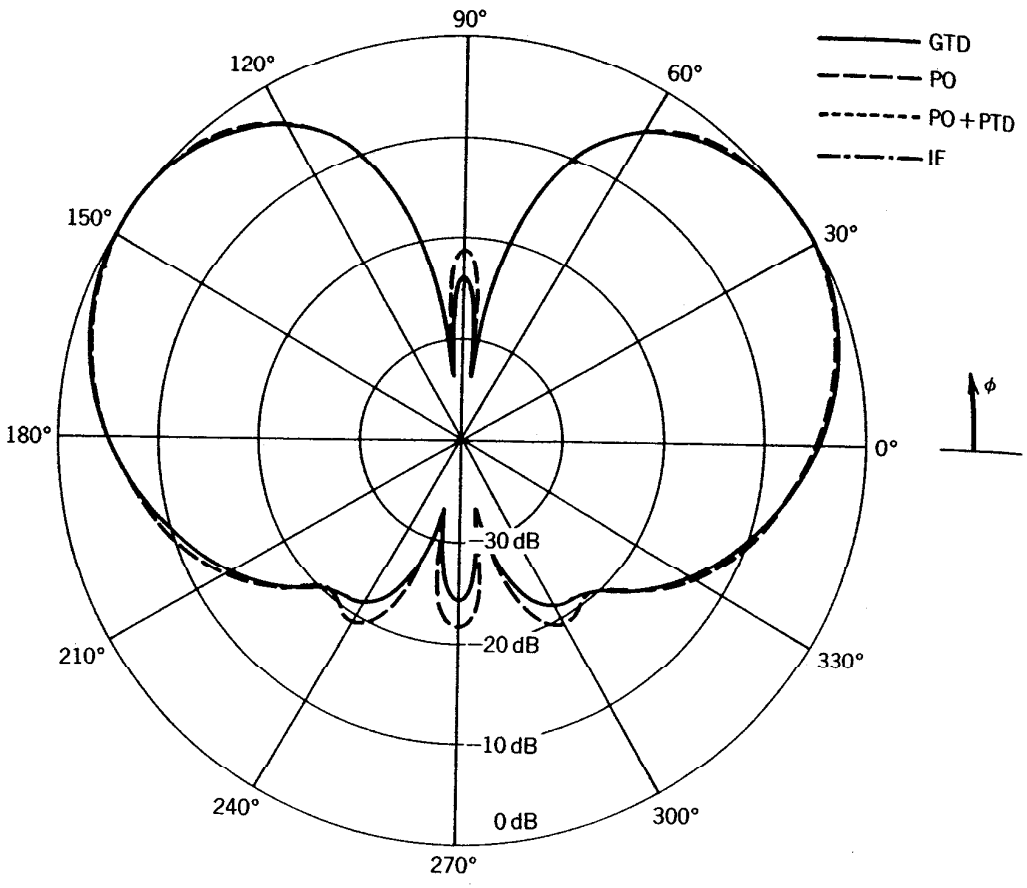

FIGURE 12-12 Normalized amplitude pattern of the line source above the finite width strip ($w = 2\lambda$, $h = 0.5\lambda$).

can be found using the standard radiation integrals. A main objective then of any solution method is to be able to predict accurately the current densities over the antenna or scatterer. This can be accomplished by the integral equation (IE) method. One form of IE, for a two-dimensional structure, was discussed in Section 12.2.2 and represented by the integral equation 12-17a.

In general there are many forms of integral equations. Two of the most popular for time-harmonic electromagnetics are the *electric field integral equation* (EFIE) and the *magnetic field integral equation* (MFIE). The EFIE enforces the boundary condition on the tangential electric field and the MFIE enforces the boundary condition on the tangential components of the magnetic field. Both of these will be discussed here as they applied to perfectly conducting structures.

12.3.1 Electric Field Integral Equation

The electric field integral equation (EFIE) is based on the boundary condition that the total tangential electric field on a perfectly electric conducting (PEC) surface of an antenna or scatterer is zero. This can be expressed as

$$\mathbf{E}_t(r = r_s) = \mathbf{E}_t^i(r = r_s) + \mathbf{E}_t^s(r = r_s) = 0 \quad \text{on } S \tag{12-53}$$

or

$$\mathbf{E}_t^s(r = r_s) = -\mathbf{E}_t^i(r = r_s) \quad \text{on } S \tag{12-53a}$$

where S is the conducting surface of the antenna or scatterer and $r = r_s$ is the distance from the origin to any point on the surface of the antenna or scatterer. The subscript t indicates tangential components.

The incident field that impinges on the surface S of the antenna or scatterer induces on it an electric current density $\mathbf{J}_s$ which in turn radiates the scattered field. If $\mathbf{J}_s$ is known, the scattered field everywhere that is due to $\mathbf{J}_s$ can be found using (6-32b), or

$$\mathbf{E}^s(r) = -j\omega\mathbf{A} - j\frac{1}{\omega\mu\varepsilon}\nabla(\nabla \cdot \mathbf{A}) = -j\frac{1}{\omega\mu\varepsilon}\left[\omega^2\mu\varepsilon\mathbf{A} + \nabla(\nabla \cdot \mathbf{A})\right] \quad (12\text{-}54)$$

where according to (6-96a)

$$\mathbf{A}(r) = \frac{\mu}{4\pi}\iint_S \mathbf{J}_s(r')\frac{e^{-j\beta R}}{R}\,ds' = \mu\iint_S \mathbf{J}_s(r')\frac{e^{-j\beta R}}{4\pi R}\,ds' \quad (12\text{-}54a)$$

Equations 12-54 and 12-54a can also be expressed by referring to Figure 6-2*b* as

$$\mathbf{E}^s(r) = -j\frac{\eta}{\beta}\left[\beta^2\iint_S \mathbf{J}_s(r')G(\mathbf{r},\mathbf{r}')\,ds' + \nabla\iint_S \nabla' \cdot \mathbf{J}_s(r')G(\mathbf{r},\mathbf{r}')\,ds'\right] \quad (12\text{-}55)$$

where

$$G(\mathbf{r},\mathbf{r}') = \frac{e^{-j\beta R}}{4\pi R} = \frac{e^{-j\beta|\mathbf{r}-\mathbf{r}'|}}{4\pi|\mathbf{r}-\mathbf{r}'|} \quad (12\text{-}55a)$$

$$R = |\mathbf{r} - \mathbf{r}'| \quad (12\text{-}55b)$$

In (12-55) ∇ and ∇' are, respectively, the gradients with respect to the observation (unprimed) and source (primed) coordinates and $G(\mathbf{r},\mathbf{r}')$ is referred to as the Green's function for a three-dimensional radiator or scatterer.

If the observations are restricted on the surface of the antenna or scatterer ($r = r_s$), then (12-55) through (12-55b) can be expressed using (12-53a) as

$$\boxed{j\frac{\eta}{\beta}\left[\beta^2\iint_S \mathbf{J}_s(r')G(\mathbf{r}_s,\mathbf{r}')\,ds' + \nabla\iint_S \nabla' \cdot \mathbf{J}_s(r')G(\mathbf{r}_s,\mathbf{r}')\,ds'\right]_t = \mathbf{E}_t^i(r = r_s)} \quad (12\text{-}56)$$

Because the right side of (12-56) is expressed in terms of the known incident electric field, it is referred to as the *electric field integral equation* (EFIE). It can be used to find the current density $\mathbf{J}_s(r')$ at any point $r = r'$ on the antenna or scatterer. It should be noted that (12-56) is actually an integrodifferential equation, but usually it is referred to as an integral equation.

Equation 12-56 can be used for closed or open surfaces. The scattered field is found, once $\mathbf{J}_s$ is determined, by using (6-32b) and (6-96a) or (12-54) and (12-54a) which assume that $\mathbf{J}_s$ radiates in one medium. Because of this $\mathbf{J}_s$ in (12-56) represents the physical equivalent electric current density of (7-53a) in Section 7.10. For open surfaces $\mathbf{J}_s$ is also the physical equivalent current density that represents the vector sum of the equivalent current densities on the opposite sides of the surface. Whenever this equivalent current density represents open surfaces, then a

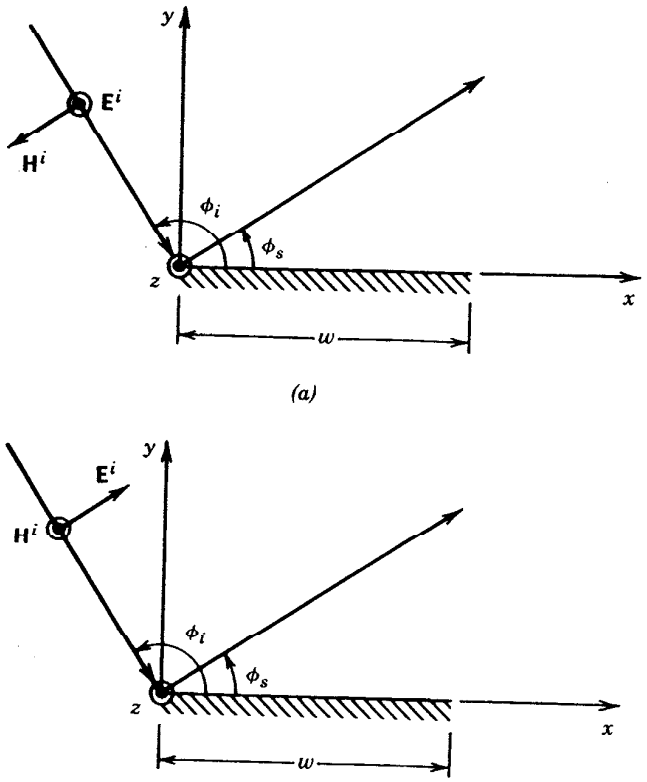

FIGURE 12-13 Uniform plane wave incident on a conducting strip of finite width. (*a*) TM^z polarization. (*b*) TE^z polarization.

boundary condition supplemental to (12-56) must be enforced to yield a unique solution for the normal component of the current density to vanish on S.

Equation 12-56 is a general surface EFIE for three-dimensional problems and its form can be simplified for two-dimensional geometries. To demonstrate this, let us derive the two-dimensional EFIEs for both TM^z and TE^z polarizations.

A. TWO-DIMENSIONAL EFIE: TM^z POLARIZATION

The best way to demonstrate the derivation of the two-dimensional EFIE for TM^z polarization is to consider a specific example. Its form can then be generalized to more complex geometries. The example to be examined here is that of a TM^z uniform plane wave incidence on a finite width strip, as shown in Figure 12-13*a*.

By referring to Figure 12-13*a* the incident electric field can be expressed as

$$\mathbf{E}^i = \hat{a}_z E_0 e^{-j\boldsymbol{\beta}^i \cdot \mathbf{r}} = \hat{a}_z E_0 e^{j\beta(x\cos\phi_i + y\sin\phi_i)} \tag{12-57}$$

which at the surface of the strip ($y = 0,\ 0 \le x \le w$) reduces to

$$\mathbf{E}^i(y = 0, 0 \le x \le w) = \hat{a}_z E_0 e^{j\beta x\cos\phi_i} \tag{12-57a}$$

Since the incident electric field has only a z component, the scattered and total fields each also has only a z component which is independent of z variations (two dimensional). Therefore the scattered field can be found by expanding (12-54) assuming $\mathbf{A}$ has only a z component which is independent of z variations. Doing

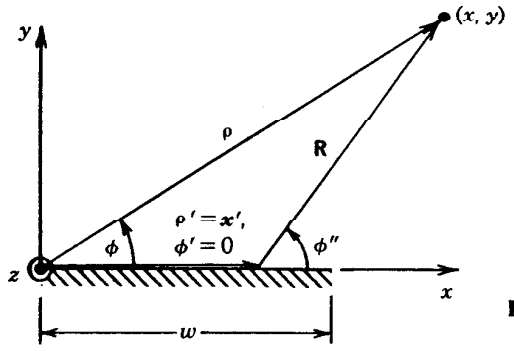

FIGURE 12-14 Geometry of the finite width strip for scattering.

this reduces (12-54) to

$$\mathbf{E}^s = -\hat{a}_z j\omega A_z \tag{12-58}$$

The vector potential component A_z is obtained using (12-54a) which in conjunction with (11-27d) and (11-28a) reduces to

$$A_z = \frac{\mu}{4\pi}\iint_S J_z(x')\frac{e^{-j\beta R}}{R}\,ds' = \frac{\mu}{4\pi}\int_0^w J_z(x')\left[\int_{-\infty}^{+\infty}\frac{e^{-j\beta\sqrt{|\rho-\rho'|^2+(z-z')^2}}}{\sqrt{|\rho-\rho'|^2+(z-z')^2}}\,dz'\right]dx'$$

$$= -j\frac{\mu}{4}\int_0^w J_z(x')H_0^{(2)}(\beta|\rho-\rho'|)\,dx' \tag{12-59}$$

where J_z is a linear current density (amperes per meter). Thus we can write the scattered electric field at any observation point, using the geometry of Figure 12-14, as

$$\mathbf{E}^s = -\hat{a}_z j\omega A_z = -\hat{a}_z\frac{\omega\mu}{4}\int_0^w J_z(x')H_0^{(2)}(\beta|\rho-\rho'|)\,dx'$$

$$= -\hat{a}_z\frac{\beta\eta}{4}\int_0^w J_z(x')H_0^{(2)}(\beta|\rho-\mathbf{x}'|)\,dx' \tag{12-60}$$

For far-field observations we can reduce (12-60) using the Hankel function approximation of (12-21b) for $\phi' = 0$ to

$$\boxed{\mathbf{E}^s \simeq -\hat{a}_z\eta\sqrt{\frac{j\beta}{8\pi}}\frac{e^{-j\beta\rho}}{\sqrt{\rho}}\int_0^w J_z(x')e^{j\beta x'\cos\phi}\,dx'} \tag{12-60a}$$

To evaluate the integral in (12-60a) in order to find the scattered field, we must know the induced current density $J_z(x')$ over the extent of the strip ($0 \le x' \le w$). This can be accomplished by observing the field on the surface of the strip ($\rho = x_m$). Under those conditions the total field over the strip must vanish. Thus

$$E_z^t(0 \le x_m \le w,\ y = 0) = E_z^i(0 \le x_m \le w,\ y = 0) + E_z^s(0 \le x_m \le w,\ y = 0) = 0 \tag{12-61}$$

or

$$E_z^s(0 \le x_m \le w,\ y = 0) = -E_z^i(0 \le x_m \le w,\ y = 0)$$

Since over the strip $\rho = x_m$, we can write the scattered field over the strip as

$$E_z^s(0 \le x_m \le w,\ y = 0) = -E_z^i(0 \le x_m \le w,\ y = 0)$$
$$= -\frac{\beta\eta}{4}\int_0^w J_z(x')\,H_0^{(2)}(\beta|x_m - x'|)\,dx' \quad (12\text{-}62)$$

or

$$\frac{\beta\eta}{4}\int_0^w J_z(x')\,H_0^{(2)}(\beta|x_m - x'|)\,dx'$$
$$= E_z^i(0 \le x_m \le w,\ y = 0) = E_0 e^{j\beta x_m \cos\phi_i} \quad (12\text{-}62a)$$

For a normalized field of unity amplitude ($E_0 = 1$) this reduces to

$$\boxed{\frac{\beta\eta}{4}\int_0^w J_z(x')\,H_0^{(2)}(\beta|x_m - x'|)\,dx' = e^{j\beta x_m \cos\phi_i}} \quad (12\text{-}63)$$

This is the desired two-dimensional electric field integral equation (EFIE) for the TM^z polarization of the conducting strip and it is equivalent to (12-56) for the general three-dimensional case. This EFIE can be solved for $J_z(x')$ using techniques similar to those used to solve the EFIE of (12-17a). It must be used to solve for the induced current density $J_z(x')$ over the surface of the strip. Since the surface of the strip is open, the aforementioned $J_z(x')$ represents the equivalent vector current density that flows on the opposite sides of the surface. For a more general geometry the EFIE of (12-63) can be written as

$$\boxed{\frac{\beta\eta}{4}\int_C J_z(\rho')\,H_0^{(2)}(\beta|\rho_m - \rho'|)\,dc' = E_z^i(\rho_m)} \quad (12\text{-}64)$$

where ρ_m = any observation point on the scatterer
ρ' = any source point on the scatterer
C = perimeter of scatterer

The solution of the preceding integral equations for the equivalent linear current density can be accomplished by using either the point-matching (collocation) method of Section 12.2.4 or the moment method of Section 12.2.8. However, using either method for the solution of the integral equation 12-63 for the strip of Figure 12-13*a*, we encounter the same problems as for the evaluation of the integral equation 12-17a for the finite strip of Figure 12-5, which are outlined in Section 12.2.6. However, these problems are overcome here using the same techniques as outlined in Section 12.2.6, namely, choosing the observation points along the bisector of the width of the strip, or using the approximations of (12-39) and (12-40).

Example 12-4. For the TM^z plane wave incidence on the conducting strip of Figure 12-13*a* perform the following.

1. Plot the induced equivalent current density for normal ($\phi_i = 90°$) incidence obtained using the EFIE of (12-63). Assume the strip has a width of

$w = 2\lambda$ and zero thickness. Use subdomain pulse expansion functions and point matching. Subdivide the strip into 250 segments.

2. Compare the current density of part 1 with the physical optics current density.
3. Compute the monostatic scattering width pattern for $0 \leq \phi_i \leq 180°$ using current density obtained using the EFIE of (12-63). Compare this pattern with those obtained with physical optics (PO), geometrical theory of diffraction (GTD) of Chapter 13, and physical optics (PO) plus physical theory of diffraction (PTD) techniques [13].

Solution.

1. Using the EFIE of (12-63) and applying point-matching methods with subdomain pulse expansion functions, the current density of Figure 12-15 for $\phi_i = 90°$ is obtained for a strip of $w = 2\lambda$. It is observed that the current density exhibits singularities toward the edges of the strip.
2. The physical optics current density is represented by

$$\mathbf{J}_s^{\text{PO}} \simeq 2\hat{n} \times \mathbf{H}^i\big|_{\text{strip}} = 2\hat{a}_y \times \left(\hat{a}_x H_x^i + \hat{a}_y H_y^i\right)\Big|_{\text{strip}}$$

$$= -\hat{a}_z 2H_x^i\big|_{\text{strip}} = \hat{a}_z 2\frac{E_0}{\eta} \sin\phi_i e^{j\beta x \cos\phi_i}$$

which is shown plotted in Figure 12-15 for $\phi_i = 90°$. It is apparent that the

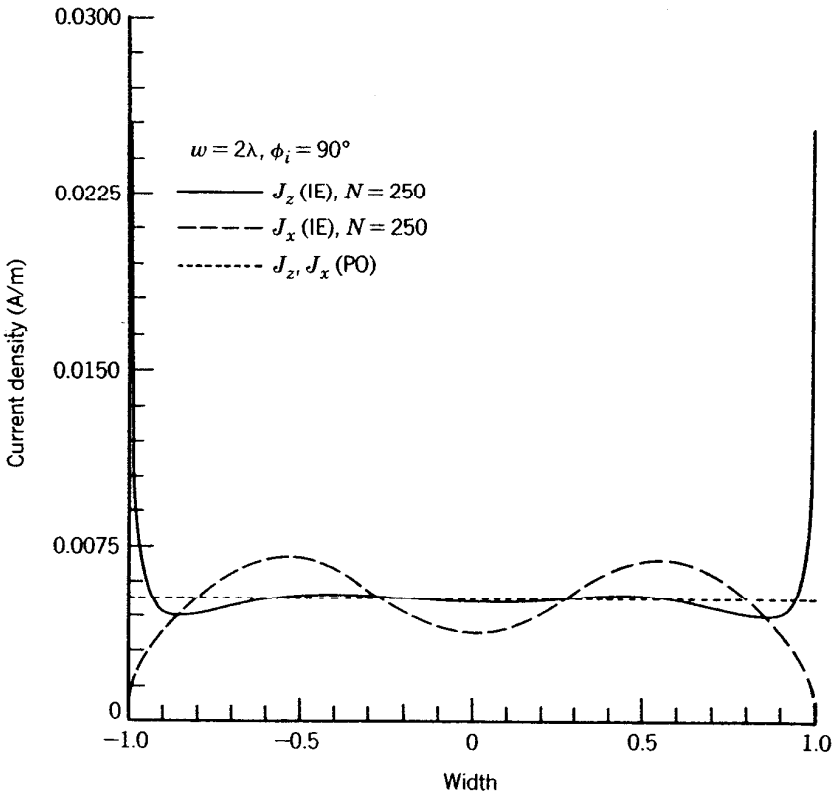

FIGURE 12-15 Current density induced on a finite width strip by a plane wave at normal incidence.

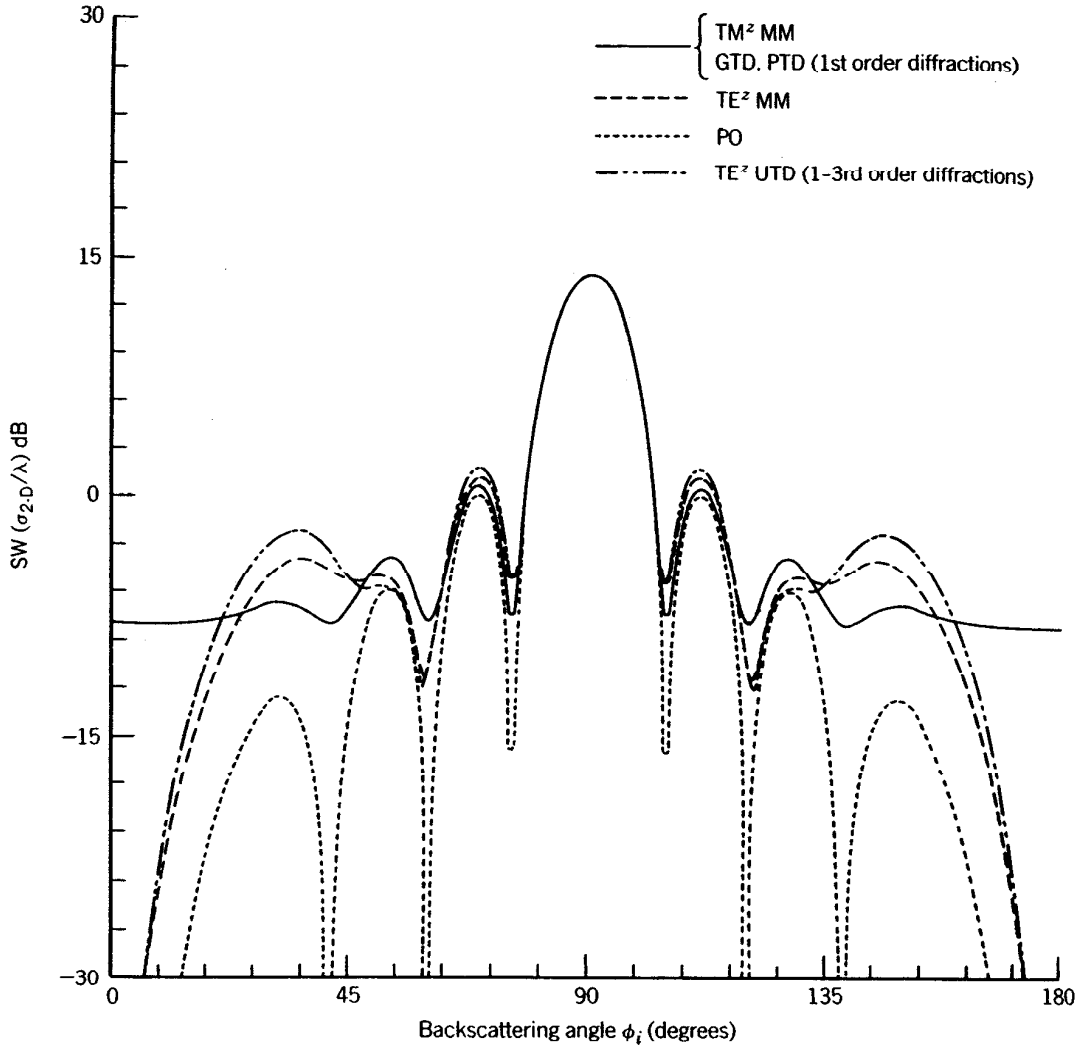

FIGURE 12-16 Monostatic scattering width of a finite width strip ($w = 2\lambda$).

PO current density does not compare well with that obtained using the IE, especially toward the edges of the strip. Therefore it does not provide a good representation of the equivalent current density induced on the strip. In Figure 12-15 we also display the equivalent current density for TE^z polarization which will be discussed in the next section and Example 12-5.

3. The monostatic scattering width patterns for $0° \leq \phi_i \leq 180°$ obtained using the methods of IE, PO, GTD, and PO plus PTD are all shown in Figure 12-16. As expected, the only one that differs from the others is that due to the PO; the other three are indistinguishable from each other and are represented by the solid curve. The pattern for the TE^z polarization for the IE method is also displayed in Figure 12-16. This will be discussed in the next section and Example 12-5.

B. TWO-DIMENSIONAL EFIE: TE^z POLARIZATION

As in the previous section, the derivation of the EFIE for TE^z polarization is best demonstrated by considering a uniform plane wave incidence on the strip, as shown in Figure 12-13*b*. Its form can then be generalized to more complex geometries.

By referring to Figure 12-13*b* the incident electric field can be expressed as

$$\mathbf{E}^i = E_0(\hat{a}_x \sin\phi_i - \hat{a}_y \cos\phi_i) e^{-j\boldsymbol{\beta}_i \cdot \mathbf{r}} = E_0(\hat{a}_x \sin\phi_i - \hat{a}_y \cos\phi_i) e^{j\beta(x\cos\phi_i + y\sin\phi_i)} \tag{12-65}$$

which at the surface of the strip ($y = 0,\ 0 \le x \le w$) reduces to

$$\mathbf{E}^i = E_0(\hat{a}_x \sin\phi_i - \hat{a}_y \cos\phi_i) e^{j\beta x\cos\phi_i} \tag{12-65a}$$

At the surface of the strip ($0 \le x \le w,\ y = 0$) the tangential components of the total field, incident plus scattered, must vanish. This can be written as

$$\begin{aligned} \hat{n} \times \mathbf{E}^t\big|_{\text{strip}} &= \hat{n} \times (\mathbf{E}^i + \mathbf{E}^s)\big|_{\text{strip}} \\ &= \hat{a}_y \times \left[(\hat{a}_x E_x^i + \hat{a}_y E_y^i) + (\hat{a}_x E_x^s + \hat{a}_y E_y^s)\right]_{\text{strip}} = 0 \end{aligned} \tag{12-66}$$

which leads to

$$-\hat{a}_z(E_x^i + E_x^s)\big|_{\text{strip}} = 0 \Rightarrow E_x^s(0 \le x \le w,\ y = 0) = -E_x^i(0 \le x \le w,\ y = 0) \tag{12-66a}$$

or

$$E_x^s(0 \le x \le w,\ y = 0) = -E_x^i(0 \le x \le w,\ y = 0) = -E_0 \sin\phi_i e^{j\beta x\cos\phi_i} \tag{12-66b}$$

The x and y components of the scattered electric field, which are independent of z variations, are obtained using (12-54) which when expanded reduce to

$$\begin{aligned} E_x^s &= -j\omega A_x - j\frac{1}{\omega\mu\varepsilon}\frac{\partial^2 A_x}{\partial x^2} = -j\frac{1}{\omega\mu\varepsilon}\left[\beta^2 A_x + \frac{\partial^2 A_x}{\partial x^2}\right] \\ &= -j\frac{1}{\omega\mu\varepsilon}\left[\left(\beta^2 + \frac{\partial^2}{\partial x^2}\right)A_x\right] \end{aligned} \tag{12-67a}$$

$$E_y^s = -j\frac{1}{\omega\mu\varepsilon}\frac{\partial^2 A_x}{\partial x\,\partial y} \tag{12-67b}$$

The vector potential A_x is obtained using (12-54a) which in conjunction with (11-27d) and (11-28a) reduces to

$$A_x = -j\frac{\mu}{4}\int_0^w J_x(x') H_0^{(2)}(\beta|\rho - \rho'|)\, dx' \tag{12-68}$$

Thus we can write that the x and y components of the scattered field can be expressed as

$$\begin{aligned} E_x^s &= -j\frac{1}{\omega\mu\varepsilon}\left(-j\frac{\mu}{4}\right)\left[\left(\beta^2 + \frac{\partial^2}{\partial x^2}\right)\int_0^w J_x(x') H_0^{(2)}(\beta|\rho - \rho'|)\, dx'\right] \\ &= -\frac{\eta}{4\beta}\left[\left(\beta^2 + \frac{\partial^2}{\partial x^2}\right)\int_0^w J_x(x') H_0^{(2)}(\beta|\rho - \rho'|)\, dx'\right] \end{aligned} \tag{12-69a}$$

$$E_y^s = -\frac{\eta}{4\beta}\frac{\partial^2}{\partial x\,\partial y}\int_0^w J_x(x') H_0^{(2)}(\beta|\rho - \rho'|)\, dx' \tag{12-69b}$$

Interchanging integration and differentiation and letting $\rho' = x'$ we can rewrite the x and y components as

$$E_x^s = -\frac{\eta}{4\beta}\int_0^w J_x(x')\left\{\left[\frac{\partial^2}{\partial x^2} + \beta^2\right]H_0^{(2)}(\beta R)\right\} dx' \tag{12-70a}$$

$$E_y^s = -\frac{\eta}{4\beta}\int_0^w J_x(x')\left\{\frac{\partial^2}{\partial x\,\partial y}H_0^{(2)}(\beta R)\right\} dx' \tag{12-70b}$$

where

$$R = |\rho - \mathbf{x}'| \tag{12-70c}$$

It can be shown using the geometry of Figure 12-14 that

$$\left[\frac{\partial^2}{\partial x^2} + \beta^2\right]H_0^{(2)}(\beta R) = \frac{\beta^2}{2}\left[H_0^{(2)}(\beta R) + H_2^{(2)}(\beta R)\cos(2\phi'')\right] \tag{12-71a}$$

$$\frac{\partial^2}{\partial x\,\partial y}H_0^{(2)}(\beta R) = \frac{\beta^2}{2}H_2^{(2)}(\beta R)\sin(2\phi'') \tag{12-71b}$$

Thus the x and y components of the electric field can be reduced to

$$E_x^s = -\frac{\beta\eta}{8}\int_0^w J_x(x')\left[H_0^{(2)}(\beta R) + H_2^{(2)}(\beta R)\cos(2\phi'')\right] dx' \tag{12-72a}$$

$$E_y^s = -\frac{\beta\eta}{8}\int_0^w J_x(x')H_2^{(2)}(\beta R)\sin(2\phi'')\, dx' \tag{12-72b}$$

The next objective is to solve for the induced current density that can then be used to find the scattered field. This can be accomplished by applying the boundary conditions on the x component of the electric field. When the observations are restricted to the surface of the strip ($\rho = x_m$), the x component of the scattered field over the strip can be written as

$$\begin{aligned} E_x^s(0 \le x_m \le w,\ y = 0) &= -E_x^i(0 \le x_m \le w,\ y = 0) = -E_0\sin\phi_i e^{j\beta x_m\cos\phi_i} \\ &= -\frac{\beta\eta}{8}\int_0^w J_x(x')\left[H_0^{(2)}(\beta R_m) + H_2^{(2)}(\beta R_m)\cos(2\phi_m'')\right] dx' \end{aligned} \tag{12-73}$$

or

$$\frac{\beta\eta}{8}\int_0^w J_x(x')\left[H_0^{(2)}(\beta R_m) + H_2^{(2)}(\beta R_m)\cos(2\phi_m'')\right] dx' = E_0\sin\phi_i e^{j\beta x_m\cos\phi_i} \tag{12-73a}$$

For a normalized field of unity amplitude ($E_0 = 1$) this reduces to

$$\boxed{\frac{\beta\eta}{8}\int_0^w J_x(x')\left[H_0^{(2)}(\beta R_m) + H_2^{(2)}(\beta R_m)\cos(2\phi_m'')\right]dx' = \sin\phi_i e^{j\beta x_m\cos\phi_i}} \tag{12-74}$$

where

$$R_m = |\rho_m - \mathbf{x}'| \tag{12-74a}$$

This is the desired two-dimensional electric field integral equation (EFIE) for the TE^z polarization of the conducting strip, and it is equivalent to (12-56) for the general three-dimensional case. This EFIE must be used to solve for the induced current density $J_x(x')$ over the surface of the strip using techniques similar to those used to solve the EFIE of (12-17a). For a more general geometry the EFIE can be written as

$$\boxed{\frac{\eta}{4\beta}\left\{\beta^2\int_C J_C(\rho')\left[\hat{c}_m\cdot\hat{c}'H_0^{(2)}(\beta|\rho_m - \rho'|)\right]dc' + \frac{d}{dc}\left[\nabla\cdot\int_C J_c(\rho')\left[\hat{c}'H_0^{(2)}(\beta|\rho_m - \rho'|)\right]dc'\right]\right\} = -E_c^i(\rho_m)} \tag{12-75}$$

where ρ_m = any observation point on the scatterer

ρ' = any source point on the scatterer

C = perimeter of the scatterer

$\hat{c}_m, \hat{c}'$ = unit vector tangent to scatterer perimeter at observation, source points

The linear current density J_x is obtained by solving the integral equation 12-74 using either the point-matching (collocation) method of Section 12.2.4 or the moment method of Section 12.2.8. Using either method the solution of the preceding integral equation for J_x is more difficult than that of the TM^z polarization of the previous example. There exist various approaches (either exact or approximate) that can be used to accomplish this.

To demonstrate this, we will discuss one method that can be used to solve the integral equation 12-74. Let us assume that the current density $J_x(x')$ is expanded into a finite series similar to (12-23). Then the integral equation can be written as

$$\sin\phi_i e^{j\beta x_m\cos\phi_i} = \frac{\beta\eta}{8}\sum_{n=1}^{N} a_n\int_0^w g_n(x')\left[H_0^{(2)}(\beta R_m) + H_2^{(2)}(\beta R_m)\cos(2\phi_m'')\right]dx' \tag{12-76}$$

If in addition the basis functions are subdomain pulse functions, as defined by (12-35), then (12-76) using point matching reduces for each observation point to

$$\sin\phi_i e^{j\beta x_m\cos\phi_i} = \frac{\beta\eta}{8}\sum_{n=1}^{N} a_n\int_{x_n}^{x_{n+1}}\left[H_0^{(2)}(\beta R_{mn}) + H_2^{(2)}(\beta R_{mn})\cos(2\phi_{mn}'')\right]dx' \tag{12-77}$$

If N observations are selected, then we can write (12-77) as

$$\left[\sin\phi_i e^{j\beta x_m \cos\phi_i}\right] = \sum_{n=1}^{N} a_n \left\{ \frac{\beta\eta}{8} \int_{x_n}^{x_{n+1}} \left[H_0^{(2)}(\beta R_{mn}) + H_2^{(2)}(\beta R_{mn}) \cos(2\phi''_{mn}) \right] dx' \right\}$$

$$m = 1, 2, \ldots, N \qquad (12\text{-}78)$$

or

$$[V_m] = [Z_{mn}][I_n] \qquad (12\text{-}78a)$$

where

$$V_m = \sin\phi_i e^{j\beta x_m \cos\phi_i} \qquad (12\text{-}78b)$$

$$I_n = a_n \qquad (12\text{-}78c)$$

$$Z_{mn} = \frac{\beta\eta}{8} \int_{x_n}^{x_{n+1}} \left[H_0^{(2)}(\beta R_{mn}) + H_2^{(2)}(\beta R_{mn}) \cos(2\phi''_{mn}) \right] dx' \qquad (12\text{-}78d)$$

One of the tasks here will be the evaluation of the integral for Z_{mn}. We will examine one technique that requires Z_{mn} to be evaluated using three different expressions depending upon the position of the segment relative to the observation point. We propose here that Z_{mn} is evaluated using

$$Z_{mn} = \begin{cases} \dfrac{\beta\eta\Delta x_n}{8} \left\{ 1 - j\dfrac{1}{\pi} \left[-1 + 2\ln\left(\dfrac{1.781\beta\Delta x_n}{4e} \right) + \dfrac{16}{(\beta\Delta x_n)^2} \right] \right\} & (12\text{-}79a) \\ \qquad e = 2.718 \qquad m = n & \\ \dfrac{\beta\eta\Delta x_n}{8} \left\{ 1 + j\dfrac{4}{\pi\beta^2} \dfrac{1}{|x_m - x_n|^2 - \dfrac{(\Delta x_n)^2}{4}} \right\} & (12\text{-}79b) \\ \qquad |m - n| \le 2 \quad m \ne n & \\ \dfrac{\beta\eta}{4} \displaystyle\int_{-\Delta x_n/2}^{\Delta x_n/2} \dfrac{H_1^{(2)}[\beta(|x_m - x_n| + x')]}{\beta(|x_m - x_n| + x')} dx' & (12\text{-}79c) \\ \qquad |m - n| > 2 & \end{cases}$$

where x_m and x_n are measured from the center of their respective segments.

The current density J_x obtained from the preceding integral equation also represents the total current density $\mathbf{J}_s$ induced on the strip. This is evident from the induced current density equation

$$\mathbf{J}_s = \hat{n} \times \mathbf{H}^t = \hat{a}_y \times \hat{a}_z H_z^t = \hat{a}_x H_z^t = \hat{a}_x \left(H_z^i + H_z^s \right) \qquad (12\text{-}80)$$

Example 12-5. For the TE^z plane wave incidence on the conducting strip of Figure 12-13*b*, perform the following tasks.

1. Plot the induced equivalent current density for normal ($\phi_i = 90°$) incidence obtained using the EFIE of (12-74) or (12-78) through (12-78d). Assume a

width of $w = 2\lambda$ and zero thickness. Use subdomain pulse expansion functions and point matching. Subdivide the strip into 250 segments.

2. Compare the current density of part 1 with the physical optics current density.
3. Compute the monostatic scattering width pattern for $0° \leq \phi_i \leq 180°$ using the current density obtained using the EFIE of (12-78) through (12-78d). Compare this pattern with those obtained with physical optics (PO), geometrical theory of diffraction (GTD) of Chapter 13, and physical optics (PO) plus physical theory of diffraction (PTD) techniques [13].

Solution.

1. Using the EFIE of (12-78) through (12-78d), the current density of Figure 12-15 for $\phi_i = 90°$ is obtained for a strip of $w = 2\lambda$. It is observed that the current density vanishes toward the edges of the strip.
2. The physical optics current density is represented by

$$\mathbf{J}_s^{\text{PO}} \sim 2\hat{n} \times \mathbf{H}^i\big|_{\text{strip}} = 2\hat{a}_y \times \hat{a}_z H_z^i\big|_{\text{strip}} = \hat{a}_x 2 H_z^i\big|_{\text{strip}} = \hat{a}_x 2 \frac{E_0}{\eta} e^{i\beta x \cos\phi_i}$$

which for normal incidence ($\phi_i = 90°$) is identical to that for the TM^z polarization, and it is shown plotted in Figure 12-15. As for the TM^z polarization, the PO TE^z polarization current density does not compare well with that obtained using the IE method. Therefore it does not provide a good representation of the equivalent current density induced on the strip. In Figure 12-15 the TE^z polarization current density is compared with that of the TM^z polarization using the different methods.

3. The monostatic scattering width pattern for $0° \leq \phi_i \leq 180°$ obtained using the IE method is shown plotted in Figure 12-16 where it is compared to those obtained by PO, PO plus PTD (first-order diffractions), and GTD (first-order diffractions) techniques. It is observed that the patterns of PO, PO plus PTD, and GTD (using first-order diffractions only) are insensitive to polarization whereby those of the integral equation with moment method solution vary with polarization. The SW patterns should vary with polarization. Therefore those obtained using the integral equation method are more accurate. It can be shown that if higher-order diffractions are included, the patterns of the PO plus PTD, and GTD will also vary with polarization. Higher-order diffractions are greater contributors to the overall scattering pattern for the TE^z polarization than for the TM^z. This is demonstrated by including in Figure 12-16 the monostatic SW for TE^z polarization obtained using higher-order GTD (UTD) diffractions [27]. It is apparent that this pattern agrees quite well with that of the IE method.

12.3.2 Magnetic Field Integral Equation

The magnetic field integral equation (MFIE) is expressed in terms of the known incident magnetic field. It is based on the boundary condition that expresses the total electric current density induced at any point $r = r'$ on the surface of a conducting surface S

$$\mathbf{J}_s(r') = \mathbf{J}_s(r = r') = \hat{n} \times \mathbf{H}^t(r = r') = \hat{n} \times \left[\mathbf{H}^i(r = r') + \mathbf{H}^s(r = r')\right] \quad (12\text{-}81)$$

Once the current density is known or determined, the scattered magnetic field can be obtained using (6-32a) and (6-96a), or

$$\mathbf{H}^s(r) = \frac{1}{\mu}\nabla \times \mathbf{A} = \nabla \times \iint_S \mathbf{J}_s(r')\frac{e^{-j\beta R}}{4\pi R}\,ds' = \nabla \times \iint_S \mathbf{J}_s(r')G(\mathbf{r},\mathbf{r}')\,ds' \tag{12-82}$$

where $G(\mathbf{r},\mathbf{r}')$ is the Green's function of (12-55a). Interchanging differentiation with integration and using the vector identity

$$\nabla \times (\mathbf{J}_s G) = G\nabla \times \mathbf{J}_s - \mathbf{J}_s \times \nabla G \tag{12-83}$$

where

$$\nabla \times \mathbf{J}_s(r') = 0 \tag{12-83a}$$

$$\nabla G = -\nabla' G \tag{12-83b}$$

(12-82) reduces to

$$\mathbf{H}^s(r) = \iint_S \mathbf{J}_s(r') \times [\nabla' G(\mathbf{r},\mathbf{r}')]\,ds' \tag{12-84}$$

On the surface S of the conductor the tangential magnetic field is discontinuous by the amount of the current density induced on the surface of the conductor. Therefore the current density is determined by (12-81) but with $\mathbf{H}^s$ found using (12-84). Thus we can write that

$$\begin{aligned}\mathbf{J}_s(r') &= \hat{n} \times \mathbf{H}^i(r = r') + \lim_{r \to S}[\hat{n} \times \mathbf{H}^s(r = r')] \\ &= \hat{n} \times \mathbf{H}^i(r = r') + \lim_{r \to S}\left\{\hat{n} \times \iint_S \mathbf{J}_s(r') \times [\nabla' G(\mathbf{r},\mathbf{r}')]\,ds'\right\}\end{aligned} \tag{12-85}$$

or

$$\boxed{\mathbf{J}_s(r') - \lim_{r \to S}\left\{\hat{n} \times \iint_S \mathbf{J}_s(r') \times [\nabla' G(\mathbf{r},\mathbf{r}')]\,ds'\right\} = \hat{n} \times \mathbf{H}^i(r = r')} \tag{12-85a}$$

where $r \to S$ indicates that S is approached by r from the outside.

Equation 12-85a is referred to as the *magnetic field integral equation* (MFIE) because its right side is in terms of the incident magnetic field, and it is valid only for *closed* surfaces. Once the current density distribution can be found using (12-85a), then the scattered fields can be found using standard radiation integrals. It should be noted that the integral of (12-85a) must be carefully evaluated. The MFIE is the most popular for TE^z polarizations, although it can be used for both TE^z and TM^z cases. Since (12-85a) is only valid for closed surfaces, the current density obtained using (12-85a) is the actual current density induced on the surface of the conducting obstacle.

Whereas (12-85a) is a general MFIE for three-dimensional problems, its form can be simplified for two-dimensional MFIEs for both TM^z and TE^z polarizations.

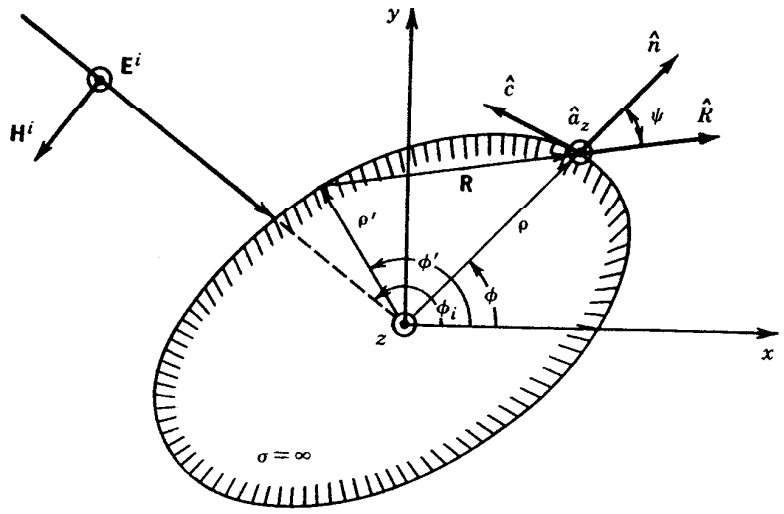

FIGURE 12-17 Geometry for two-dimensional MFIE TM^z polarization scattering.

A. TWO-DIMENSIONAL MFIE: TM^z POLARIZATION

The best way to demonstrate the derivation of the two-dimensional MFIE for TM^z polarization is to consider a TM^z uniform plane wave incident upon a two-dimensional smooth curved surface, as shown in Figure 12-17.

Since the incident field has only a z component of the electric field, and x and y components of the magnetic field, the electric current density induced on the surface of the scatterer will only have a z component. That is

$$\mathbf{J}_s(\rho) = \hat{a}_z J_z(\rho)\big|_C \tag{12-86}$$

On the surface of the scatterer the current density is related to the incident and scattered magnetic fields by (12-81), which for the geometry of Figure 12-17 can be written as

$$\mathbf{J}_s(\rho)\big|_C = \hat{a}_z J_z(\rho)\big|_C = \hat{n} \times (\mathbf{H}^i + \mathbf{H}^s)\big|_C = \hat{n} \times \mathbf{H}^i + \lim_{\rho \to C} (\hat{n} \times \mathbf{H}^s) \tag{12-87}$$

where $\rho \to C$ indicates that the boundary C is approached by ρ from the outside. Since the left side of (12-87) has only a z component, then the right side of (12-87) must also have only z components. Therefore the only component of $\mathbf{H}^i$ that contributes to (12-87) is that which is tangent to C and coincides with the surface of the scatterer. Thus we can rewrite (12-87) as

$$J_z(\rho)\big|_C = H_c^i(\rho)\big|_C + \lim_{\rho \to C} [\hat{a}_z \cdot (\hat{n} \times \mathbf{H}^s)] \tag{12-88}$$

The scattered magnetic field $\mathbf{H}^s$ can be expressed according to (12-82) as

$$\begin{aligned}
\mathbf{H}^s &= \frac{1}{\mu}\nabla \times \mathbf{A} = \frac{1}{\mu}\nabla \times \left[\frac{\mu}{4\pi}\int_C\int_{-\infty}^{+\infty} \mathbf{J}_s(\rho')\frac{e^{-j\beta R}}{R}\,dz'\,dc'\right] \\
&= \frac{1}{4\pi}\nabla \times \left\{\int_C \mathbf{J}_s(\rho')\left[\int_{-\infty}^{+\infty}\frac{e^{-j\beta R}}{R}\,dz'\right]dc'\right\} = -j\frac{1}{4}\nabla \times \int_C \mathbf{J}_s(\rho')H_0^{(2)}(\beta R)\,dc' \\
\mathbf{H}^s &= -j\frac{1}{4}\int_C \nabla \times [\mathbf{J}_s(\rho')H_0^{(2)}(\beta R)]\,dc'
\end{aligned} \tag{12-89}$$

Using (12-83) and (12-83a) reduces (12-89) to

$$\mathbf{H}^s = j\frac{1}{4}\int_C \mathbf{J}_s(\rho') \times \nabla H_0^{(2)}(\beta R)\, dc' \tag{12-90}$$

Since $\mathbf{J}_s(\rho')$ has only a z component, then the second term within the brackets on the right side of (12-88) can be written using (12-90) as

$$\begin{aligned}\hat{a}_z \cdot (\hat{n} \times \mathbf{H}^s) &= \hat{a}_z \cdot \hat{n} \times \left\{ j\frac{1}{4}\int_C [\hat{a}_z' J_z(\rho')] \times [\nabla H_0^{(2)}(\beta R)]\, dc' \right\} \\ &= j\frac{1}{4}\int_C J_z(\rho')\{\hat{a}_z \cdot [\hat{n} \times \hat{a}_z \times \nabla H_0^{(2)}(\beta R)]\}\, dc' \end{aligned} \tag{12-91}$$

since $\hat{a}_z' = \hat{a}_z$. Using the vector identity of

$$\mathbf{A} \times (\mathbf{B} \times \mathbf{C}) = (\mathbf{A} \cdot \mathbf{C})\mathbf{B} - (\mathbf{A} \cdot \mathbf{B})\mathbf{C} \tag{12-92}$$

we can write that

$$\begin{aligned}\hat{n} \times [\hat{a}_z \times \nabla H_0^{(2)}(\beta R)] &= \hat{a}_z[\hat{n} \cdot \nabla H_0^{(2)}(\beta R)] - (\hat{n} \cdot \hat{a}_z)\nabla H_0^{(2)}(\beta R) \\ &= \hat{a}_z[\hat{n} \cdot \nabla H_0^{(2)}(\beta R)] \end{aligned} \tag{12-93}$$

since $\hat{n} \cdot \hat{a}_z = 0$. Substituting (12-93) into (12-91) reduces it to

$$\begin{aligned}\hat{a}_z \cdot (\hat{n} \times \mathbf{H}^s) &= j\frac{1}{4}\int_C J_z(\rho')[\hat{n} \cdot \nabla H_0^{(2)}(\beta R)]\, dc' \\ &= j\frac{1}{4}\int_C J_z(\rho')[-\beta \cos\psi H_1^{(2)}(\beta R)]\, dc' \\ \hat{a}_z \cdot (\hat{n} \times \mathbf{H}^s) &= -j\frac{\beta}{4}\int_C J_z(\rho') \cos\psi H_1^{(2)}(\beta R)\, dc' \end{aligned} \tag{12-94}$$

where the angle ψ is defined in Figure 12-17. Thus we can write (12-88) using (12-94) as

$$J_z(\rho)\big|_C = H_c^i(\rho)\big|_C + \lim_{\rho \to C}\left[-j\frac{\beta}{4}\int_C J_z(\rho') \cos\psi H_1^{(2)}(\beta R)\, dc'\right] \tag{12-95}$$

or

$$\boxed{J_z(\rho)\Big|_C + j\frac{\beta}{4}\lim_{\rho \to C}\left[\int_C J_z(\rho') \cos\psi H_1^{(2)}(\beta R)\, dc'\right] = H_c^i(\rho)\Big|_C} \tag{12-95a}$$

B. TWO-DIMENSIONAL MFIE: TE^z POLARIZATION

To derive the MFIE for the TE^z polarization, let us consider a TE^z uniform plane wave incidence upon a two-dimensional curved surface, as shown in Figure 12-18. Since the incident field has only a z component of the magnetic field, the current induced on the surface of the scatterer will have only a component that is tangent to C and it will coincide with the surface of the scatterer. That is

$$\mathbf{J}_s = \hat{c} J_c(\rho) \tag{12-96}$$

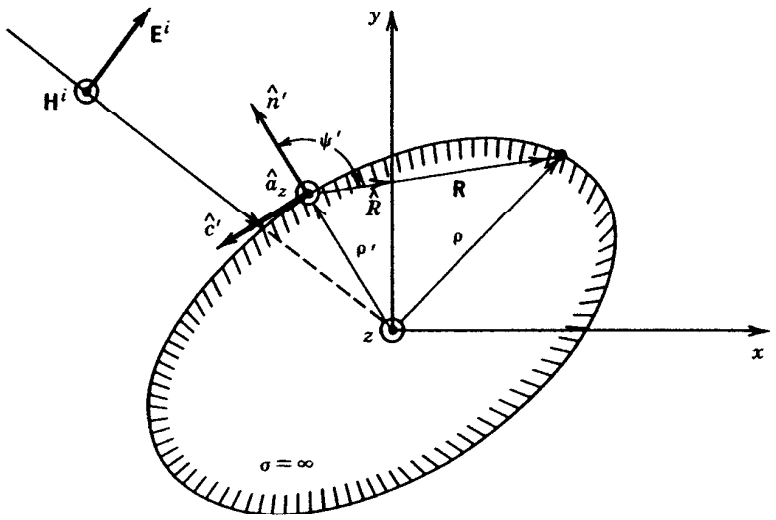

FIGURE 12-18 Geometry for two-dimensional MFIE TE^z polarization scattering.

On the surface of the scatterer the current density is related to the incident and scattered magnetic fields by (12-81), which for the geometry of Figure 12-18 can be written as

$$\mathbf{J}_s\big|_C = \hat{c}J_c(\rho)\big|_C = \hat{n} \times (\mathbf{H}^i + \mathbf{H}^s)\big|_C = \hat{n} \times \mathbf{H}^i + \lim_{\rho \to C} (\hat{n} \times \mathbf{H}^s)$$

$$= \hat{n} \times \hat{a}_z H^i\big|_C + \lim_{\rho \to C} (\hat{n} \times \mathbf{H}^s)$$

$$\mathbf{J}_s\big|_C = \hat{c}J_c(\rho)\big|_C = -\hat{c}H_z^i\big|_C + \lim_{\rho \to C} (\hat{n} \times \mathbf{H}^s) \tag{12-97}$$

where $\rho \to C$ indicates that the boundary C is approached by ρ from the outside. Since the left side and the first term of the right side of (12-97) have only c components, then the second term of the right side of (12-97) must also have only a c component. Thus we can write (12-97) as

$$J_c(\rho)\big|_C = -H_z^i(\rho)\big|_C + \lim_{\rho \to C} [\hat{c} \cdot (\hat{n} \times \mathbf{H}^s)] \tag{12-98}$$

Using the scattered magnetic field of (12-90) we can write the second term within the brackets of (12-98) as

$$\hat{c} \cdot (\hat{n} \times \mathbf{H}^s) = \hat{c} \cdot \hat{n} \times \left\{ j\frac{1}{4} \int_C [\hat{c}' J_c(\rho') \times \nabla H_0^{(2)}(\beta R)] \right\} dc'$$

$$= j\frac{1}{4} \int_C J_c(\rho') \{ \hat{c} \cdot \hat{n} \times [\hat{c}' \times \nabla H_0^{(2)}(\beta R)] \} \tag{12-99}$$

Since from Figure 12-18

$$\hat{c}' = -\hat{n}' \times \hat{a}_z' = -\hat{n}' \times \hat{a}_z \tag{12-100}$$

then with the aid of (12-92)

$$\begin{aligned}\hat{c}' \times \nabla H_0^{(2)}(\beta R) &= (-\hat{n}' \times \hat{a}_z) \times \nabla H_0^{(2)}(\beta R) = \nabla H_0^{(2)}(\beta R) \times (\hat{n}' \times \hat{a}_z) \\ &= -\hat{a}_z[\hat{n}' \cdot \nabla H_0^{(2)}(\beta R)] + \hat{n}'[\hat{a}_z \cdot \nabla H_0^{(2)}(\beta R)] \\ &= -\hat{a}_z[\hat{n} \cdot \nabla H_0^{(2)}(\beta R)] \end{aligned} \tag{12-100a}$$

since $\hat{a}_z \cdot \nabla H_0^{(2)}(\beta R) = 0$. Thus the terms within the brackets in (12-99) can be written as

$$\begin{aligned}&\hat{c} \cdot \hat{n} \times [\hat{c}' \times \nabla H_0^{(2)}(\beta R)] \\ &\quad = -\hat{c} \cdot (\hat{n} \times \hat{a}_z)[\hat{n}' \cdot \nabla H_0^{(2)}(\beta R)] = (\hat{c} \cdot \hat{c})[\hat{n}' \cdot \nabla H_0^{(2)}(\beta R)] \\ &\quad = \hat{n}' \cdot \nabla H_0^{(2)}(\beta R) \end{aligned} \tag{12-101}$$

since $-\hat{c} = \hat{n} \times \hat{a}_z$. Substituting (12-101) into (12-99) reduces it to

$$\hat{c} \cdot \hat{n} \times \mathbf{H}^s = j\frac{1}{4}\int_C J_c(\rho')[\hat{n}' \cdot \nabla H_0^{(2)}(\beta R)]\, dc' = j\frac{1}{4}\int_C J_c(\rho')[-\beta \cos\psi' H_1^{(2)}(\beta R)]\, dc'$$

$$\hat{c} \cdot \hat{n} \times \mathbf{H}^s = -j\frac{\beta}{4}\int_C J_c(\rho') \cos\psi' H_1^{(2)}(\beta R)\, dc' \tag{12-102}$$

where the angle ψ' is defined in Figure 12-18. Thus we can write (12-98) using (12-102) as

$$J_c(\rho)\big|_C = -H_z^i(\rho)\big|_C + \lim_{\rho \to C}\left[-j\frac{\beta}{4}\int_C J_c(\rho') \cos\psi' H_1^{(2)}(\beta R)\, dc'\right] \tag{12-103}$$

or

$$\boxed{J_c(\rho)\Big|_C + j\frac{\beta}{4}\lim_{\rho \to C}\left[\int_C J_c(\rho') \cos\psi' H_1^{(2)}(\beta R)\, dc'\right] = -H_z^i\Big|_C} \tag{12-103a}$$

C. SOLUTION OF THE TWO-DIMENSIONAL MFIE TE^z POLARIZATION

The two-dimensional MFIEs of (12-95a) for TM^z polarization and (12-103a) for TE^z polarization are of identical form and their solutions are then similar. Since TM^z polarizations are very conveniently solved using the EFIE, usually the MFIEs are mostly applied to TE^z polarization problems where the magnetic field has only a z component. Therefore we will demonstrate here the solution to the TE^z MFIE of (12-103a).

In the evaluation of the scattered magnetic field at $\rho = \rho_m$ from all points on C (including the point $\rho = \rho_m$ where the observation is made), the integral of (12-103a) can be split into two parts; one part coming from ΔC and the other part outside $\Delta C(C - \Delta C)$, as shown in Figure 12-19.Thus we can write the integral of (12-103a) as

$$\begin{aligned}&j\frac{\beta}{4}\lim_{\rho \to C}\int_C J_c(\rho') \cos\psi' H_1^{(2)}(\beta R)\, dc' \\ &\quad = j\frac{\beta}{4}\lim_{\rho \to C}\left\{\int_{\Delta C} J_c(\rho') \cos\psi' H_1^{(2)}(\beta R)\, dc' + \int_{C-\Delta C} J_c(\rho') \cos\psi' H_1^{(2)}(\beta R)\, dc'\right\} \end{aligned} \tag{12-104}$$

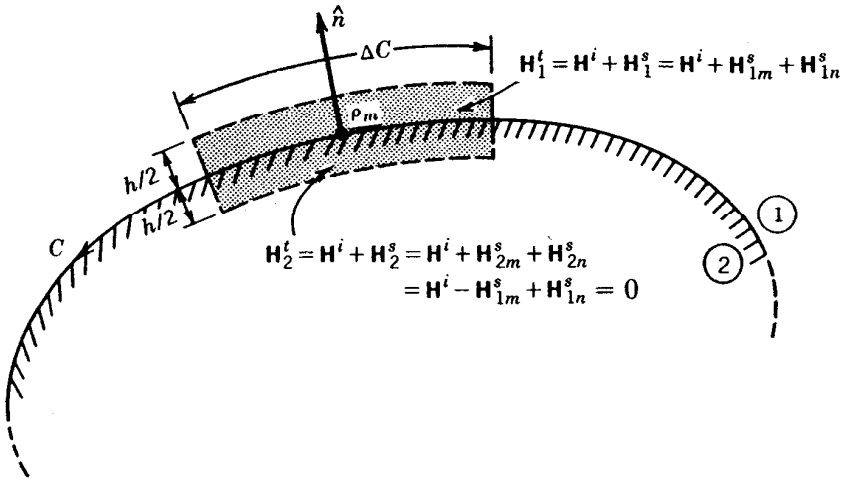

FIGURE 12-19 Geometry and fields along the scattering surface for a two-dimensional MFIE.

In a solution of (12-103a) where C is subdivided into segments, ΔC would typically represent one segment (the self-term) and $C - \Delta C$ would represent the other segments (the non-self-terms). Let us now examine the evaluation of each of the integrals in (12-104).

At any point the total magnetic field is equal to the sum of the incident and scattered parts. Within the scattered conducting obstacle the total magnetic field is zero whereby above the conducting surface the field is nonzero. The discontinuity of the two along C is used to represent the current density along C. Within the thin rectangular box with dimensions of h and ΔC (in the limit $h \to 0$), the total magnetic field above ($\mathbf{H}_1^t$) and below ($\mathbf{H}_2^t$) the interface can be written as

$$\mathbf{H}_1^t = \mathbf{H}^i + \mathbf{H}_1^s = \mathbf{H}^i + (\mathbf{H}_{1m}^s + \mathbf{H}_{1n}^s) \tag{12-105a}$$

$$\mathbf{H}_2^t = \mathbf{H}^i + \mathbf{H}_2^s = \mathbf{H}^i + (\mathbf{H}_{2m}^s + \mathbf{H}_{2n}^s) = \mathbf{H}^i + (-\mathbf{H}_{1m}^s + \mathbf{H}_{1n}^s) = 0 \tag{12-105b}$$

or $$\mathbf{H}_{1n}^s = \mathbf{H}_{1m}^s - \mathbf{H}^i \tag{12-105c}$$

where $\mathbf{H}_{1m}^s$ ($\mathbf{H}_{2m}^s$) = scattered field in region 1 (2) within the box that is due to ΔC (self-term) which is discontinuous across the boundary along ΔC

$\mathbf{H}_{1n}^s$ ($\mathbf{H}_{2n}^s$) = scattered field in region 1 (2) within the box that is due to $C - \Delta C$ (non-self-terms) which is continuous across the boundary along ΔC

It is assumed here that ΔC along C becomes a straight line as the segment becomes small. The current density along ΔC can then be represented using (12-105a) and (12-105b) by

$$\mathbf{J}_c(\rho)\big|_{\Delta C} = \hat{n} \times (\mathbf{H}_1^t - \mathbf{H}_2^t)\big|_{\Delta C} = \hat{n} \times (\mathbf{H}_{1m}^s + \mathbf{H}_{1m}^s) = 2\hat{n} \times \mathbf{H}_{1m}^s = -2\hat{c}H_{1m}^s \tag{12-106}$$

or

$$J_c(\rho_m) = -2H_{1m}^s(\rho_m) \Rightarrow H_{1m}^s(\rho_m) = -\frac{J_c(\rho_m)}{2} \tag{12-106a}$$

Therefore the integral along ΔC in (12-104), which can be used to represent the

scattered magnetic field at $\rho = \rho_m$ that is due to the ΔC, can be replaced by (12-106a). The non-self terms can be found using the integral along $C - \Delta C$ in (12-104). Thus using (12-104) and (12-106a) we can reduce (12-103a) for $\rho = \rho_m$ to

$$J_c(\rho_m) - \frac{J_c(\rho_m)}{2} + j\frac{\beta}{4}\int_{C-\Delta C} J_c(\rho')\cos\psi'_m H_1^{(2)}(\beta R_m)\,dc' = -H_z^i(\rho_m) \quad (12\text{-}107)$$

or

$$\boxed{\frac{J_c(\rho_m)}{2} + j\frac{\beta}{4}\int_{C-\Delta C} J_c(\rho')\cos\psi'_m H_1^{(2)}(\beta R_m)\,dc' = -H_z^i(\rho_m)} \quad (12\text{-}107a)$$

An analogous procedure can be used to reduce (12-95a) to a form similar to that of (12-107a).

Let us now represent the current density $J_c(\rho)$ of (12-107a) by the finite series of (12-23)

$$J_c(\rho) \simeq \sum_{n=1}^{N} a_n g_n(\rho) \quad (12\text{-}108)$$

where $g_n(\rho)$ represents the basis (expansion) functions. Substituting (12-108) into (12-107a) and interchanging integration and summation, we can write that at any point $\rho = \rho_m$ on C (12-107a) can be written as

$$-H_z^i(\rho_m) = \frac{1}{2}\sum_{n=1}^{N} a_n g_n(\rho_m) + j\frac{\beta}{4}\sum_{n=1}^{N} a_n \int_{C-\Delta C} g_n(\rho')\cos\psi'_m H_1^{(2)}(\beta R_m)\,dc' \quad (12\text{-}109)$$

If the g_n's are subdomain piecewise constant pulse functions with each basis function existing only over its own segment, then (12-109) reduces to

$$-H_z^i(\rho_m) = \frac{\delta_{mn}}{2}a_n + j\frac{\beta}{4}\sum_{\substack{n=1\\ n\neq m}}^{N} a_n \int_{\rho_n}^{\rho_{n+1}} \cos\psi'_{mn} H_1^{(2)}(\beta R_{mn})\,dc' \quad (12\text{-}110)$$

or

$$-H_z^i(\rho_m) = \sum_{n=1}^{N} a_n \left[\frac{\delta_{mn}}{2} + j\frac{\beta}{4}\int_{\substack{\rho_n\\ n\neq m}}^{\rho_{n+1}} \cos\psi'_{mn} H_1^{(2)}(\beta R_{mn})\,dc'\right] \quad (12\text{-}110a)$$

where δ_{mn} is the Kronecker delta function defined by

$$\delta_{mn} = \begin{cases} 1 & m = n \\ 0 & m \neq n \end{cases} \quad (12\text{-}110b)$$

The Kronecker delta function is used to indicate that for a given observation point m only the segment itself ($n = m$) contributes to the first term on the right side of (12-110a).

If (12-110a) is applied to m points on C, then it can be written as

$$\boxed{\left[-H_z^i(\rho_m)\right] = \sum_{n=1}^{N} a_n \left[\frac{\delta_{mn}}{2} + j\frac{\beta}{4}\int_{\rho_n}^{\rho_{n+1}} \cos\psi'_{mn} H_1^{(2)}(\beta R_{mn})\, dc'\right]} \quad (12\text{-}111)$$

$$n \neq m$$

$$m = 1, 2, \ldots, N$$

In general matrix notation (12-111) can be expressed as

$$[V_m] = [Z_{mn}][I_n] \quad (12\text{-}112)$$

where

$$V_m = -H_z^i(\rho_m) \quad (12\text{-}112a)$$

$$Z_{mn} = \left[\frac{\delta_{mn}}{2} - j\frac{\beta}{4}\int_{\rho_n}^{\rho_{n+1}} \cos\psi'_{mn} H_1^{(2)}(\beta R_{mn})\, dc'\right] \quad (12\text{-}112b)$$

$$I_n = a_n \quad (12\text{-}112c)$$

To demonstrate the applicability of (12-111), let us consider an example.

Example 12-6. A TE^z uniform plane wave is normally incident upon a circular conducting cylinder of radius a, as shown in Figure 12-20.

1. Using the MFIE of (12-107a) determine and plot the current density induced on the surface of the cylinder when $a = 2\lambda$. Assume the incident magnetic field is of unity amplitude. Use subdomain piecewise constant pulse functions. Subdivide the circumference into 540 segments. Compare the current density obtained using the IE with the exact modal solution of (11-113).
2. Based on the electric current density, derive and then plot the normalized $(\sigma_{2\text{-D}}/\lambda)$ bistatic scattering width (in decibels) for $0° \leq \phi \leq 360°$ when

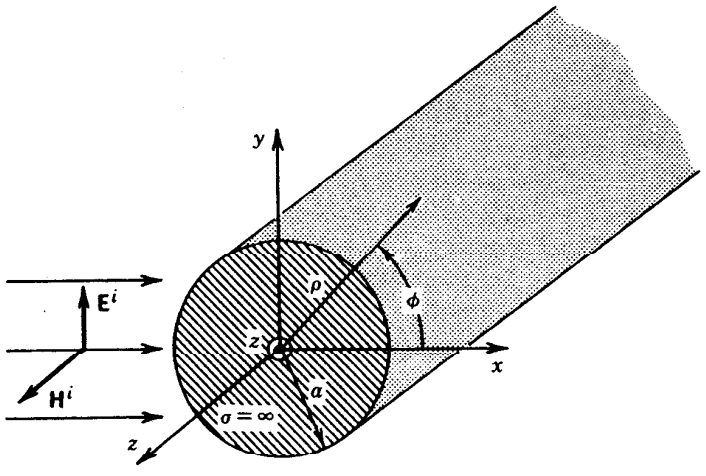

FIGURE 12-20 TE^z uniform plane wave incident on a circular conducting cylinder.

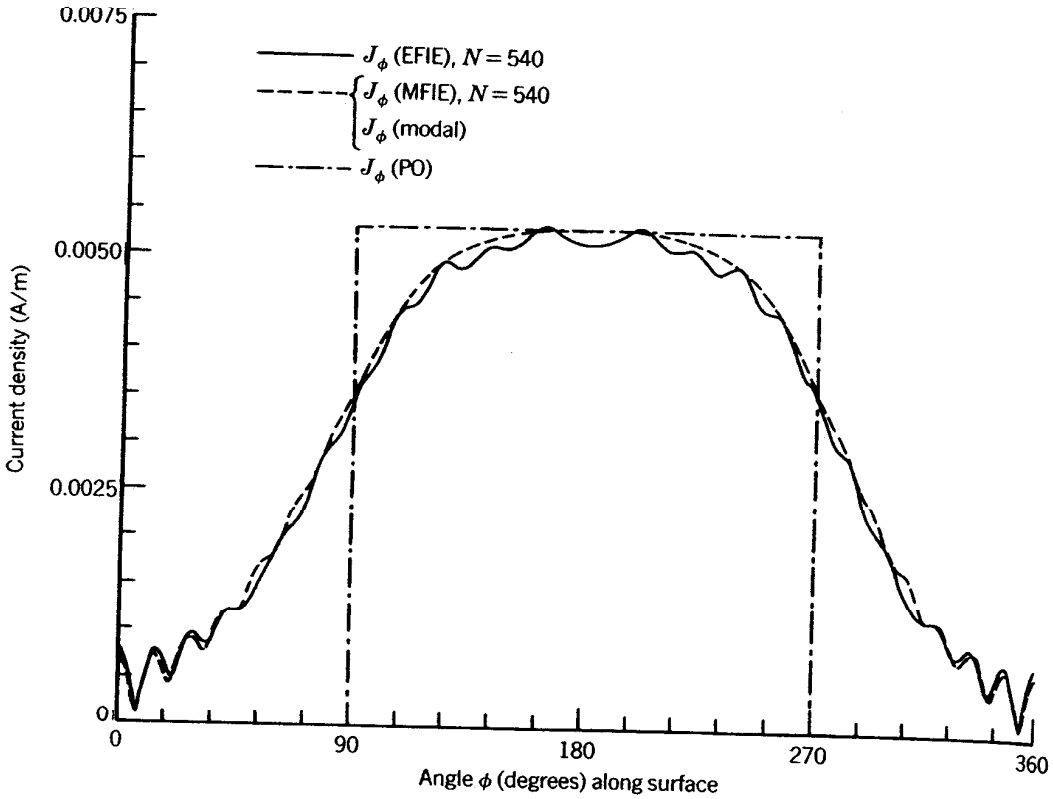

FIGURE 12-21 Current density induced on the surface of a circular conducting cylinder by TE^z plane wave incidence ($a = 2\lambda$).

$a = 2\lambda$. Compare these values with those obtained using the exact modal solution of (11-117).

Solution.

1. Since for subdomain piecewise constant pulse functions (12-103a) or (12-107a) reduces to (12-111) or (12-112) through (12-112c), then a solution of (12-112) for I_n leads to the current density shown in Figure 12-21. In the same figure we have plotted the current density of (11-113) based on the modal solution, and an excellent agreement between the two is indicated. We also have plotted the current densities based on the EFIE for TE^z polarization of Section 12.3.1B and on the physical optics of (7-54) over the illuminated portion of the cylinder surface. The results of the EFIE do not agree with the modal as accurately as those of the MFIE. However, they still are very good. As expected, the physical optics current density is not representative of the true solution.
2. Based on the current densities obtained in part 1, the far-zone scattered field was derived and the corresponding bistatic scattering width was formulated. The computed SW results are shown in Figure 12-22. Besides the results based on the physical optics approximation, the other three (MFIE, EFIE, and modal solution) give almost indistinguishable data and are shown in Figure 12-22 almost as one curve.

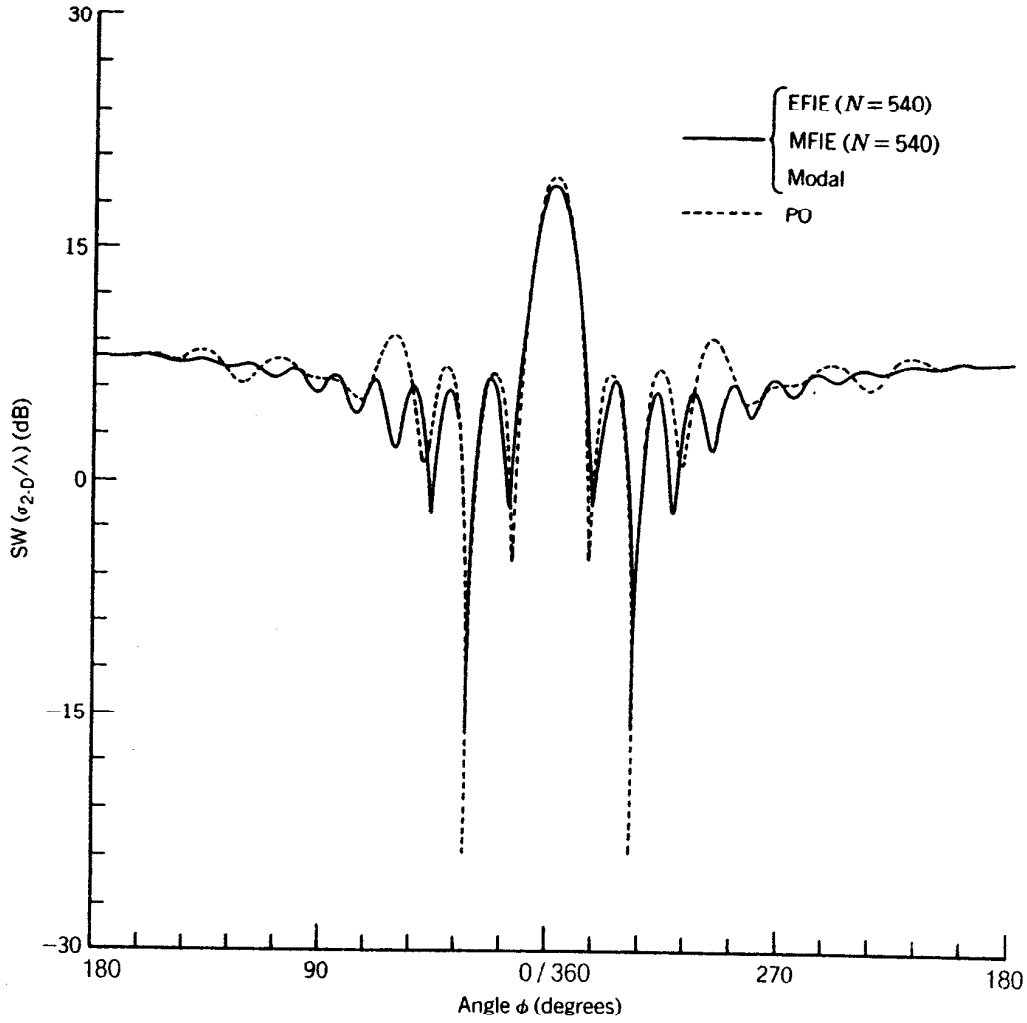

FIGURE 12-22 TE^z bistatic scattering width of a circular conducting cylinder ($a = 2\lambda$).

12.4 FINITE DIAMETER WIRES

In this section we want to derive and apply two classic three-dimensional integral equations, referred to as *Pocklington's integrodifferential equation* and *Hallén's integral equation* [28–36], that can be used most conveniently to find the current distribution on conducting wires. Hallén's equation is usually restricted to the use of a *delta-gap* voltage source model at the feed of a wire antenna. Pocklington's equation, however, is more general and it is adaptable to many types of feed sources (through alteration of its excitation function or excitation matrix), including a magnetic frill [37]. In addition, Hallén's equation requires the inversion of an $N + 1$ order matrix (where N is the number of divisions of the wire) while Pocklington's equation requires the inversion of an N order matrix.

For very thin wires, the current distribution is usually assumed to be of sinusoidal form [24]. For finite diameter wires (usually diameters d of $d > 0.05\lambda$), the sinusoidal current distribution is representative but not accurate. To find a more accurate current distribution on a cylindrical wire, an integral equation is usually derived and solved. Previously, solutions to the integral equation were obtained

using iterative methods [30]; presently, it is most convenient to use moment method techniques [1–3].

If we know the voltage at the feed terminals of a wire antenna and find the current distribution, the input impedance and radiation pattern can then be obtained. Similarly if a wave impinges upon the surface of a wire scatterer, it induces a current density that in turn is used to find the scattered field. Whereas the linear wire is simple, most of the information presented here can be readily extended to more complicated structures.

12.4.1 Pocklington's Integral Equation

In deriving Pocklington's integral equation, the integral equation approach of Section 12.3.1 will be used. However, each step, as applied to the wire scatterer, will be repeated here to indicate the simplicity of the method.

Refer to Figure 12-23*a*. Let us assume that an incident wave impinges on the surface of a conducting wire. The total tangential electric field (E_z) at the surface of the wire is given by (12-53) or (12-53a), that is

$$E_z^t(r = r_s) = E_z^i(r = r_s) + E_z^s(r = r_s) = 0 \tag{12-113}$$

or

$$E_z^s(r = r_s) = -E_z^i(r = r_s) \tag{12-113a}$$

At any observation point, the field scattered by the induced current density on the surface of the wire is given by (12-54). However, for observations at the wire surface only the z component of (12-54) is needed and we can write it as

$$E_z^s(r) = -j\frac{1}{\omega\mu\varepsilon}\left(\beta^2 A_z + \frac{\partial^2 A_z}{\partial z^2}\right) \tag{12-114}$$

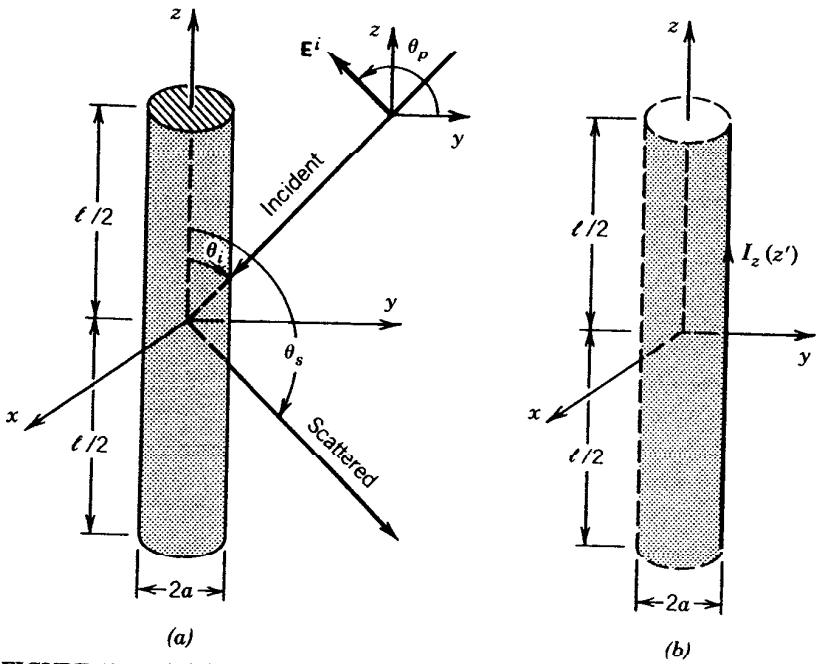

FIGURE 12-23 (*a*) Uniform plane wave obliquely incident on a conducting wire and (*b*) equivalent current.

According to (12-54a) and neglecting edge effects

$$A_z = \frac{\mu}{4\pi}\iint_S J_z \frac{e^{-j\beta R}}{R}\,ds' = \frac{\mu}{4\pi}\int_{-\ell/2}^{+\ell/2}\int_0^{2\pi} J_z \frac{e^{-j\beta R}}{R}\,a\,d\phi'\,dz' \tag{12-115}$$

If the wire is very thin, the current density J_z is not a function of the azimuthal angle ϕ, and we can write it as

$$2\pi a J_z = I_z(z') \Rightarrow J_z = \frac{1}{2\pi a} I_z(z') \tag{12-116}$$

where $I_z(z')$ is assumed to be an equivalent filament line-source current located a radial distance $\rho = a$ from the z axis, as shown in Figure 12-23*b*. Thus (12-115) reduces to

$$A_z = \frac{\mu}{4\pi}\int_{-\ell/2}^{+\ell/2}\left[\frac{1}{2\pi a}\int_0^{2\pi} I_z(z')\frac{e^{-j\beta R}}{R}\,a\,d\phi'\right] dz' \tag{12-117}$$

$$R = \sqrt{(x-x')^2 + (y-y')^2 + (z-z')^2}$$
$$= \sqrt{\rho^2 + a^2 - 2\rho a\cos(\phi - \phi') + (z-z')^2} \tag{12-117a}$$

where ρ is the radial distance to the observation point and a is the radius.

Because of the symmetry of the scatterer, the observations are not a function of ϕ. For simplicity let us then choose $\phi = 0$. For observations at the surface $\rho = a$ of the scatterer (12-117) and (12-117a) reduce to

$$A_z(\rho = a) = \mu\int_{-\ell/2}^{+\ell/2} I_z(z')\left(\frac{1}{2\pi}\int_0^{2\pi}\frac{e^{-j\beta R}}{4\pi R}\,d\phi'\right) dz' = \mu\int_{-\ell/2}^{+\ell/2} I_z(z')G(z,z')\,dz' \tag{12-118}$$

$$\boxed{G(z,z') = \frac{1}{2\pi}\int_0^{2\pi}\frac{e^{-j\beta R}}{4\pi R}\,d\phi'} \tag{12-118a}$$

$$\boxed{R(\rho = a) = \sqrt{4a^2\sin^2\left(\frac{\phi'}{2}\right) + (z-z')^2}} \tag{12-118b}$$

Thus for observations at the surface $\rho = a$ of the scatterer the z component of the scattered electric field can be expressed as

$$E_z^s(\rho = a) = -j\frac{1}{\omega\varepsilon}\left(\beta^2 + \frac{d^2}{dz^2}\right)\int_{-\ell/2}^{+\ell/2} I_z(z')G(z,z')\,dz' \tag{12-119}$$

which by using (12-113a) reduces to

$$-j\frac{1}{\omega\varepsilon}\left(\frac{d^2}{dz^2} + \beta^2\right)\int_{-\ell/2}^{+\ell/2} I_z(z')G(z,z')\,dz' = -E_z^i(\rho = a) \tag{12-120}$$

or

$$\left(\frac{d^2}{dz^2} + \beta^2\right)\int_{-\ell/2}^{+\ell/2} I_z(z')G(z,z')\,dz' = -j\omega\varepsilon E_z^i(\rho = a) \tag{12-120a}$$

Interchanging integration with differentiation, we can rewrite (12-120a) as

$$\boxed{\int_{-\ell/2}^{+\ell/2} I_z(z')\left[\left(\frac{\partial^2}{\partial z^2}+\beta^2\right)G(z,z')\right]dz' = -j\omega\varepsilon E_z^i(\rho=a)} \tag{12-121}$$

where $G(z, z')$ is given by (12-118a).

Equation 12-121 is referred to as *Pocklington's integrodifferential equation* [28], and it can be used to determine the equivalent filamentary line-source current of the wire, and thus current density on the wire, by knowing the incident field on the surface of the wire. It is a simplified form of (12-56) as applied to a wire scatterer, and it could have been derived directly from (12-56).

If we assume that the wire is very thin ($a \ll \lambda$) such that (12-118a) reduces to

$$G(z,z') = G(R) = \frac{e^{-j\beta R}}{4\pi R} \tag{12-122}$$

(12-121) can also be expressed in a more convenient form as [32]

$$\boxed{\int_{-\ell/2}^{+\ell/2} I_z(z')\frac{e^{-j\beta R}}{4\pi R^5}\left[(1+j\beta R)(2R^2-3a^2)+(\beta a R)^2\right]dz' = -j\omega\varepsilon E_z^i(\rho=a)} \tag{12-123}$$

where for observations along the center of the wire ($\rho = 0$)

$$R = \sqrt{a^2+(z-z')^2} \tag{12-123a}$$

In (12-121) or (12-123) $I(z')$ represents the equivalent filamentary line-source current located on the surface of the wire, as shown in Figure 12-23*b*, and it is obtained by knowing the incident electric field at the surface of the wire. By point-matching techniques this is solved by matching the boundary conditions at discrete points on the surface of the wire. Often it is easier to choose the matching points to be at the interior of the wire, especially along the axis as shown in Figure 12-24*a*, where $I_z(z')$ is located on the surface of the wire. By reciprocity the configuration of Figure 12-24*a* is analogous to that of Figure 12-24*b* where the equivalent filamentary line-source current is assumed to be located along the center axis of the wire and the matching points are selected on the surface of the wire. Either of the two configurations can be used to determine the equivalent filamentary line-source current $I_z(z')$; the choice is left to the individual.

12.4.2 Hallén's Integral Equation

Referring again to Figure 12-23*a* let us assume that the length of the cylinder is much larger than its radius ($\ell \gg a$) and its radius is much smaller than the wavelength ($a \ll \lambda$) so that the effects of the end faces of the cylinder can be neglected. Therefore the boundary conditions for a wire with infinite conductivity are those of vanishing total tangential E fields on the surface of the cylinder and vanishing current at the ends of the cylinder [$I_z(z' = \pm\ell/2) = 0$].

Since only an electric current density flows on the cylinder and it is directed

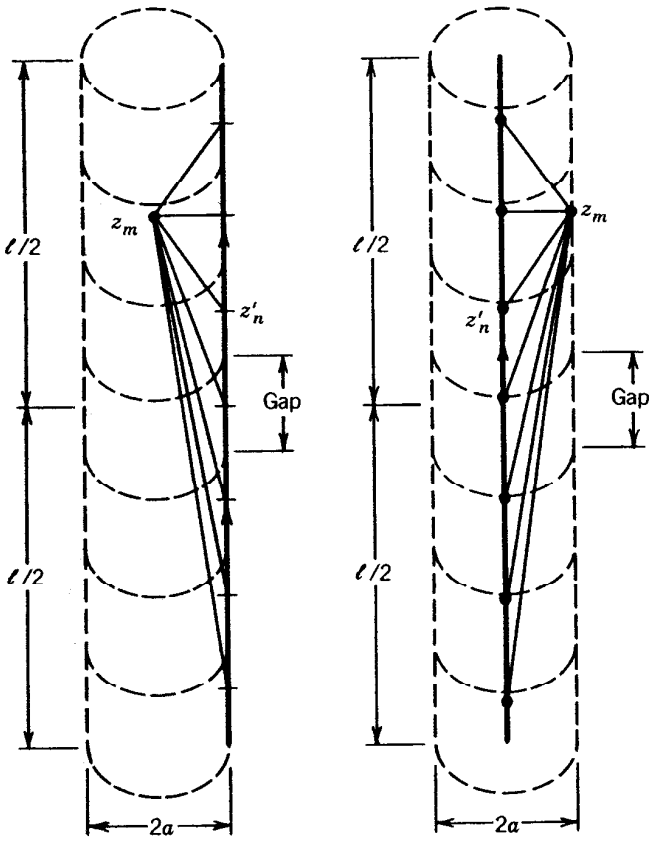

FIGURE 12-24 Dipole segmentation and its equivalent current (a) on the surface and (b) along its center.

along the z axis ($\mathbf{J} = \hat{a}_z J_z$), then according to (6-30) and (6-96a) $\mathbf{A} = \hat{a}_z A_z(z')$, which for small radii is assumed to be only a function of z'. Thus (6-34) reduces for $\mathbf{F} = 0$ to

$$E_z^t = -j\omega A_z - j\frac{1}{\omega\mu\varepsilon}\frac{\partial^2 A_z}{\partial z^2} = -j\frac{1}{\omega\mu\varepsilon}\left[\frac{d^2 A_z}{dz^2} + \omega^2\mu\varepsilon A_z\right] \tag{12-124}$$

Since the total tangential electric field E_z^t vanishes on the surface of the cylinder, (12-124) reduces to

$$\frac{d^2 A_z}{dz^2} + \beta^2 A_z = 0 \tag{12-124a}$$

Because the current density on the cylinder is symmetrical [$J_z(z') = J_z(-z')$], the potential A_z is also symmetrical [i.e., $A_z(z') = A_z(-z')$]. Thus the solution of (12-124a) is given by

$$A_z(z) = -j\sqrt{\mu\varepsilon}\left[B_1 \cos(\beta z) + C_1 \sin(\beta|z|)\right] \tag{12-125}$$

where B_1 and C_1 are constants. For a current-carrying wire, its potential is also

given by (6-97a). Equating (12-125) to (6-97a) leads to

$$\boxed{\int_{-\ell/2}^{+\ell/2} I_z(z') \frac{e^{-j\beta R}}{4\pi R}\, dz' = -j\sqrt{\frac{\varepsilon}{\mu}} \left[B_1 \cos(\beta z) + C_1 \sin(\beta|z|)\right]} \quad (12\text{-}126)$$

If a voltage V_i is applied at the input terminals of the wire, it can be shown that the constant $C_1 = V_i/2$. The constant B_1 is determined from the boundary condition that requires the current to vanish at the end points of the wire.

Equation 12-126 is referred to as *Hallén's integral equation* for a perfectly conducting wire. It was derived by solving the differential equation 6-34 or 12-124a with the enforcement of the appropriate boundary conditions.

12.4.3 Source Modeling

Let us assume that the wire of Figure 12-23 is symmetrically fed by a voltage source, as shown in Figure 12-25*a*, and the element acting as a dipole antenna. To use, for example, Pocklington's integrodifferential equation 12-121 or 12-123 we need to know how to express $E_z^i(\rho = a)$. Traditionally there have been two methods used to model the excitation to represent $E_z^i(\rho = a, 0 \le \phi \le 2\pi, -\ell/2 \le z \le +\ell/2)$ at all points on the surface of the dipole: One is referred to as the *delta-gap* excitation and the other as the *equivalent magnetic ring current* (better known as *magnetic frill generator*) [37].

A. DELTA GAP

The delta-gap source modeling is the simplest and most widely used of the two, but it is also the least accurate, especially for impedances. Usually it is most accurate for smaller width gaps. Using the delta gap, it is assumed that the excitation voltage at the feed terminals is of a constant V_i value, and zero elsewhere. Therefore the incident electric field $E_z^i(\rho = a, 0 \le \phi \le 2\pi, -\ell/2 \le z \le +\ell/2)$ is also a constant (V_i/Δ where Δ is the gap width) over the feed gap and zero elsewhere, hence the name delta gap. For the delta-gap model, the feed gap Δ of Figure 12-25*a* is replaced by a narrow band of strips of equivalent magnetic current density of

$$\mathbf{M}_i = -\hat{n} \times \mathbf{E}^i = -\hat{a}_\rho \times \hat{a}_z \frac{V_i}{\Delta} = \hat{a}_\phi \frac{V_i}{\Delta} \qquad -\frac{\Delta}{2} \le z' \le \frac{\Delta}{2} \quad (12\text{-}127)$$

The magnetic current density $\mathbf{M}_i$ is sketched in Figure 12-25*a*.

B. MAGNETIC FRILL GENERATOR

The magnetic frill generator was introduced to calculate the near- as well as the far-zone fields from coaxial apertures [37]. To use this model the feed gap is replaced with a circumferentially directed magnetic current density that exists over an annular aperture with inner radius a, which is usually chosen to be the radius of the wire, and an outer radius b, as shown in Figure 12-25*b*. Since the dipole is usually fed by transmission lines, the outer radius b of the equivalent annular aperture of the magnetic frill generator is found using the expression for the characteristic impedance of the transmission line.

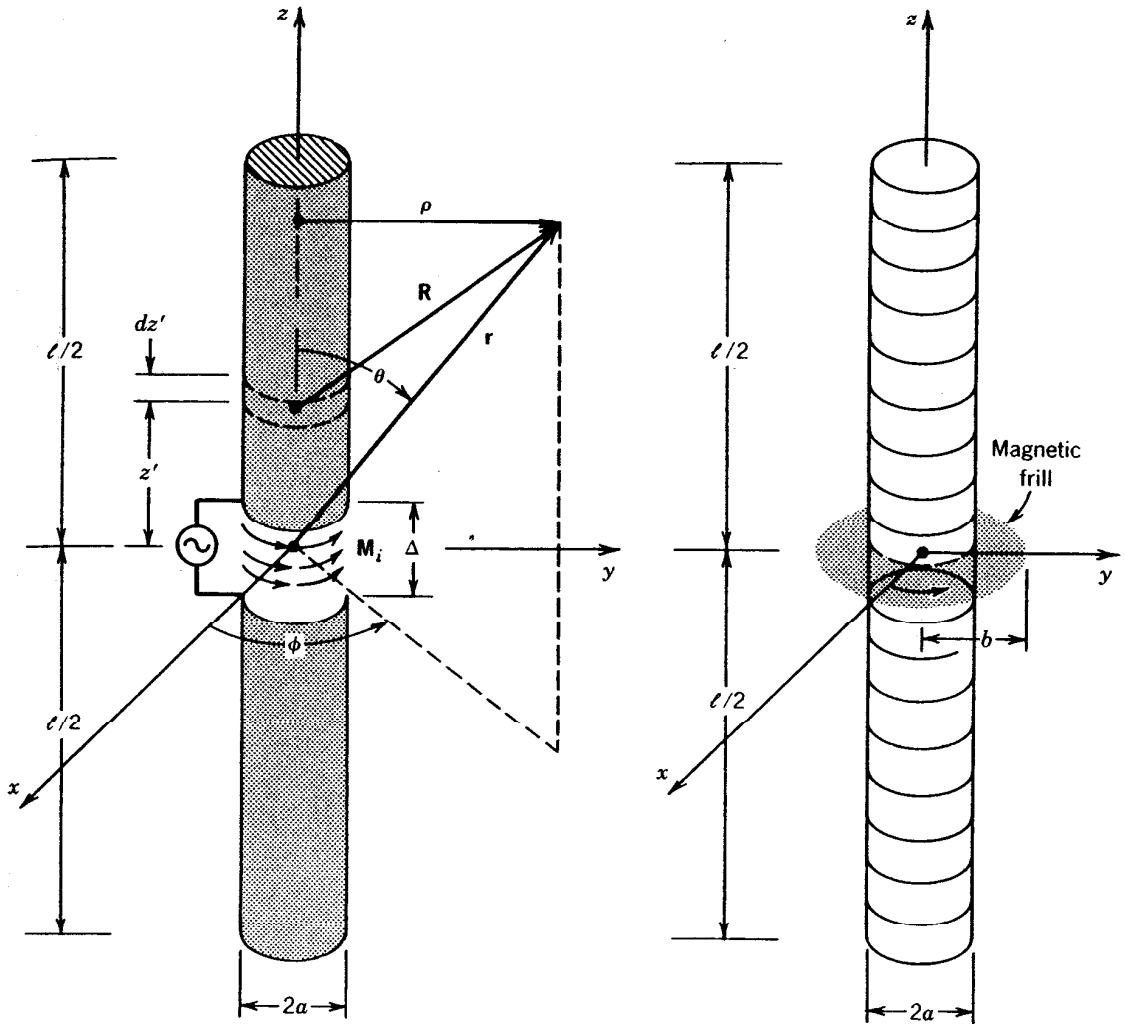

FIGURE 12-25 Cylindrical dipole, its segmentation, and gap modeling. (*Source:* C. A. Balanis, *Antenna Theory: Analysis and Design*, copyright © 1982, John Wiley & Sons, Inc. Reprinted by permission of John Wiley & Sons, Inc.) (*a*) Cylindrical dipole. (*b*) Segmented dipole.

Over the annular aperture of the magnetic frill generator the electric field is represented by the TEM mode field distribution of a coaxial transmission line given by

$$\mathbf{E}_f = \hat{a}_\rho \frac{V_i}{2\rho' \ln(b/a)} \tag{12-128}$$

Therefore the corresponding equivalent magnetic current density $\mathbf{M}_f$ for the magnetic frill generator used to represent the aperture is equal to

$$\mathbf{M}_f = -2\hat{n} \times \mathbf{E}_f = -2\hat{a}_z \times \hat{a}_\rho E_\rho = -\hat{a}_\phi \frac{V_i}{\rho' \ln(b/a)} \tag{12-129}$$

The fields generated by the magnetic frill generator of (12-129) on the surface of the wire are found using [37]

$$E_z^i\left(\rho = a, 0 \le \phi \le 2\pi, -\frac{\ell}{2} \le z \le \frac{\ell}{2}\right)$$

$$= -V_i\left(\frac{\beta(b^2-a^2)e^{-j\beta R_0}}{8\ln(b/a)R_0^2}\left\{2\left[\frac{1}{\beta R_0} + j\left(1 - \frac{b^2-a^2}{2R_0^2}\right)\right]\right.\right.$$

$$\left.\left. + \frac{a^2}{R_0}\left[\left(\frac{1}{\beta R_0} + j\left(1 - \frac{(b^2+a^2)}{2R_0^2}\right)\right)\left(-j\beta - \frac{2}{R_0}\right) + \left(-\frac{1}{\beta R_0^2} + j\frac{b^2+a^2}{R_0^3}\right)\right]\right\}\right) \quad (12\text{-}130)$$

where

$$R_0 = \sqrt{z^2 + a^2} \quad (12\text{-}130a)$$

The fields generated on the surface of the wire computed using (12-130) can be approximated by those found along the axis ($\rho = 0$). Doing this leads to a simpler expression of the form [37]

$$E_z^i\left(\rho = 0, -\frac{\ell}{2} \le z \le \frac{\ell}{2}\right) = -\frac{V_i}{2\ln(b/a)}\left[\frac{e^{-j\beta R_1}}{R_1} \quad \frac{e^{-j\beta R_2}}{R_2}\right] \quad (12\text{-}131)$$

where

$$R_1 = \sqrt{z^2 + a^2} \quad (12\text{-}131a)$$

$$R_2 = \sqrt{z^2 + b^2} \quad (12\text{-}131b)$$

To compare the results using the two source modelings (delta gap and magnetic frill generator), an example will be performed.

Example 12-7. Assume a center-fed linear dipole of $\ell = 0.47\lambda$ and $a = 0.005\lambda$.

1. Determine the voltage and normalized current distribution over the length of the dipole using $N = 21$ segments to subdivide the length. Plot the current distribution.
2. Determine the input impedance using segments of $N = 7, 11, 21, 29, 41, 51, 61, 71$, and 79.

Use Pocklington's integrodifferential equation 12-123 with piecewise constant subdomain basis functions and point matching to solve the problems, model the gap with one segment, and use both the delta gap and magnetic frill generator to model the excitation. Use (12-131) for the magnetic frill generator. Because the current at the ends of the wire vanishes, the piecewise constant subdomain basis functions are not the most judicious choice. However, because of their simplicity, they are chosen here to illustrate the principles even though the results are not the most accurate. Assume that the characteristic impedance of the annular aperture is 50 ohms and the excitation voltage V_i is 1 V.

Solution.

1. Since the characteristic impedance of the annular aperture is 50 ohms, then

$$Z_c = \sqrt{\frac{\mu_0}{\varepsilon_0}}\,\frac{\ln(b/a)}{2\pi} = 50 \Rightarrow \frac{b}{a} = 2.3$$

Subdividing the total length ($\ell = 0.47\lambda$) of the dipole to 21 segments makes the gap and each segment equal to

$$\Delta = \frac{0.47\lambda}{21} = 0.0224\lambda$$

Using (12-131) to compute E_z^i, the corresponding induced voltages obtained by multiplying the value of $-E_z^i$ at each segment by the length of the segment are found listed in Table 12-1, where they are compared with those of the delta gap. $N = 1$ represents the outermost segment and $N = 11$ represents the center segment. Because of the symmetry, only values for the center segment and half of the other segments are shown. Although the two distributions are not identical, the magnetic frill distribution voltages decay quite rapidly away from the center segment and they very quickly reach almost vanishing values.

The corresponding unnormalized and normalized currents are obtained using (12-123) with piecewise constant pulse functions and the point-matching technique for both the delta gap and magnetic frill generator.

TABLE 12-1
Unnormalized and normalized dipole induced voltage[a] differences for delta gap and magnetic frill generator ($\ell = 0.47\lambda$, $a = 0.005\lambda$, $N = 21$)

Segment number	Delta gap voltage		Magnetic frill generator voltage	
n	Unnormalized	Normalized	Unnormalized	Normalized
1	0	0	$1.11 \times 10^{-4} \angle -26.03°$	$7.30 \times 10^{-5} \angle -26.03°$
2	0	0	$1.42 \times 10^{-4} \angle -20.87°$	$9.34 \times 10^{-5} \angle -20.87°$
3	0	0	$1.89 \times 10^{-4} \angle -16.13°$	$1.24 \times 10^{-4} \angle -16.13°$
4	0	0	$2.62 \times 10^{-4} \angle -11.90°$	$1.72 \times 10^{-4} \angle -11.90°$
5	0	0	$3.88 \times 10^{-4} \angle -8.23°$	$2.55 \times 10^{-4} \angle -8.23°$
6	0	0	$6.23 \times 10^{-4} \angle -5.22°$	$4.10 \times 10^{-4} \angle -5.22°$
7	0	0	$1.14 \times 10^{-3} \angle -2.91°$	$7.5 \times 10^{-4} \angle -2.91°$
8	0	0	$2.52 \times 10^{-3} \angle -1.33°$	$1.66 \times 10^{-3} \angle -1.33°$
9	0	0	$7.89 \times 10^{-3} \angle -0.43°$	$5.19 \times 10^{-3} \angle -0.43°$
10	0	0	$5.25 \times 10^{-2} \angle -0.06°$	$3.46 \times 10^{-2} \angle -0.06°$
11	1	1	$1.52 \angle 0°$	$1.0 \angle 0°$

[a]Voltage differences as defined here represent the product of the incident electric field at the center of each segment and the corresponding segment length.

TABLE 12-2
Dipole input impedance for delta gap and magnetic frill generator using Pocklington's integral equation ($\ell = 0.47\lambda$, $a = 0.005\lambda$)

N	Delta gap	Magnetic frill
7	$122.8 + j113.9$	$26.8 + j24.9$
11	$94.2 + j49.0$	$32.0 + j16.7$
21	$77.7 - j0.8$	$47.1 - j0.2$
29	$75.4 - j6.6$	$57.4 - j4.5$
41	$75.9 - j2.4$	$68.0 - j1.0$
51	$77.2 + j2.4$	$73.1 + j4.0$
61	$78.6 + j6.1$	$76.2 + j8.5$
71	$79.9 + j7.9$	$77.9 + j11.2$
79	$80.4 + j8.8$	$78.8 + j12.9$

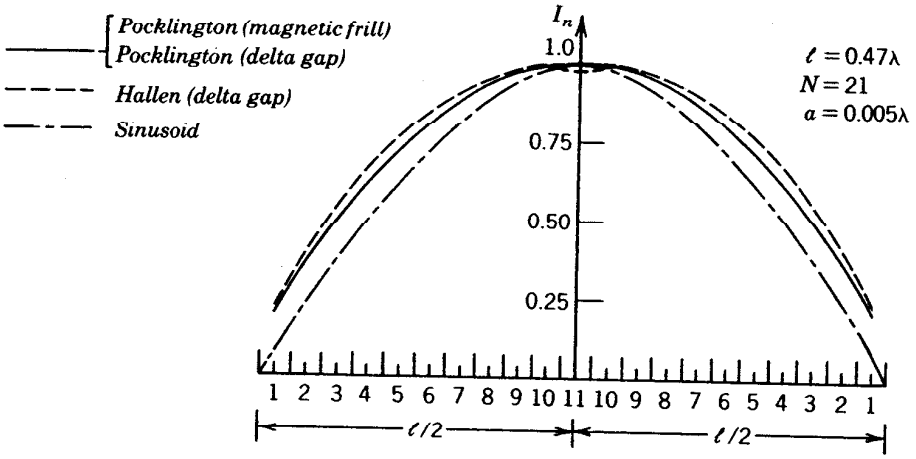

FIGURE 12-26 Current distribution along a dipole antenna.

The normalized magnitudes of the se currents are shown plotted in Figure 12-26. It is apparent that the two distributions are almost identical in shape, and they resemble that of the ideal sinusoidal current distribution which is more valid for very thin wires and very small gaps. The distributions obtained using Pocklington's integral equation do not vanish at the ends because of the use of piecewise constant subdomain basis functions.

2. The input impedances computed using both the delta gap and the magnetic frill generator are shown listed in Table 12-2. It is evident that the values begin to stabilize and compare favorably to each other once 61 or more segments are used.

12.5 COMPUTER CODES

With the advent of the computer there has been a proliferation of computer program development. Many of these programs are based on algorithms that are suitable for efficient computer programming for the analysis and synthesis of

electromagnetic boundary-value problems. Some of these computer programs are very sophisticated and can be used to solve complex radiation and scattering problems. Others are much simpler and have limited applications. Many programs are public domain; others are restricted.

Five computer programs based on integral equation formulations and moment method solutions will be described here. The first computes the radiation or scattering by a two-dimensional perfectly electric conducting (PEC) body. It is referred to here as TDRS (two-dimensional radiation and scattering), and it is based on the two-dimensional formulations of the electric field integral equation (EFIE) of Section 12.3.1. It can be used for both electric and magnetic line-source excitation or TM^z and TE^z plane wave incidence. The listing of this program is included in the solutions manual available to the instructors. It can also be obtained from the author. The second program, referred to here as PWRS (Pocklington's wire radiation and scattering) is based on Pocklington's integral equation of Section 12.4.1, and it is used for both radiation and scattering by a perfect electric conducting (PEC) wire. The listing of this program is found at the end of this chapter.

The remaining three programs are more general, public domain moment method programs. A very brief description of these programs is given here. Information as to where these programs can be obtained is also included. It should be stated, however, that there are numerous other codes, public domain and restricted, that utilize moment method and other techniques, such as geometrical optics, geometrical theory of diffraction, physical optics, and physical theory of diffraction, which are too numerous to mention here.

12.5.1 Two-Dimensional Radiation and Scattering

The two-dimensional radiation and scattering (TDRS) program is used to analyze four different two-dimensional perfectly electric conducting problems: the strip, and the circular, elliptical, and rectangular cylinders. The algorithm is based on the electric field integral equation of Section 12.3.1, and it is used for both electric and magnetic line-source excitation, or plane wave incidence of arbitrary polarization. For simplicity, piecewise constant pulse expansion functions and point-matching techniques have been adopted. The listing of this program is included in the solutions manual available to the instructors. It can also be obtained from the author.

A. STRIP

For the strip problem, the program can analyze either of the following:

1. A line source (electric or magnetic). It computes the electric current density over the width of the strip and the normalized radiation amplitude pattern (in decibels) for $0° \leq \phi \leq 360°$. The user must specify the width of the strip (in wavelengths), the type of line source (either electric or magnetic), and the location x_s, y_s of the source (in wavelengths).
2. Plane wave incidence of arbitrary polarization. The program can analyze either monostatic or bistatic scattering.

For monostatic scattering the program computes the two-dimensional normalized (with respect to λ) monostatic SW $\sigma_{2\text{-D}}/\lambda$ (in decibels) for all angles of

incidence ($0° \leq \phi \leq 360°$). The program starts at $\phi = 0°$ and then completes the entire 360° monostatic scattering pattern. The user must specify the width w of the strip (in wavelengths) and the polarization angle θ_p (in degrees) of the incident plane wave. The polarization of the incident wave is specified by the direction θ_p of the incident electric field relative to the z axis ($\theta_p = 0°$ implies TM^z; $\theta_p = 90°$ implies TE^z; otherwise arbitrary polarization). The polarization angle θ_p needs to be specified only when the polarization is neither TM^z nor TE^z.

For bistatic scattering, the program computes for the specified incidence angle the current density over the width of the strip and the two-dimensional normalized (with respect to λ) bistatic SW $\sigma_{2\text{-D}}/\lambda$ (in decibels) for all angles of observation ($0° \leq \phi_s \leq 360°$). The user must specify the width w of the strip (in wavelengths), the angle of incidence ϕ_i (in degrees), and the polarization angle θ_p (in degrees) of the incident plane wave. The polarization angle of the incident wave is specified in the same manner as for the monostatic case.

B. CIRCULAR, ELLIPTICAL, OR RECTANGULAR CYLINDER

For the cylinder program, the program can analyze either a line source (electric or magnetic) or plane wave scattering of arbitrary polarization by a two-dimensional circular, or elliptical or rectangular cylinder.

1. For the line source excitation, the program computes the current distribution over the entire surface of the cylinder and the normalized radiation amplitude pattern (in decibels). The user must specify for each cylinder the type of line source (electric or magnetic), the location x_s, y_s of the line source, and the size of the cylinder. For the circular cylinder the size is specified by its radius a (in wavelengths) and for the elliptical and rectangular cylinders by the principal semiaxes lengths a and b (in wavelengths), with a measured along the x axis and b along the y axis.
2. For the plane wave incidence the program computes monostatic or bistatic scattering of arbitrary polarization by a circular, elliptical, or rectangular cylinder.

For monostatic scattering the program computes the two-dimensional normalized (with respect to λ) monostatic SW $\sigma_{2\text{-D}}/\lambda$ (in decibels) for all angles of incidence ($0° \leq \phi \leq 360°$). The program starts at $\phi = 0°$ and then computes the entire 360° monostatic scattering pattern. The user must specify the size of the cylinder, as was done for the line-source excitation, and the polarization angle θ_p (in degrees) of the incident plane wave. The polarization of the incident wave is specified by the direction θ_p of the incident electric field relative to the z axis ($\theta_p = 0°$ implies TM^z; $\theta_p = 90°$ implies TE^z; otherwise arbitrary polarization). The polarization angle θ_p needs to be specified only when the polarization is neither TM^z nor TE^z.

For bistatic scattering, the program computes for the specified incidence angle the current density over the entire surface of the cylinder and the two-dimensional normalized (with respect to λ) bistatic SW $\sigma_{2\text{-D}}/\lambda$ (in decibels) for all angles of observation ($0° \leq \phi_s \leq 360°$). The user must specify the size of the cylinder, as was done for the line-source excitation, the incidence angle ϕ_i (in degrees), and the polarization angle θ_p (in degrees) of the incident plane wave. The polarization angle of the incident wave is specified in the same manner as for the monostatic case.

12.5.2 Pocklington's Wire Radiation and Scattering

Pocklington's wire radiation and scattering (PWRS) program computes the radiation characteristics of a center-fed wire antenna and the scattering characteristics of a perfectly electric conducting (PEC) wire, each of radius a and length ℓ. Both are based on Pocklington's integral equation 12-123.

A. RADIATION

For the wire antenna of Figure 12-25 the excitation is modeled by either a delta gap or a magnetic frill feed modeling, and it computes the current distribution, normalized amplitude radiation pattern, and the input impedance. The user must specify the length of the wire, its radius (both in wavelengths), and the type of feed modeling (delta gap or magnetic frill). A computer program based on Hallén's integral equation can be found at the end of Chapter 7 of [24].

B. SCATTERING

The geometry for the plane wave scattering by the wire is shown in Figure 12-23(a). The program computes the monostatic or bistatic scattering of arbitrary polarization.

For monostatic scattering the program computes the normalized (with respect to m^2) RCS $\sigma_{3\text{-D}}/m^2$ (in dBsm) for all angles of incidence ($0° \leq \theta_i \leq 180°$). The program starts at $\theta_i = 0°$ and then computes the entire 180° monostatic scattering pattern. The user must specify the length and radius of the wire (both in wavelengths) and the polarization angle θ_p (in degrees) of the incident plane wave. The polarization of the incident wave is specified by the direction θ_p of the incident electric field relative to the plane of incidence, where the plane of incidence is defined as the plane that contains the vector of the incident wave and the wire scatterer ($\theta = 0°$ implies that the electric field is on the plane of incidence; $\theta = 90°$ implies that the electric field is perpendicular to the plane of incidence and to the wire; thus no scattering occurs for this case).

For bistatic scattering, the program computes for the specified incidence angle the current distribution over the length of the wire and the normalized (with respect to m^2) bistatic RCS $\sigma_{3\text{-D}}/m^2$ (in dBsm) for all angles of observation ($0° \leq \theta_s \leq 180°$). The user must specify the length and radius of the wire (both in wavelengths), the angle of incidence θ_i (in degrees), and the polarization angle θ_p of the incident plane wave. The polarization angle is specified in the same manner as for the monostatic case.

12.5.3 Numerical Electromagnetics Code

The numerical electromagnetics code (NEC) [38] is a user-oriented program developed at Lawrence Livermore Laboratory. It is a moment method code for analyzing the interaction of electromagnetic waves with arbitrary structures consisting of conducting wires and surfaces. It combines an integral equation for smooth surfaces with one for wires to provide convenient and accurate modeling for a wide range of applications. The code can model nonradiating networks and transmission lines, perfect and imperfect conductors, lumped element loading, and perfect and imperfect conducting ground planes. It uses the electric field integral equation (EFIE) for thin wires and the magnetic field integral equation (MFIE) for surfaces. The

excitation can be either an applied voltage source or an incident plane wave. The program computes induced currents and charges, near- or far-zone electric and magnetic fields, radar cross section, impedances or admittances, gain and directivity, power budget, and antenna to antenna coupling.

Information concerning the code and its availability can be directed to:

Professor Richard W. Adler
Naval Postgraduate School
Code 62 AB
Monterey, California 93943

12.5.4 Mini-Numerical Electromagnetics Code

The mini-numerical electromagnetics code (MININEC) [39, 40] is a user-oriented compact version of NEC developed at the Naval Ocean Systems Center. It is also a moments method code, but coded in BASIC, and has retained the most frequently used options of NEC. It is intended to be used in mini, micro, and personal computers, and it is most convenient to analyze wire antennas. It computes currents, and near- and far-field patterns. It also optimizes the feed excitation voltages that yield a desired radiation patterns.

Information concerning the MININEC and its availability can be directed to:

Professor Richard W. Adler
Naval Postgraduate School
Code 62 AB
Monterey, California 93943

or

Artech House, Inc.
685 Canton Street
Norwood, Massachusetts 02062

12.5.5 Electromagnetic Surface Patch Code

The electromagnetic surface patch (ESP) [41] code is a user-oriented program developed at the ElectroScience Laboratory at Ohio State University. It is a moment method, surface patch code based on the piecewise sinusoidal reaction formulation, which is basically equivalent to the electric field integral equation (EFIE). It can treat (perfectly conducting or thin dielectric) geometries that consist of thin wires, rectangular or polygonal plates, wire-plate or plate-plate attachments, and open or closed surfaces. The excitation can be either by a delta gap voltage generator or an incident plane wave. The program computes current distribution, input impedance, radiation efficiency, mutual coupling, near- or far-field gain patterns, and near- or far-field radar cross section patterns. ESP also incorporates an efficient impedance matrix interpolation scheme for obtaining data over a wide frequency bandwidth [42].

Information concerning the code and its availability can be directed to:

Dr. Edward H. Newman
The Ohio State University
ElectroScience Laboratory
1320 Kinnear Road
Columbus, Ohio 43212

REFERENCES

1. R. F. Harrington, "Matrix methods for field problems," *Proc. IEEE*, vol. 55, no. 2, pp. 136–149, February 1967.
2. R. F. Harrington, *Field Computation By Moment Methods*, Macmillan, New York, 1968.
3. J. H. Richmond, "Digital computer solutions of the rigorous equations for scattering problems," *Proc. IEEE*, vol. 53, pp. 796–804, August 1965.
4. L. L. Tsai, "Moment methods in electromagnetics for undergraduates," *IEEE Trans. on Education*, vol. E-21, no. 1, pp. 14–22, February 1978.
5. R. Mittra (Ed.), *Computer Techniques for Electromagnetics*, Pergamon, New York, 1973.
6. J. Moore and R. Pizer, *Moment Methods in Electromagnetics*, Wiley, New York, 1984.
7. P. Y. Ufimtsev, "Method of edge waves in the physical theory of diffraction," translated by U.S. Air Force Foreign Technology Division, Wright-Patterson AFB, Ohio, September 1971.
8. P. Y. Ufimtsev, "Approximate computation of the diffraction of plane electromagnetic waves at certain metal bodies," *Sov. Phys.–Tech. Phys.*, vol. 27, pp. 1708–1718, 1957.
9. P. Y. Ufimtsev, "Secondary diffraction of electromagnetic waves by a strip," *Sov. Phys.–Tech. Phys.*, vol. 3, pp. 535–548, 1958.
10. K. M. Mitzner, "Incremental length diffraction coefficients," Tech. Rep. AFAL-TR-73-296, Northrop Corp., Aircraft Division, April 1974.
11. E. F. Knott and T. B. A. Senior, "Comparison of three high-frequency diffraction techniques," *Proc. IEEE*, vol. 62, no. 11, pp. 1468–1474, November 1974.
12. E. F. Knott, "A progression of high-frequency RCS prediction techniques," *Proc. IEEE*, vol. 73, no. 2, pp. 252–264, February 1985.
13. T. Griesser and C. A. Balanis, "Backscatter analysis of dihedral corner reflectors using physical optics and the physical theory of diffraction," *IEEE Trans. Antennas Propagat.*, vol. AP-35, no. 10, pp. 1137–1147, October 1987.
14. J. B. Keller, "Diffraction by an aperture," *J. Appl. Phys.*, vol. 28, no. 4, pp. 426–444, April 1957.
15. J. B. Keller, "Geometrical theory of diffraction," *J. Opt. Soc. Amer.*, vol. 52, no. 2, pp. 116–130, February 1962.
16. R. G. Kouyoumjian and P. H. Pathak, "A uniform geometrical theory of diffraction for an edge in a prefectly conducting surface," *Proc. IEEE*, vol. 62, no. 11, pp. 1448–1461, November 1974.
17. G. L. James, *Geometrical Theory of Diffraction for Electromagnetic Waves*, Third Edition Revised, Peregrinus, London, 1986.
18. J. D. Lilly, "Application of the moment method to antenna analysis," MSEE Thesis, Department of Electrical Engineering, West Virginia University, 1980.
19. J. D. Lilly and C. A. Balanis, "Current distributions, input impedances, and radiation patterns of wire antennas," North American Radio Science Meeting of URSI, Université Laval, Quebec, Canada, June 2–6, 1980.
20. D. K. Cheng, *Field and Wave Electromagnetics*, Addison-Wesley, Reading, Mass., 1983, p. 88.

21. R. Mittra and C. A. Klein, "Stability and convergence of moment method solutions," in *Numerical and Asymptotic Techniques in Electromagnetics*, R. Mittra (Ed.), Springer-Verlag, New York, 1975, Chapter 5, pp. 129–163.
22. T. K. Sarkar, "A note on the choice weighting functions in the method of moments," *IEEE Trans. Antennas Propagat.*, vol. AP-33, no. 4, pp. 436–441, April 1985.
23. T. K. Sarkar, A. R. Djordjević, and E. Arvas, "On the choice of expansion and weighting functions in the numerical solution of operator equations," *IEEE Trans. Antennas Propagat.*, vol. AP-33, no. 9, pp. 988–996, September 1985.
24. C. A. Balanis, *Antenna Theory: Analysis and Design*, Wiley, New York, 1982.
25. E. K. Miller and F. J. Deadrick, "Some computational aspects of thin-wire modeling," in *Numerical and Asymptotic Techniques in Electromagnetics*, R. Mittra (Ed.), Springer-Verlag, New York, 1975, Chapter 4, pp. 89–127.
26. L. Kantorovich and G. Akilov, *Functional Analysis in Normed Spaces*, Pergamon, Oxford, pp. 586–587, 1964.
27. D. P. Marsland, C. A. Balanis, and S. Brumley, "Higher order diffractions from a circular disk," *IEEE Trans. Antennas Propagat.*, vol. AP-35, no. 12, pp. 1436–1444, December 1987.
28. H. C. Pocklington, "Electrical oscillations in wire," *Cambridge Philos. Soc. Proc.*, vol. 9, pp. 324–332, 1897.
29. E. Hallén, "Theoretical investigations into the transmitting and receiving qualities of antennae," *Nova Acta Regiae Soc. Sci. Upsaliensis*, Ser. IV, no. 4, pp. 1–44, 1938.
30. R. King and C. W. Harrison, Jr., "The distribution of current along a symmetrical center-driven antenna," *Proc. IRE*, vol. 31, pp. 548–567, October 1943.
31. J. H. Richmond, "A wire-grid model for scattering by conducting bodies," *IEEE Trans. Antennas Propagat.*, vol. AP-14, no. 6, pp. 782–786, November 1966.
32. G. A. Thiele, "Wire antennas," in *Computer Techniques for Electromagnetics*, R. Mittra (Ed.), Pergamon, New York, Chapter 2, pp. 7–70, 1973.
33. C. M. Butler and D. R. Wilton, "Evaluation of potential integral at singularity of exact kernel in thin-wire calculations," *IEEE Trans. Antennas Propagat.*, vol. AP-23, no. 2, pp. 293–295, March 1975.
34. L. W. Pearson and C. M. Butler, "Inadequacies of collocation solutions to Pocklington-type models of thin-wire structures," *IEEE Trans. Antennas Propagat.*, vol. AP-23, no. 2, pp. 293–298, March 1975.
35. C. M. Butler and D. R. Wilton, "Analysis of various numerical techniques applied to thin-wire scatterers," *IEEE Trans. Antennas Propagat.*, vol. AP-23, no. 4, pp. 534–540, July 1975.
36. D. R. Wilton and C. M. Butler, "Efficient numerical techniques for solving Pocklington's equation and their relationships to other methods," *IEEE Trans. Antennas Propagat.*, vol. AP-24, no. 1, pp. 83–86, January 1976.
37. L. L. Tsai, "A numerical solution for the near and far fields of an annular ring of magnetic current," *IEEE Trans. Antennas Propagat.*, vol. AP-20, no. 5, pp. 569–576, September 1972.
38. G. J. Burke and A. J. Poggio, "Numerical electromagnetics code (NEC)–method of moments," Technical Document 116, Naval Ocean Systems Center, San Diego, Calif., January 1981.
39. A. J. Julian, J. M. Logan, and J. W. Rockway, "MININEC: A mini-numerical electromagnetics code," Technical Document 516, Naval Ocean Systems Center, San Diego, Calif., September 6, 1982.
40. J. Rockway, J. Logan, D. Tam, and S. Li, *The MININEC SYSTEM: Microcomputer Analysis of Wire Antennas*, Artech House, Inc., 1988.
41. E. H. Newman and D. L. Dilsavor, "A user's manual for the electromagnetic surface patch code: ESP version III," Technical Report No. 716148-19, ElectroScience Laboratory, The Ohio State University, May 1987.
42. E. H. Newman, "Generalization of wideband data from the method of moments by interpolating the impedance matrix," *IEEE Trans. Antennas Propagat.*, to be published.

PROBLEMS

12.1. A circular loop of radius $a = 0.2$ m is constructed out of a wire of radius $b = 10^{-3}$ m, as shown in Figure P12-1. The entire loop is maintained at a constant potential of 1 V. Using integral equation techniques, determine and plot for $0° \leq \phi \leq 360°$ the surface charge density on the wire. Assume that at any given angle the charge is uniformly distributed along the circumference of the wire.

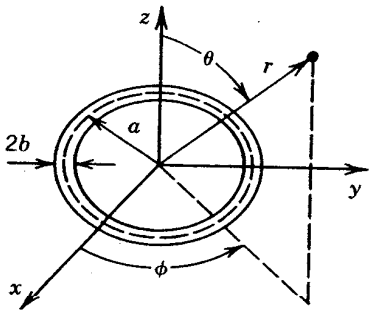

FIGURE P12-1

12.2. Repeat Problem 12.1 when the loop is split into two parts; one part (from 0 to 180°) is maintained at a constant potential of 1 V and the other part (from 180 to 360°) is maintained at a constant potential of 2 V.

12.3. Repeat Example 12.3 for a strip with $w = 2\lambda$, $h = 0.25\lambda$, and $t = 0.01\lambda$.

12.4. An infinite electric line source of constant current I_e is placed next to a circular conducting cylinder of radius a, as shown in Figure P12-4. The line source is positioned a distance b ($b > a$) from the center of the cylinder. Use the EFIE, piecewise constant subdomain basis functions, and point-matching techniques.

(a) Formulate the problem current density induced on the surface of the cylinder.
(b) Compute the induced current density when $a = 5\lambda$ and $b = 5.25\lambda$. Assume a unity line-source current. Compare with the modal solution current density of (11-168a).
(c) Compute for part b the normalized far-zone amplitude pattern (in decibels). Normalize so that the maximum is 0 dB.

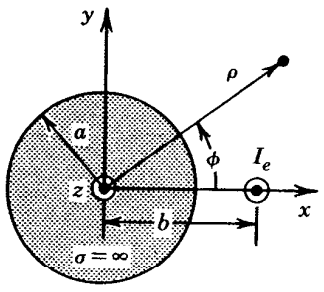

FIGURE P12-4

12.5. Repeat Problem 12.4 for $a = 5\lambda$ and $b = 5.5\lambda$.

12.6. An infinite electric line source of constant current I_e is placed next to a rectangular cylinder of dimensions a and b, as shown in the Figure P12-6. The line source is positioned a distance c ($c > a$) from the center of the cylinder along the x axis. Use

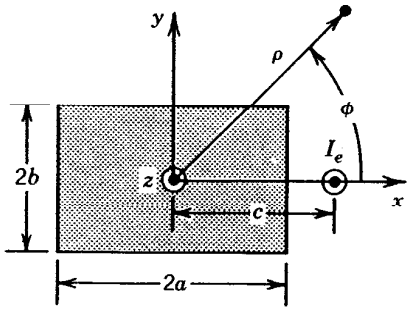

FIGURE P12-6

the EFIE and piecewise subdomain basis functions and point-matching techniques, and do the following.

(a) Compute the induced current on the surface of the cylinder when $a = 5\lambda$, $b = 2.5$, and $c = 5.25\lambda$. Assume a unity line-source current.
(b) Compute for part a the normalized far-zone amplitude pattern (in decibels). Normalize so that the maximum is 0 dB.

12.7. Repeat Problem 12.6 for an electric line source near an elliptic cylinder with $a = 5\lambda$, $b = 2.5\lambda$, and $c = 5.25\lambda$.

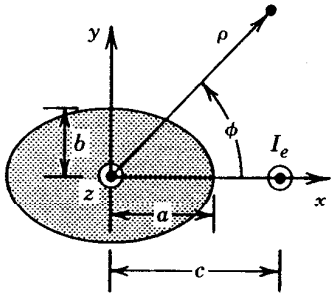

FIGURE P12-7

12.8. A TM^z uniform plane wave traveling in the $+x$ direction is normally incident upon a conducting circular cylinder of radius a, as shown in Figure P12-8. Use the EFIE, piecewise constant subdomain basis functions, and point-matching techniques, write your own program, and do the following.

(a) Plot the current density induced on the surface of the cylinder when $a = 2\lambda$. Assume the incident field is of unity amplitude. Compare with the modal solution current density of (11-97).
(b) Plot the normalized $\sigma_{2\text{-D}}/\lambda$ bistatic scattering width (in decibels) for $0° \leq \phi \leq 360°$ when $a = 2\lambda$. Compare with the modal solution of (11-102).

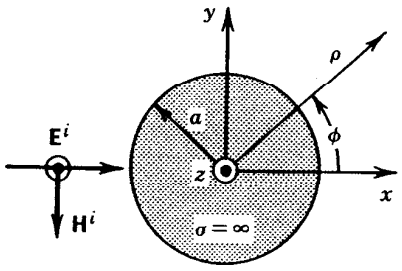

FIGURE P12-8

12.9. A TM^z uniform plane wave traveling in the $+x$ direction is normally incident upon a conducting rectangular cylinder of dimensions a and b, as shown in Figure P12-9. Use the EFIE, piecewise constant subdomain basis functions and point-matching techniques, write your own program, and do the following.

(a) Compute the induced current density on the surface of the cylinder when $a = 5\lambda$ and $b = 2.5\lambda$. Assume a unity line-source current.

(b) Compute and plot for part a the two-dimensional normalized $\sigma_{2\text{-D}}/\lambda$ bistatic scattering width (in decibels) for $0° \leq \phi \leq 360°$.

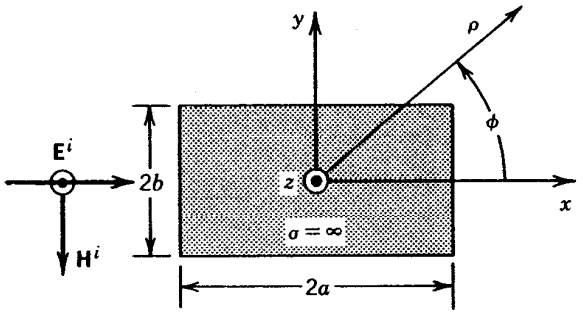

FIGURE P12-9

12.10. Repeat Problem 12.9 for a TM^z uniform plane wave impinging upon an elliptic conducting cylinder with $a = 5\lambda$ and $b = 2.5\lambda$.

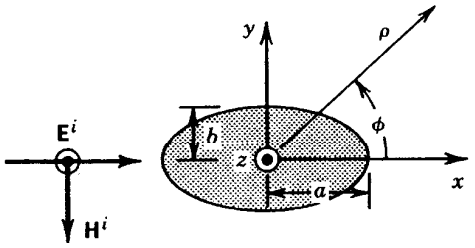

FIGURE P12-10

12.11. Using the geometry of Figure 12-14 verify (12-71a) and (12-71b), and that (12-70a) reduces to (12-72a) and (12-70b) to (12-72b).

12.12. Show that the integral of (12-78d) can be evaluated using (12-79a) through (12-79c).

12.13. Repeat Problem 12.4 for a magnetic line source of constant current $I_m = 1$ when $a = b = 5\lambda$. This problem is representative of a very thin axial slot on the surface of the cylinder. Compare the current density on the surface of the cylinder from part b with that of the modal solution of (11-177a).

12.14. Repeat Problem 12.6 for a magnetic line source of constant current $I_m = 1$ when $a = 5\lambda$, $b = 2.5\lambda$, and $c = 5\lambda$. This problem is representative of a very thin axial slot on the surface of the cylinder.

12.15. Repeat Problem 12.7 for a magnetic line source of constant current $I_m = 1$ when $a = 5\lambda$, $b = 2.5\lambda$, and $c = 5\lambda$. This problem is representative of a very thin axial slot on the surface of the cylinder.

12.16. Repeat Problem 12.8 for a TE^z uniform plane wave of unity amplitude. Compare the current density with the modal solution of (11-113) and the normalized $\sigma_{2\text{-D}}/\lambda$ bistatic scattering width with the modal solution of (11-117).

12.17. Repeat Problem 12.9 for a TE^z uniform plane wave at unity amplitude.

12.18. Repeat Problem 12.10 for a TE^z uniform plane wave of unity amplitude.

12.19. Using the geometry of Figure 12-17 show that

$$\hat{n} \cdot \nabla H_0^{(2)}(\beta R) = -\beta \cos\psi H_1^{(2)}(\beta R)$$

12.20. Repeat Problem 12.4 using the MFIE.

12.21. Repeat Problem 12.8 using the MFIE. You must write your own computer program to solve this problem.

12.22. Using the geometry of Figure 12-18 show that

$$\hat{n}' \cdot \nabla H_0^{(2)}(\beta R) = -\beta \cos\psi' H_1^{(2)}(\beta R)$$

12.23. Repeat Problem 12.13 using the MFIE.

12.24. Derive Pocklington's integral equation 12-123 using (12-121) and (12-122).

12.25. Derive the solution of (12-125) to the differential equation of (12-124a). Show that Hallén's integral equation can be written as (12-126).

12.26. Show that the incident tangential electric field (E_z^i) generated on the surface of a wire of radius a by a magnetic field generator of (12-129) is given by (12-130).

12.27. Reduce (12-130) to (12-131) valid only along the z axis ($\rho = 0$).

12.28. For the center-fed dipole of Example 12-7, write the $[Z]$ matrix for $N = 21$ using for the gap the delta-gap generator and the magnetic frill generator.

12.29. For an infinitesimal center fed dipole of $\ell = \lambda/50$ of radius $a = 0.005\lambda$ derive the input impedance using Pocklington's integral equation with piecewise constant subdomain basis functions and point matching. Use $N = 21$ and model the gap as a delta-gap generator and as a magnetic-frill generator. Use the PWRS computer program at the end of the chapter.

12.30. A conducting wire of length $\ell = 0.47\lambda$ and radius $a = 0.005\lambda$ is placed symmetrically along the z axis. Assuming a TM^z uniform plane wave is incident on the wire at an angle $\theta_i = 30°$ from the z axis, do the following.

(a) Compute and plot the current induced on the surface of the wire.
(b) Compute and plot the bistatic RCS for $0° \leq \theta_s \leq 180°$.
(c) Compute and plot the monostatic RCS for $0° \leq \theta_i = \theta_s \leq 180°$.

The amplitude of the incident electric field is 10^{-3} V/m. Use Pocklington's integral equation and the PWRS computer program. Determine the number of segments that lead to a stable solution.

12.31. Repeat Problem 12.30 for a TE^z uniform plane wave incidence.

COMPUTER PROGRAM PWRS

```
C*************************************************************************
C   THIS PROGRAM USES POCKLINGTON'S INTEGRAL EQUATIONS  OF ( 12 - 123 )*
C   ON A SYMMETRICAL DIPOLE, AND IT COMPUTES THE CURRENT DISTRIBTUION,  *
C   INPUT IMPEDANCE, NORMALIZED AMPLITUDE RADIATION PATTERN, AND        *
C   SCATTERING PATTERNS                                                 *
C                                                                       *
C   GEOMETRY                                                            *
C   HL  — HALF OF THE DIPOLE LENGTH (IN WAVELENGTHS)                    *
C   RA  — RADIUS OF THE WIRE (IN WAVELENGTHS)                           *
C   NM  — TOTAL NUMBER OF SUBSECTIONS (MUST BE AN ODD INTEGER)          *
C                                                                       *
C   IOPT— OPTIONS TO USE POCKLINGTON'S FORMULATION OF ( 12 - 123 )      *
C   TO SOLVE THE WIRE ANTENNA PROBLEM OR THE WIRE SCATTERER PROBLEM.    *
C                                                                       *
C       IOPT=1 :  ANTENNA PROBLEM                                       *
C       IOPT=2 :  WIRE SCATTERING PROBLEM                               *
C         *** IGNORE OPTION ISCAT WHEN IOPT=1 ***                       *
C                 ISCAT=1, MONOSTATIC RADAR CROSS SECTON                *
C                 ISCAT=2, BISTATIC RADAR CROSS SECTION                 *
C                          NEEDS TO SPECIFY INCIDENT ANGLE              *
C   IEX  — OPTION TO USE EITHER MAGNETIC-FRILL GENERATOR OR DELTA GAP   *
C         *** IGNORE OPTION IEX WHEN IOPT=2 ***                         *
C       IEX =1 :  MAGNETIC-FRILL GENERATOR                              *
C       IEX =2 :  DELTA GAP                                             *
C                                                                       *
C         *** IGNORE POLRD, AND THETD WHEN IOPT=1 ***                   *
C   POLRD— ELECTRIC FIELD POLARIZATION RELATIVE TO THE PLANE OF         *
C          INCIDENCE, WHICH IS DEFINED AS THE PLANE CONTAINING THE      *
C          INCIDENT WAVE VECTOR AND THE WIRE SCATTERER.  REFER TO       *
C          FIGURE 12 - 23(A) FOR THE SCATTERER'S GEOMETRY(IN DEGREES).  *
C   THETD— THE INCIDENT ANGLE RELATIVE TO THE Z-AXIS (IN DEGREES).      *
C         *** THETD IS NEEDED FOR BISTATIC CASE ONLY ***                *
C                                                                       *
C   THIS PROGRAM USES PULSE EXPANSION FOR THE ELECTRIC CURRENT MODE     *
C   AND POINT-MATCHING THE ELECTRIC FIELD AT THE CENTER OF EACH         *
C   WIRE SEGMENT.                                                       *
C                                                                       *
C*************************************************************************
C  EXAMPLE A: HOW TO SPECIFY THE NUMBER OF SUBSECTIONS OF THE ANTENNA
C             OR SCATTERER.  NM=21 FOR THIS EXAMPLE.
      PARAMETER  ( NM=21, NMT=2*NM-1 )
      COMMON/SIZE/HL,RA,DZ,ZM,ZN,NMH
      COMMON/CONST/BETA,ETA,RAD,J
      COMPLEX ZMN(NMT),WA(NMT),CGA(NM),ZIN,J,CRT
      DIMENSION INDEX(NM),ETMM(181)
      EXTERNAL CGP
      DATA POLRD,THETD,ISCAT/0.0,0.0,0/
C  EXAMPLE B: HOW TO SPECIFY THE ANTENNA PROBLEM USING MAGNETIC FRILL
C     IOPT=1
C     IEX=1
C  EXAMPLE C: HOW TO SPECIFY THE ANTENNA PROBLEM USING DELTA GAP
C     IOPT=1
C     IEX=2
C  EXAMPLE D: HOW TO SPECIFY THE MONOSTATIC SCATTERING PROBLEM
C             AT A POLARIZATION ANGLE OF 45 DEGREES
C     IOPT=2
C     ISCAT=1
C     POLRD=45.0
C  EXAMPLE E: HOW TO SPECIFY THE BISTATIC SCATTERING PROBLEM
C             AT A POLARIZATION ANGLE OF 45 DEGREES,
C             AND AN INCIDENT ANGLE OF 60 DEGREES
C     IOPT=2
C     ISCAT=2
```

```
C      POLRD=45.0
C      THETD=60.0
C   THE PRESET EXAMPLE HERE IS THE WIRE ANTENNA PROBLEM OF MAGNETIC
C   FRILL GENERATOR MODEL
       IOPT=1
C      IEX=1
C.. GEOMETRY DATA
C.. EXAMPLE: DIPOLE HALF LENGTH  OF 0.235 WAVELENGTHS
C..          AND WIRE RADIUS OF 0.005 WAVELENGTHS.
       HL=.235
       RA=.005
C.. SOME CONSTANTS
       PI=3.14159265
       RAD =PI/180.
       BETA=2.0*PI
       ETA =120.*PI
       NMH=0.5*(NM+1)
       J=CMPLX(0.,1.)
       DZ=2.*HL/NM
       IF(IOPT.EQ.1) THEN
        WRITE(6,50) HL,RA
        IF(IEX.EQ.1) WRITE(6,100)
        IF(IEX.EQ.2) WRITE(6,102)
       ELSE
        WRITE(6,52) HL,RA
       ENDIF
        WRITE(6,54) NM
C.. THE IMPEDANCE MATRIX HAS A TOEPLITZ PROPERTY, THEREFORE ONLY
C.. NM ELEMENTS NEED TO BE COMPUTED, AND THE MATRIX IS FILLED IN
C.. A FORM THAT CAN BE SOLVED BY A TOEPLITZ MATRIX SOLVING SUBROUTINE
       ZM=HL-0.5*DZ
       B=0.5*DZ
       A=-0.5*DZ
       DO 4 I=1,NM
         ZN=HL-(I-0.5)*DZ
         CALL CSINT(CGP,A,B,79,CRT)
         ZMN(I)=CRT
         IF(I.EQ.1) GOTO 4
         ZMN(NM+I-1)=CRT
  4    CONTINUE
       IF(IOPT.EQ.2.AND.ISCAT.EQ.1) GOTO 60
       IF(IOPT.EQ.1) THEN
         RB=2.3*RA
         TLAB=2.*ALOG(2.3)
         DO 10 I=1,NM
         ZI=HL-(I-0.5)*DZ
         R1=BETA*SQRT(ZI*ZI+RA*RA)
         R2=BETA*SQRT(ZI*ZI+RB*RB)
         IF(IEX.EQ.1) THEN
           CGA(I)=-J*BETA**2/(ETA*TLAB)*(CEXP(-J*R1)/R1-CEXP(-J*R2)/R2)
         ELSE
         IF(IEX.NE.2) WRITE(6,999)
           IF(I.NE.NMH) THEN
             CGA(I)=0.
           ELSE
             CGA(I)=-J*BETA/(ETA*DZ)
           ENDIF
         ENDIF
  10     CONTINUE
       CALL TSLZ(ZMN,CGA,WA,NM)
C.. OUTPUT THE CURRENT DISTRIBUTION ALONG OF THE DIPOLE
```

```
      WRITE(6,104)
      DO 12 I=1,NMH
        XI=HL-(I-.5)*DZ
        YI=CABS(CGA(I))
        WRITE(6,106)I, XI,CGA(I),YI
 12   CONTINUE
C..  COMPUTATION OF THE INPUT IMPEDANCE
      ZIN=1./CGA(NMH)
      WRITE(6,108) ZIN
C.. COMPUTATION OF AMPLITUDE RADIATION PATTERN OF THE ANTENNA
      CALL PATN(CGA,NM,ETMM,IOPT)
      WRITE(6,110)
      DO 14 I=1,181
        XI=I-1.
 14     WRITE(6,112)  XI,ETMM(I)
      ELSE
C.. WIRE SCATTERER PROBLEM, BISTATIC CASE
        IF(IOPT.NE.2) WRITE(6,999)
        IF(ISCAT.NE.2) WRITE(6,999)
        CTH=COS(THETD*RAD)
        STH=SIN(THETD*RAD)
        CSPL=COS(POLRD*RAD)
        DO 15 I=1,NM
        ZI=HL- (I-0.5)*DZ
 15     CGA(I)=-J*BETA/ETA*CSPL*STH*CEXP(J*BETA*ZI*CTH)
C.. NOW SOLVE FOR THE CURRENT DISTRIBUTION
      CALL TSLZ(ZMN,CGA,WA,NM)
C.. COMPUTE THE PATTERN
      WRITE(6,120)
      WRITE(6,122) THETD,POLRD
      DO 20 I=1,NM
        XI=HL-(I-0.5)*DZ
        YI=CABS(CGA(I))
        WRITE(6,124) XI,CGA(I),YI
 20   CONTINUE
C.. COMPUTATION OF BISTATIC RCS  PATTERNS
      CALL PATN(CGA,NM,ETMM,IOPT)
      WRITE(6,126)
      DO 40 I=1,181
        XI=I-1.
        WRITE(6,128)  XI,ETMM(I)
 40   CONTINUE
      ENDIF
      GOTO 200
C.. THE MONOSTATIC CASE
 60   WRITE(6,140)
      DO 70 M=1,91
      THETA=(M-1.)*RAD
        CTH=COS(THETA)
        STH=SIN(THETA)
        CSPL=COS(POLRD*RAD)
        DO 62 I=1,NM
        ZI=HL-(I-0.5)*DZ
 62     CGA(I)=-J*BETA/ETA*CSPL*STH*CEXP(J*BETA*ZI*CTH)
      CALL TSLZ(ZMN,CGA,WA,NM)
      IF(ABS(CTH).LE.1.E-3) THEN
        FT=1.
      ELSE
        FT=SIN(BETA*DZ*CTH*.5)/(BETA*DZ*CTH*.5)
      ENDIF
      CRT=0.
      DO 64 I=1,NM
        ZI=HL-(I-.5)*DZ
        CRT=CRT+CEXP(J*BETA*ZI*CTH)*FT*CGA(I)*DZ
```

```
 64   CONTINUE
      PTT=CABS(CRT)*STH*STH*ETA*0.5
      PTT=PTT*PTT*BETA*2.
      IF(PTT.LE.1.E-10) PTT=1.E-10
      PTT=10.*ALOG10(PTT)
      ETMM(M)=PTT
 70   ETMM(182-M)=PTT
      WRITE(6,142) POLRD
      WRITE(6,144)
      DO 72 I=1,181
      XI=I-1
 72   WRITE(6,146) XI,ETMM(I)
 50   FORMAT(15X,'WIRE ANTENNA PROBLEM'//5X,'LENGTH = 2 X ',F6.4,
     +' (WLS)', 4X,'RADIUS OF THE WIRE=',F6.4,' (WLS) '/)
 52   FORMAT(15X,'WIRE SCATTERER PROBLEM'//5X,'LENGTH = 2 X ',F6.4,
     +' (WLS)', 4X,'RADIUS OF THE WIRE=',F6.4,' (WLS) '/)
 54   FORMAT(15X,'NUMBER OF SUBSECTIONS = ', I3/)
 100  FORMAT(5X,'POCKLINGTON''S EQUATION AND MAGNETIC FRILL MODEL'/)
 102  FORMAT(5X,'POCKLINGTON''S EQUATION AND DELTA GAP MODEL'/)
 104  FORMAT(10X,'CURRENT DISTRIBUTION ALONG ONE HALF OF THE DIPOLE'/
     +8X,'POSITION Z',3X,'REAL PART',3X,'IMAGINARY ',3X,'MAGNITUDE'/)
 106  FORMAT(3X,I3,4X,F6.4,5X,F9.6,3X,F9.6,3X,F9.6)
 108  FORMAT(/3X,'INPUT IMPEDANCE = ',F7.1,'+ J',F7.1,' (OHMS)')
 110  FORMAT(/3X,'RADIATION POWER PATTERN VS OBSERVATION ANGLE THETA'//
     +3X,'THETA (IN DEGREES)',2X,'POWER (IN DB)')
 112  FORMAT(8X,F6.1,8X,F8.2)
 120  FORMAT(4X,'BISTATIC WIRE SCATTERER PROBLEM WITH POCKLINGTON''S',
     +' EQUATION'//)
 122  FORMAT(8X,'INCIDENT ANGLE=',F5.1,' DEGREES, POLARIZATION=',F5.1,
     +' DEGREEES'//10X,'CURRENT DISTRIBUTION ALONG THE DIPOLE'//
     +8X,'POSITION Z',3X,'REAL PART',3X,'IMAGINARY ',3X,'MAGNITUDE'/)
 124  FORMAT(10X,F6.4,5X,F9.6,3X,F9.6,3X,F9.6)
 126  FORMAT(/4X,'BISTATIC RADAR CROSS SECTION PATTERN VS OBSERVATION',
     +' ANGLE THETA '//8X,'THETA(IN DEGREES) ',2X,'RCS (IN DBSM)')
 128  FORMAT(12X,F6.1,8X,F10.2)
 140  FORMAT(4X,'MONOSTATIC WIRE SCATTERER PROBLEM WITH POCKLINGTON''S',
     +' EQUATION'/)
 142  FORMAT(4X,'THE POLARIZATION TO THE PLANE OF INCIDENCE = ',F5.1,
     +' DEGREES '/)
 144  FORMAT(14X,'THE MONOSTATIC RADAR CROSS SECTION PATTERN'
     +//10X,'    INCIDENT ANGLE (THETA)',5X,'  RCS IN (DBSM)')
 146  FORMAT(20X,F7.2,15X,F10.2)
 999  FORMAT(5X,'******WARNING: NO SUCH OPTION. CHOOSE A VALID OPTION'/
     +20X,'AND TRY AGAIN.')
 200  STOP
      END
C..
      COMPLEX FUNCTION CGP(Z)
C.. POCKLINGTON'S KERNEL
      COMMON/SIZE/HL,RA,DZ,ZM,ZN,NMH
      COMMON/CONST/BETA,ETA,RAD,J
      COMPLEX J
      Z1=ZN-ZM +Z
      R=SQRT(RA*RA+Z1*Z1)
      CGP=CEXP(-J*BETA*R)*((1.+J*BETA*R)*(2.*R*R-3.*RA*RA)+
     +(BETA*RA*R)**2)/(2.*BETA*R**5)
      RETURN
      END
C.
      SUBROUTINE PATN(CGA,NM,ETMM,IOPT)
C.. THE SUBROUTINE TO COMPUTE THE RADIATION PATTERN
      COMMON/SIZE/HL,RA,DZ,ZM,ZN,NMH
      COMMON/CONST/BETA,ETA,RAD,J
      COMPLEX CGA(NM),J,CRT
```

```
      DIMENSION ETMM(181)
      DO 4 I=1,181
      THETA=(I-1.)*RAD
      CTH=COS(THETA)
      STH=SIN(THETA)
      IF(ABS(CTH).LE.1.E-3) THEN
        FT=1.
      ELSE
        FT=SIN(BETA*DZ*CTH*.5)/(BETA*DZ*CTH*.5)
      ENDIF
      CRT=0.
      DO 2 M=1,NM
        ZM=HL-(M-.5)*DZ
        CRT=CRT+CEXP(J*BETA*ZM*CTH)*FT*CGA(M)*DZ
 2    CONTINUE
      PTT=CABS(CRT)*STH*STH*ETA*0.5
 4    ETMM(I)=PTT
      IF(IOPT.EQ.1) THEN
       AMAX=ETMM(1)
       DO 6 I=2,181
       IF(ETMM(I).GT.AMAX) AMAX=ETMM(I)
 6    CONTINUE
      DO 8 I=1,181
      PTT=ETMM(I)/AMAX
      IF(PTT.LE.1.E-5) PTT=1.E-5
 8    ETMM(I)=20.*ALOG10(PTT)
      ELSE
      DO 10 I=1,181
      PTT=ETMM(I)**2*BETA*2.
      IF(PTT.LT.1.E-10) PTT=1.E-10
 10   ETMM(I)=10.*ALOG10(PTT)
      ENDIF
      RETURN
      END
C*******************************************************************************
C     SUBROUTINE TSLZ          NETLIB
C     INPUT:
C       (C)A(2*M - 1)          THE FIRST ROW OF THE T-MATRIX FOLLOWED BY
C                              ITS FIRST COLUMN BEGINNING WITH THE SECOND
C                              ELEMENT.  ON RETURN A IS UNALTERED.
C       (C)B(M)                THE RIGHT HAND SIDE VECTOR B.
C       (C)WA(2*M-2)           A WORK AREA VECTOR
C       (I)M                   ORDER OF MATRIX A.
C     OUTPUT:
C       (C)B(M)                THE SOLUTION VECTOR.
C     PURPOSE:
C       SOLVE A SYSTEM OF EQUATIONS DESCRIBED BY A TOEPLITZ MATRIX.
C       A * X = B
C     SUBROUTINES AND FUNCTIONS:
C       TOEPLITZ PACKAGE ... TSLZ1
C*******************************************************************************
      SUBROUTINE TSLZ(A,B,WA,M)
      INTEGER M
      COMPLEX A(2*M-1),B(M),WA(2*M-2)
      CALL TSLZ1(A,A(M+1),B,B,WA,WA(M-1),M)
      RETURN
      END
C..
      SUBROUTINE TSLZ1(A1,A2,B,X,C1,C2,M)
      INTEGER M
      COMPLEX A1(M),A2(M-1),B(M),X(M),C1(M-1),C2(M-1)
      INTEGER I1,I2,N,N1,N2
      COMPLEX R1,R2,R3,R5,R6
      R1 = A1(1)
```

```
      X(1) = B(1)/R1
      IF (M .EQ. 1) GO TO 80
      DO 70 N = 2, M
         N1 = N - 1
         N2 = N - 2
         R5 = A2(N1)
         R6 = A1(N)
         IF (N .EQ. 2) GO TO 20
            C1(N1) = R2
            DO 10 I1 = 1, N2
               I2 = N - I1
               R5 = R5 + A2(I1)*C1(I2)
               R6 = R6 + A1(I1+1)*C2(I1)
   10       CONTINUE
   20    CONTINUE
         R2 = -R5/R1
         R3 = -R6/R1
         R1 = R1 + R5*R3
         IF (N .EQ. 2) GO TO 40
            R6 = C2(1)
            C2(N1) = (0.0D0,0.0D0)
            DO 30 I1 = 2, N1
               R5 = C2(I1)
               C2(I1) = C1(I1)*R3 + R6
               C1(I1) = C1(I1) + R6*R2
               R6 = R5
   30       CONTINUE
   40    CONTINUE
         C2(1) = R3
         R5 = (0.0D0,0.0D0)
         DO 50 I1 = 1, N1
            I2 = N - I1
            R5 = R5 + A2(I1)*X(I2)
   50    CONTINUE
         R6 = (B(N) - R5)/R1
         DO 60 I1 = 1, N1
            X(I1) = X(I1) + C2(I1)*R6
   60    CONTINUE
         X(N) = R6
   70 CONTINUE
   80 CONTINUE
      RETURN
      END
C..
      SUBROUTINE CSINT(CF,XL,XU,N,CRT)
C.. FAST ALGORITHM FORM OF THE SIMPSON'S INTEGRAL ROUTINE
      IMPLICIT COMPLEX (C)
      CRT=CF(XL)+CF(XU)
      HD=(XU-XL)/(N+1)
      DO 20 I=1,N
        XI=XL+I*HD
        IF(MOD(I,2).NE.0) THEN
          CRT=CRT+4.*CF(XI)
        ELSE
          CRT=CRT+2.*CF(XI)
        ENDIF
   20 CONTINUE
      CRT=CRT*HD*0.33333333
      RETURN
      END
```